NASA Contractor Report 195042

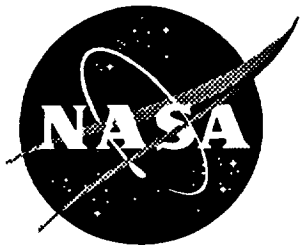

Effects of Through-the-Thickness Stitching on Impact and Interlaminar Fracture Properties of Textile Graphite/Epoxy Laminates

Suresh K. Sharma and Bhavani V. Sankar
University of Florida, Gainesville, Florida

Grant NAG1-1226

February 1995

National Aeronautics and
Space Administration
Langley Research Center
Hampton, Virginia 23681-0001

TABLE OF CONTENTS

LIST OF TABLES

LIST OF FIGURES

SUMMARY

This study investigated the effects of through-the-thickness stitching on impact damage resistance, impact damage tolerance, Mode I and Mode II fracture toughness of textile graphite/epoxy laminates. Uniweave resin-transfer-molded (RTM) 48 ply graphite/epoxy (AS4/3501-6) laminates were stitched with Kevlar® and Glass yarns of different linear and stitch densities. Delaminations were implanted during processing to simulate impact damage. Sublaminate Buckling Tests were performed to measure compression strength and to understand the effect of stitching on the failure mode of the sublaminates. The results showed outstanding improvements of up to 400% in the compression strength over the unstitched laminates. The stitches change the failure mode of laminates radically as compared to the unstitched laminates. In addition, the effect on the impact damage resistance and tolerance of 16 ply plain weave stitched laminates (Hercules A193-P/3501-6) was studied by conducting Static Indentation-Flexure (SIF) test followed by a CAI test. Though the onset of damage occurred at the same load levels as the unstitched laminates, the damage area was less and the CAI strength was significantly more even for these thin stitched laminates.

Mode I fracture toughness of 24 ply Uniweave unidirectional (AS4/3501-6) stitched laminates was measured by conducting Double-Cantilever-Beam (DCB) tests. The crack propagation in the stitched laminates was observed to be intermittent and dynamic. The critical strain energy release rate (G_{Ic}) was found to be about 30 times higher than the unstitched laminates for even a low stitch density like 16 stitches/in^2. The G_{Ic} values for higher stitch density are expected to be much higher. The G_{Ic} was not measured as the specimens failed in bending before the crack could start propagating during the DCB test.

Mode II fracture toughness of the Uniweave laminates was measured by performing End-Notched-Flexure (ENF) test in stroke control mode. The crack propagation in the stitched laminates is gradual and steady unlike the unstitched laminates where it is sudden and dynamic. In order to calculate the critical strain energy release rate (G_{IIc}), the existing beam theory formula can not be applied as the stitches change the crack propagation mechanism altogether. The material together with the stitches seems to behave more like a structure. Therefore, two new methods to compute the apparent G_{IIc} are presented. First one is Area Method using C-Scan and the other one is Equivalent Area Method using the Compliance of the Unloading Curve. The apparent G_{IIc} was found to be at least 5-15 times higher for the stitched laminates. The stitches plough through the matrix and do not break as the crack propagates. Thus, the apparent G_{IIc} increases with the increase in crack length as more and more stitches become involved in the matrix ploughing.

CHAPTER - 1
INTRODUCTION

Literature Review

Although man-made composites have existed for many thousands of years, the advanced fibrous composites have evolved in the aerospace industry during the last three decades. These composite materials are well known for their high strength-to-weight and stiffness-to-weight ratios. They offer flexibility in tailoring the composite structure to meet performance requirements in an optimum way. Other advantages of composite materials include superior corrosion resistance, high energy absorption, favorable thermal insulation and electrical resistivity [1,2]. The materials have the potential for revolutionizing the way present day products are made. Today, these materials are finding increasing applications in automotive, sports, marine, transportation, building construction and biomedical industry [3]. However, despite the diverse potential of their applications the production volume of advanced composites has not risen significantly in recent past [4]. Primary problem areas of unidirectional fiber composites are: high processing cost, low impact damage resistance and impact damage tolerance, and poor interlaminar fracture toughness. To alleviate some of the high processing costs, Textile Structural Composites are fast emerging as low cost - high performance alternative due to adaptation of many cost effective mass production techniques well known to the textile industry [5].

This research study focusses on the effects of through-the-thickness stitching on the low velocity impact damage resistance and damage tolerance, and the interlaminar fracture toughness of textile graphite/epoxy laminates.

Impact Damage Resistance and Impact Damage Tolerance

Impact damage resistance deals with the damage state brought about by an impact event. Impact damage tolerance concerns the changes in structural performance due to the damage state. Impact of any foreign object on a composite structure may cause matrix cracking and delaminations. Damage due to low velocity impact may not be always visible. Damage, once initiated will propagate during the service life of a structure due to a variety of loading factors. The effect of low velocity impact on advanced composites have been widely reported by researchers in the past several years, experimentally and analytically.

Kwon and Sankar [6] studied applicability of static indentation response in predicting damage due to large impact mass at low velocity. Jackson and Poe [7] showed use of impact force as a scale parameter for delamination damage for impacts of simple plates. They assessed other impact parameters, namely, impact energy and delamination damage. Low velocity impact damage testing is ususally carried out using a pendulum, drop tower or gas-gun. Quasi-isotropic graphite/epoxy laminates have virtually become the bench mark for testing and comparison of analytical and experimental data. Prasad et al. [8] developed an experimentally validated analysis to determine transient response of simply supported, rectangular composite plates subjected to low velocity impact. Recently,

a synthesis and treatise of the vast research carried out in the area of low velocity impact response of composites has been published by Sankar [9]. Whereas the impact force and impact damage area characterize the impact damage resistance of a laminate, the impact damage tolerance is invariably characterized by residual compression-after-impact (CAI) strength [10-13]. These references are representative of only a cross-section of literature on a wide variety of impact related issues. Results of all studies indicate that significant drop in compression strength can result from a low velocity impact even if the damage is not visible to the eye. Impact causes interply delaminations. The delaminations make the laminate behave like thinner sublaminates which buckle at lower compressive loads. However, the effect of through-the-thickness stitching on limiting impact damage and sublaminate buckling, and increasing the CAI strength of the laminate needs further understanding.

Interlaminar Fracture Toughness

Although conventional laminated composites have high strength in the fiber direction, they lack through-the-thickness reinforcement. Hence, they have poor interlaminar fracture toughness and are susceptible to delaminations. One of the ways to reinforce a laminate through the thickness is by stitching. The idea of stitching the textile preform fits well with textile technology. Mignery et al. [14] investigated the use of stitching by Kevlar® yarn to suppress delamination in graphite/epoxy laminates. The results showed that stitches effectively arrested delamination. Dexter and Funk [15] investigated characterization of impact resistance and interlaminar fracture toughness of

quasi-isotropic graphite-epoxy laminates made of unidirectional Thornel 300-6K fibers/Hercules 3501-6 resin and stitched with polyester or Kevlar® yarns. They experimented with stitch parameters and found a significant drop in damage areas of stitched laminates compared to unstitched laminates for the same impact energy. The Mode I fracture toughness, characterized by the critical strain energy release rate, G_{Ic} , was found to be about 30 times higher for the stitched laminates. Effect on Mode II fracture toughness was not investigated in this study. Ogo [16] investigated the effect of through-the-thickness stitching of plain woven graphite/epoxy laminates with Kevlar® yarn. The study showed a manifold increase in G_{Ic} values at the expense of slight drops of in-plane properties. However, his results did not show any significant increase (8%) in Mode II fracture toughness as characterized by the critical strain energy release rate, G_{IIc}. Pelstring and Madan [17] developed semiempirical formulae relating damage tolerance of a composite laminate to stitching parameters. Mode I critical strain energy release rate was found to be 15 times greater than in unstitched laminates, and the critical strain energy release rates decreased exponentially with increase in stitch spacing. Correlation existed between strain energy release rate, damage area, and CAI strength. Byun et al. [18] conducted a finite element analysis on 3-D woven double cantilever beam (DCB) specimen and evaluated Mode I critical strain energy release rate to investigate the influence of through-the-thickness fibers on crack driving force and crack length. Chen et al. [19] proposed effective critical strain energy release rate to measure Mode I fracture toughness of stitched laminates using a finite element model. Recently, Jain and Mai [20] have analytically modeled the Mode I delamination toughness of stitched laminated

composites.

It is evident from the above studies that through-the-thickness stitching significantly improves Mode I fracture toughness in laminates made of unidirectional tapes or plain woven fabric cloth of graphite and epoxy resin. However, effect on Mode II fracture toughness has not been fully investigated. Further, variations of stitch density, stitch failure mechanisms and their contribution to Mode I and Mode II fracture toughness are not completely understood.

Objectives and Scope

To investigate the effects of stitching on sublaminate buckling failure, CAI strength, and interlaminar fracture toughness, the tests given below were conducted on stitched and unstitched specimens made of AS4 uniweave graphite fabric and 3501-6 epoxy resin. Stitch yarns of 1600 denier Kevlar® (2790 yd/lb) and 3570 and 5952 denier Glass (1250 and 750 yd/lb respectively) with different stitch densities were investigated. A denier is a measure of linear density in grams per 9000 meters of yarn. This can also be represented by yarn number which is given by yards/lb for the yarn. Further, we define stitch density in a composite laminate by the number of stitches per square inch and represent this density by the stitching pattern as: (Number of stitches per inch) × (Spacing between two stitch lines), e.g., 8×1/8" means a stitch density of 64 where pitch is 8 stitches per inch and distance between two adjoining stitch rows is 1/8". The specimens were cut from plates that were processed using Resin-Transfer-Molding (RTM) at Douglas Aircraft Co., and provided to us by NASA Langley Research Center, Hampton VA. The

RTM process can be used for high volume manufacturing process for large structural parts. Details of the material system for these uniweave laminates and the stitch density of each plate are described in the section following the types of tests conducted in this study.

Sublaminate Buckling Test. To understand the effect of stitching on sublaminate buckling failure. Sublaminate Buckling Tests were conducted at NASA Langley Research Center, Hampton, VA. The delamination damage in the specimens was simulated by implanting teflon film inserts at various ply interfaces during the processing. Four different types (i.e., extent) of delamination damage were investigated by varying the size, number, and location of the teflon inserts. In addition, control specimens were processed without any teflon inserts in them. The variation in stitch density was also studied for each type of delamination damage. Details of the test and results are in Chapter - 2.

Mode I Fracture Toughness Test. Double-Cantilever-Beam (DCB) tests were performed to measure Mode I fracture toughness. The effects of stitch yarn, stitch density and yarn denier on G_{Ic} were studied. Stitch damage mechanisms were investigated using Photomicrography and Scanning Electron Microscopy (SEM). Details of the test and results are described in Chapter - 3.

Mode II Fracture Toughness Test. End-Notched-Flexure (ENF) tests were performed to measure Mode II fracture toughness. The effects of stitch yarn, stitch density, yarn number, starter crack length, crack surface and contact roller pin friction and

unstitched length on G_{IIc} were studied. The unstitched length is defined as the distance between the starter crack and the first stitch. Stitch damage mechanisms were investigated using X-Radiography, Ultrasonic C-Scanning and Photomicrography. Details of the test and results are described in Chapter - 4.

In addition to the above tests on the uniweave laminates provided to us by NASA Langley Research Center, thin plain weave graphite/epoxy laminates were processed at the Center for Studies of Advanced Structural Composites, University of Florida, Gainesville FL, to gain insight into some of the processing aspects and to study impact damage resistance and damage tolerance of thin stitched laminates. Towards this end, Static Indentation-Flexure (SIF) tests followed by Compression-After-Impact (CAI) tests were performed on these thin laminates. The indentation damage area due to the SIF test and the propagation of the damage during the CAI test were studied by Ultrasonic C-Scanning. Details of the material system of thin plain weave laminates along with the SIF and CAI test findings are described in Chapter - 5.

Material System of Uniweave Laminates

The AS4 uniweave graphite fabric preforms were stitched using automated sewing machines. The modified lock stitch as shown in Fig. 1-1 and Resin-Transfer-Molding (RTM) process [21] were used by Douglas Aircraft Company to fabricate plates from which the specimens were machined. Three different bobbin stitch yarns each with two different stitch densities of 4×1/4" and 8×1/8" were used for stitching. Needle stitching yarn used in all the cases was Kevlar®-29 (400 denier). Top and bottom plies of the

uniweave preform were covered by one layer of plain weave fiberglass cloth to act as retainer cloth for the stitches. The details of the stitch yarns used are given in Table 1-1. For the purposes of this document, the three bobbin stitch yarns will be referred to as: Kevlar-2790, Glass-1250 and Glass-750. In addition, one unstitched plate for each type of testing was processed for control specimens. Thus, seven plates (#31 to 37) were processed for Sublaminate Buckling Test specimens as per details given in Table 1-2 and Fig. 1-2, and another set of seven plates (#24 to 30) were processed for Mode I and Mode II Fracture Toughness Tests as per details shown in Table 1-3 and Fig. 1-3. The plates were Ultrasonically C-Scanned for quality and location of teflon inserts. Representative C-Scans of the plates are shown in Figs. 1-4 and 1-5.

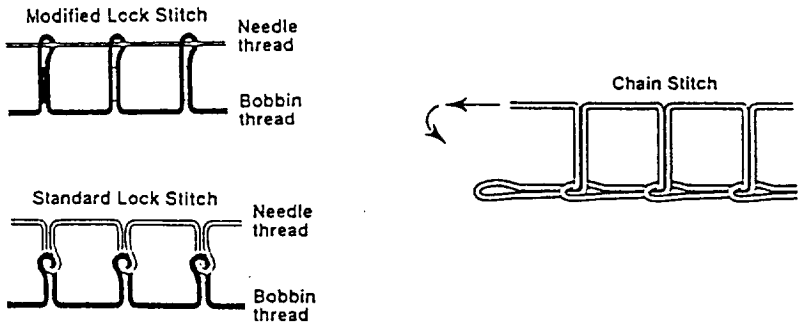

Figure 1-1: Types of stitch locks [Courtesy; Palmer, Dow and Smith: Ref. 21]

Table 1-1: Details of stitch yarns used

STITCH YARN	BREAKING STRENGTH (Newton)	BREAKING STRENGTH (lbf)
Kevlar (1600 denier ~ 2790 yd/lb) bobbin yarn	347	78
Glass (3570 denier ~ 1250 yd/lb) bobbin yarn	262	59
Glass (5952 denier ~ 750 yd/lb) bobbin yarn	436	98
Kevlar (400 denier ~ 11160 yd/lb) needle yarn	53	12

Table 1-2: Material system for Sublaminate Buckling Tests

PLATE #	LAY UP	STITCH DENSITY	STITCH YARN	YARN‡ NUMBER (yd/lb)	YARN‡ DENIER (gm/9000 meters)	AVERAGE THICKNESS OF PLATES (mm)
31	$[(45/0/-45)_s]_{4s}$ (Total 48 plies)†	4×1/4"	Kevlar	2790	1600	6.90
32		8×1/8"	Kevlar	2790	1600	7.20
33		4×1/4"	Glass	1250	3570	7.00
34		8×1/8"	Glass	1250	3570	7.20
35		4×1/4"	Glass	750	5952	6.85
36		8×1/8"	Glass	750	5952	7.45
37		None	-	-	-	6.60

† Each ply is AS4 uniweave graphite fabric. The stitching is in 0° fiber direction. The top and bottom plies of the laminate have one plain weave fiberglass cloth layer each to retain the stitches.

‡ The units for the linear density of a yarn can be Yarn Number (yards/lb) or Denier (grams/9000 meters of yarn). The product of the Yarn Number and Denier will be a constant approximately equal to 4,463,728.

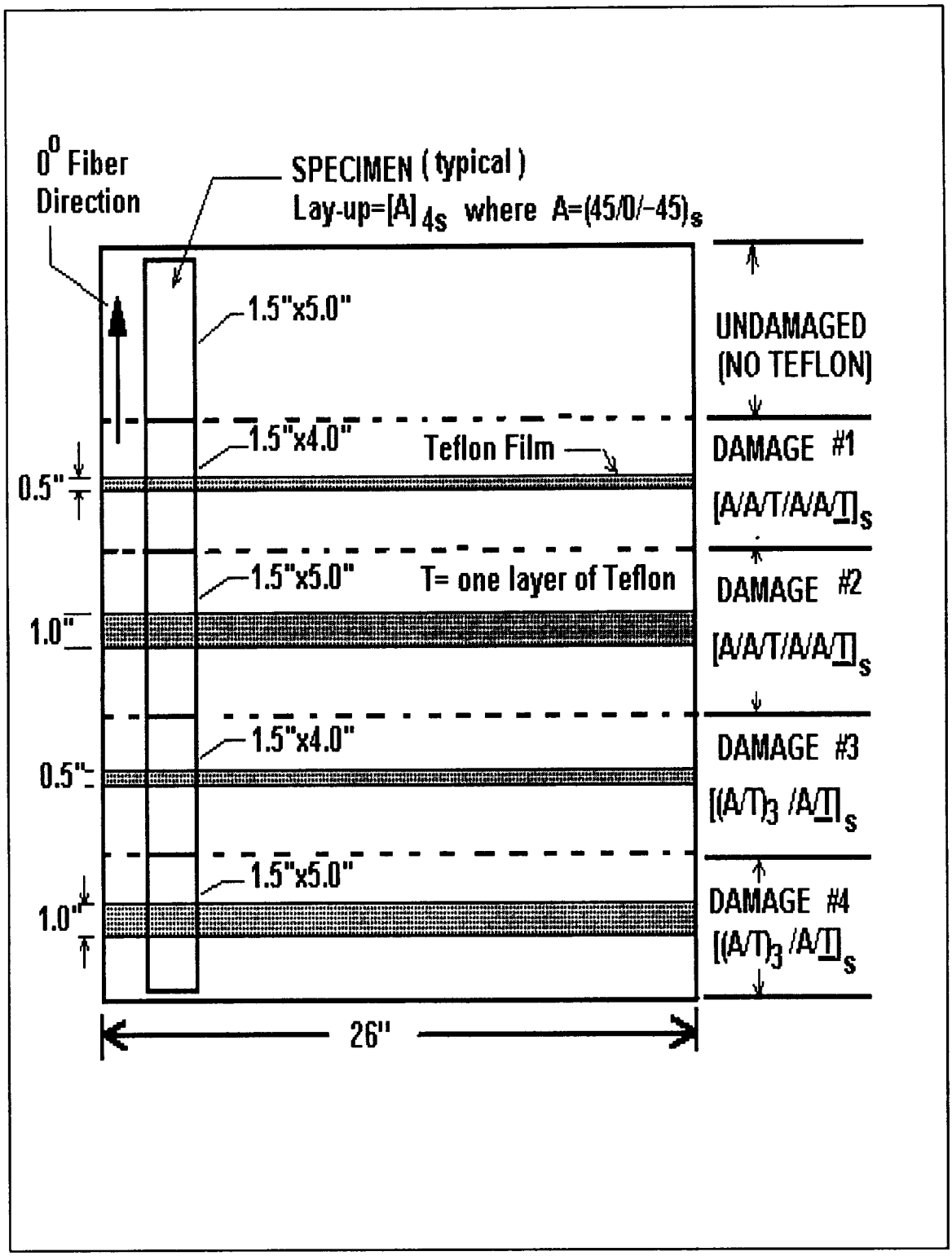

Figure 1-2: Details of a typical RTMed plate for Sublaminate Buckling Test specimens

Table 1-3: Material system for Mode I and Mode II Fracture Toughness Tests

PLATE #	LAY UP	STITCH DENSITY	STITCH YARN	YARN NUMBER (yards/lb)	DENIER (gm/9000 meters)	AVERAGE THICKNESS OF PLATES (mm)
24	Uni-directional 24 plies†	4×1/4"	Kevlar	2790	1600	3.683
25		8×1/8"	Kevlar	2790	1600	4.191
26		4×1/4"	Glass	1250	3570	3.810
27		8×1/8"	Glass	1250	3570	4.191
28		4×1/4"	Glass	750	5952	4.318
29		8×1/8"	Glass	750	5952	4.445
30		None	-	-	-	3.556

† Each ply is AS4 uniweave graphite fabric. The stitching is in 0° fiber direction. A 26"×2.5"×0.0005" thick teflon crack starter film is located at the midplane along the edge as shown in Figs.1-3 and 1-5. No stitching is within 1/2" of the film. Top and bottom plies are covered by plain weave fiberglass cloth to retain the stitches.

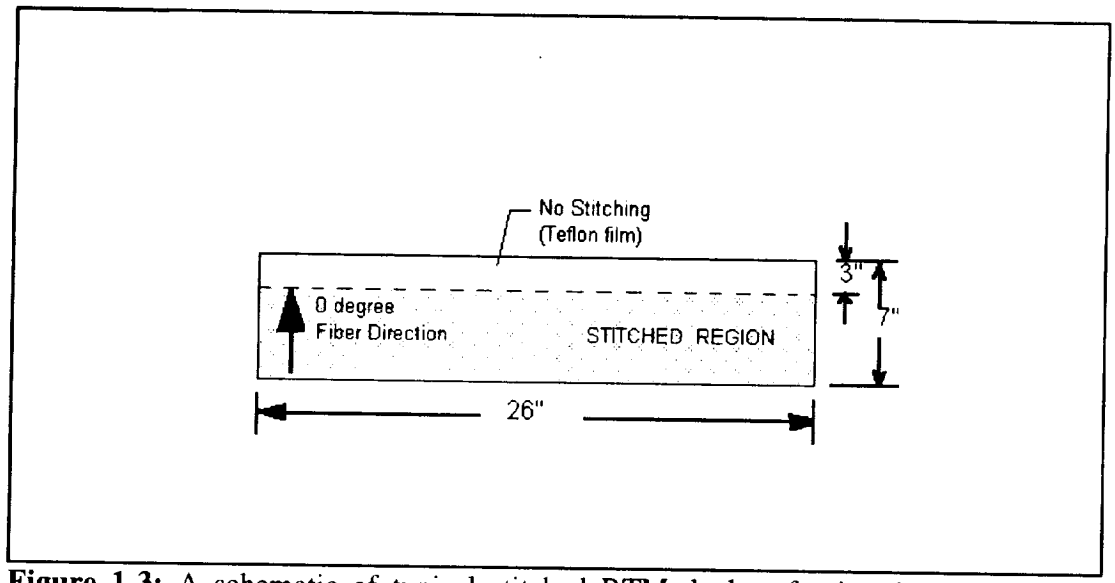

Figure 1-3: A schematic of typical stitched RTMed plate for interlaminar fracture toughness test specimens

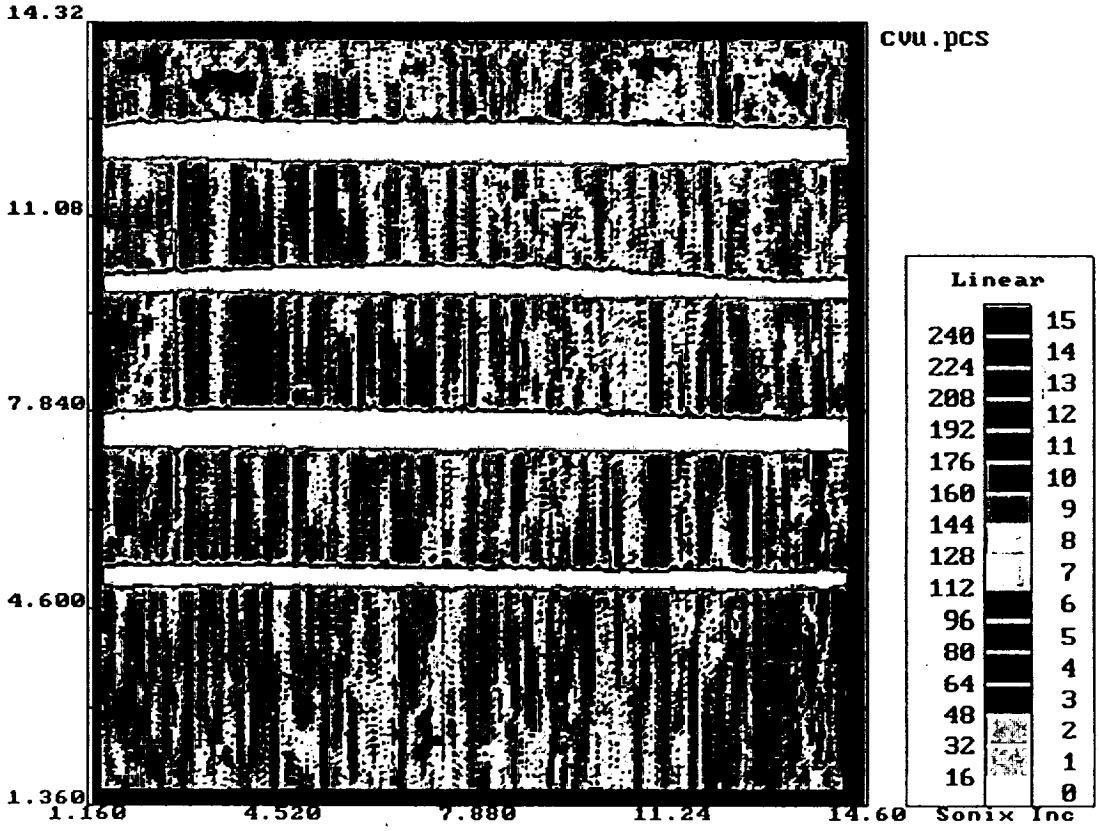

Figure 1-4: A typical C-Scan of a stitched plate for Sublaminate Buckling Test shows position of teflon film strips.

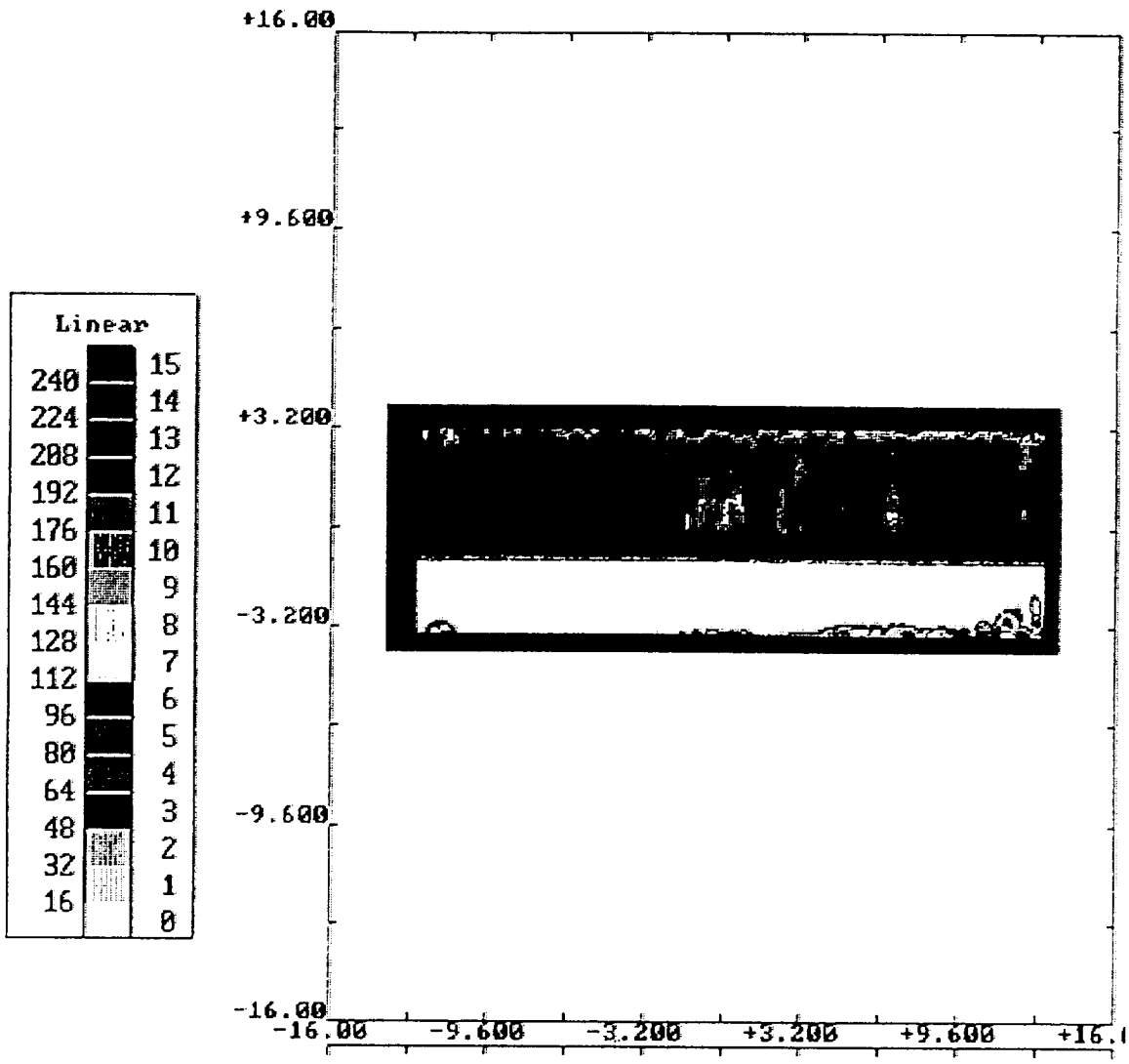

Figure 1-5: A typical C-Scan of a plate for Mode I and Mode II Fracture Toughness Test shows the teflon film strip for creating starter crack.

CHAPTER 2
SUBLAMINATE BUCKLING TEST

Sublaminate Buckling and Test Approach

Residual compression strength of a laminate for a given impact damage is used to compare and characterize different material systems for damage tolerance. In fiber composites, impact damage leads to delaminations, matrix cracking and fiber breaking. The delaminations create sublaminates of different sizes in a laminate. These sublaminates tend to buckle at much smaller loads during compression. Therefore, sublaminate buckling is an important failure mode in fiber composite laminates [11]. This study investigated effects of stitching on sublaminate buckling behavior which is expected to correlate with the CAI strength. Specimens with different stitch densities and known delaminations were subjected to compression loading. The delaminations simulate the impact damage and were created by inserting teflon film strips at various ply interfaces during processing as described in Chapter-1. The University of Florida Compression-After-Impact (UF-CAI) test fixture was used for the tests. The fixture allows end compression loading and can be adapted for different gage lengths as shown in Fig. 2-1. The fixture evolved from an existing NASA post-impact compression fatigue test fixture at the Center for Studies of Advanced Structural Composites, University of Florida. The design considerations and its experimental validation are given in Appendix-A.

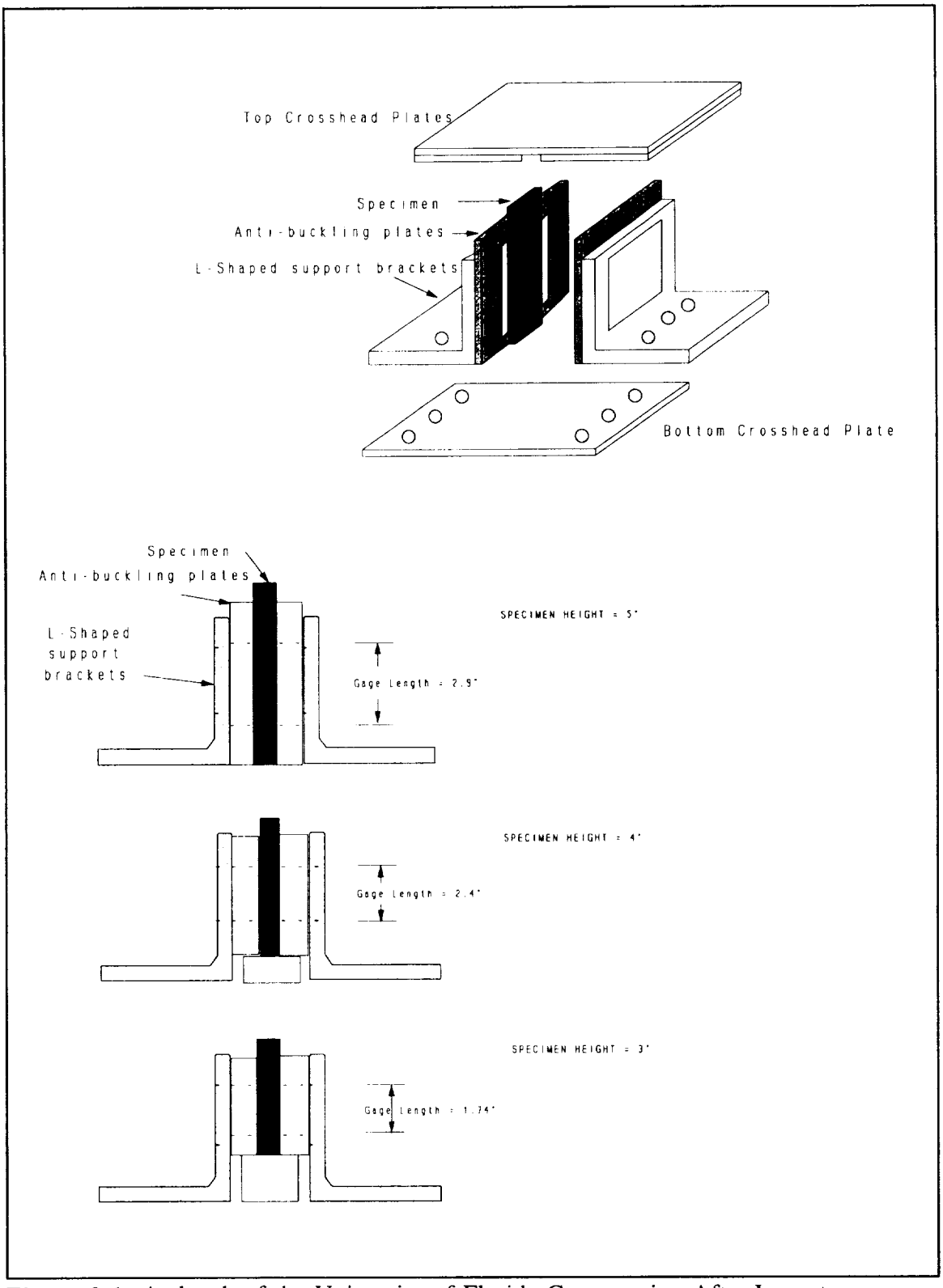

Figure 2-1: A sketch of the University of Florida Compression-After-Impact (UF-CAI) test fixture along with adaptations required for different specimen heights

Specimen Geometry and Test Variables

Each of the seven RTMed plates of the material system processed had four different types of delaminations (numbered Damage Type #1 to 4 for purpose of this report, see Fig. 1-2). The part of the plate without delaminations i.e., no teflon (numbered Damage Type #Zero in this report) was used to cut control specimens. At least 3 specimens each of every damage category were cut and mounted with back to back Micro-Measurement group type CEA-06-250-UW-350 strain gages. The strain gages were mounted to observe global instabilities during compression. The details of a typical specimen are shown in a sketch in Fig. 2-2.

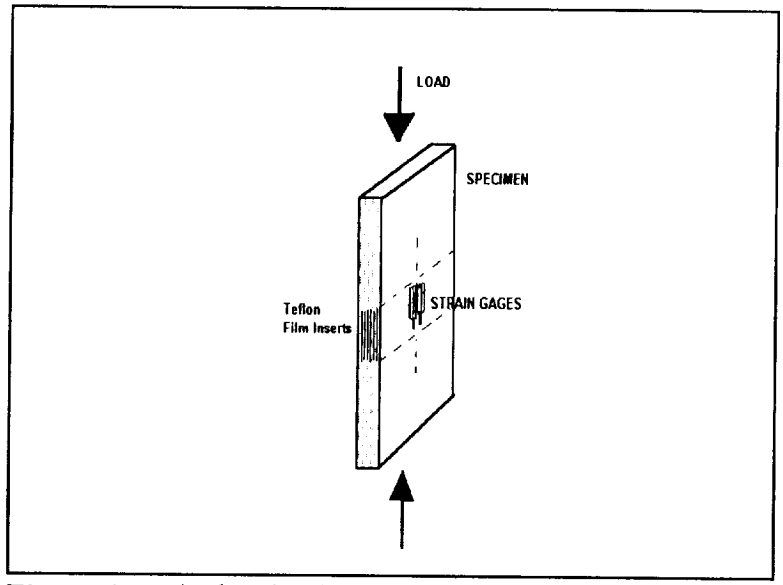

Figure 2-2: A sketch of typical sublaminate buckling specimen

The specimens were cut such that the gage length was 1.9" longer than the length of the delaminations, and the delaminations were located centrally in the specimen. The delaminations ran through the entire width of the specimen. Thus, the specimens with 0.5" teflon inserts had a total gage length of 2.4" and the specimens with 1.0" teflon inserts had a total gage length of 2.9". The specimens having 2.4" gage length were 4" tall and therefore tested using the 4" adaptation of the UF-CAI test fixture (see Fig. 2-1). The other specimens were 5" tall and were tested using the 5" adaptation of the UF-CAI fixture. The side edge surfaces were painted white with typewriter correction fluid to facilitate easy visualization of sublaminate buckling.

Test Procedures and Data Reduction

The tests were performed at the facilities of NASA Langley Research Center at Hampton, VA using a 50 kips capacity MTS 810 testing system, type 647 hydraulic wedge grips and an MTS 458.20 microprofiler controller to conduct the test in stroke control mode. The loading end edges were machined flat and parallel to each other. It is important that the fixture surfaces on which the specimen rests are clean and devoid of any foreign matter as these spots may become potential stress concentration points at which the failure may initiate leading to end brooming. Further, adequate care must be exercised to align the specimen, fixture and the loading platform to ensure vertical axial loading. Rate of compression loading was 0.03"/min. Real time load, displacement and strain signals were acquired using Micro-Measurements System 4000 data acquisition system. The compression failure could mostly be anticipated by strain gage signals

"flaring outward" after the initial superimposed movement indicative of compression. As the strain gage signals begin to flare out significantly (indicative of buckling in the strain gage mounted region), a loud "bang" sound could be heard after a few crackling sounds in quick succession. This is almost immediately accompanied with a drop in load signal. The specimen is unloaded thereafter. The acquired load, displacement and strain gage signals were transferred to a spreadsheet software (Excel) accompanying the Micro-Measurements System 4000 data acquisition system for plotting and analysis. The compression strength was computed from the peak load and the average cross-sectional area. An average thickness of the region without the teflon inserts was used to calculate cross-sectional area. The results of the CAI strength from the tests of 126 specimens cut from the seven plates are given in Tables A-1 to A-7 in Appendix A. A representative stress-strain curve obtained for an unstitched and a stitched laminate are shown in Figs. 2-3 and 2-4 respectively. A total of 131 specimens were tested including 5 additional repeats for cases where end brooming was observed.

Results and Discussions

Effect of stitching on sublaminate buckling strength

It is established by previous studies [22] that compression strength increases with reduction in gage length. In this study the two selected gage lengths (2.9" and 2.4") showed a similar trend. Therefore, the compression strength pertaining to 2.9" gage length was scaled for 2.4" gage length specimens for study of trend analysis only. An example of a scale factor used is as follows:

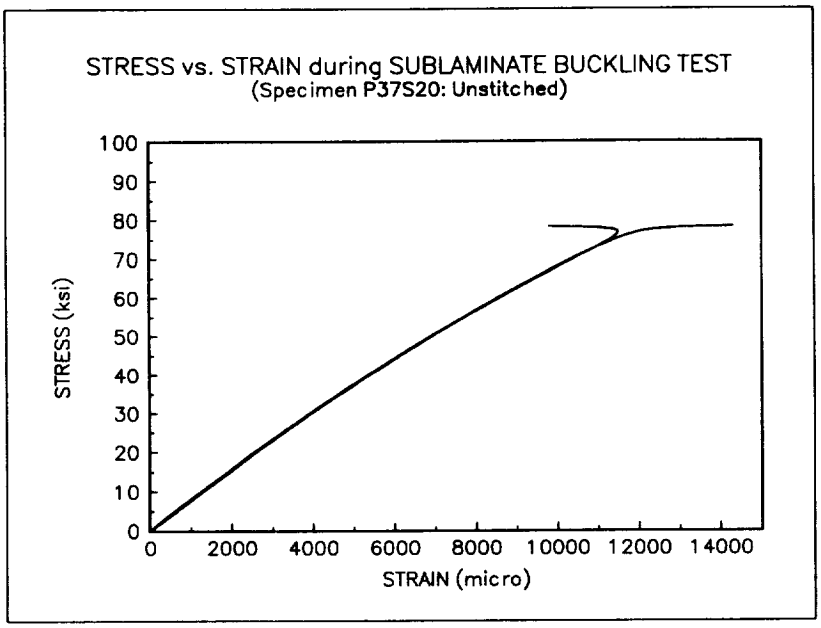

Figure 2-3: A typical stress-strain response for an unstitched laminate.

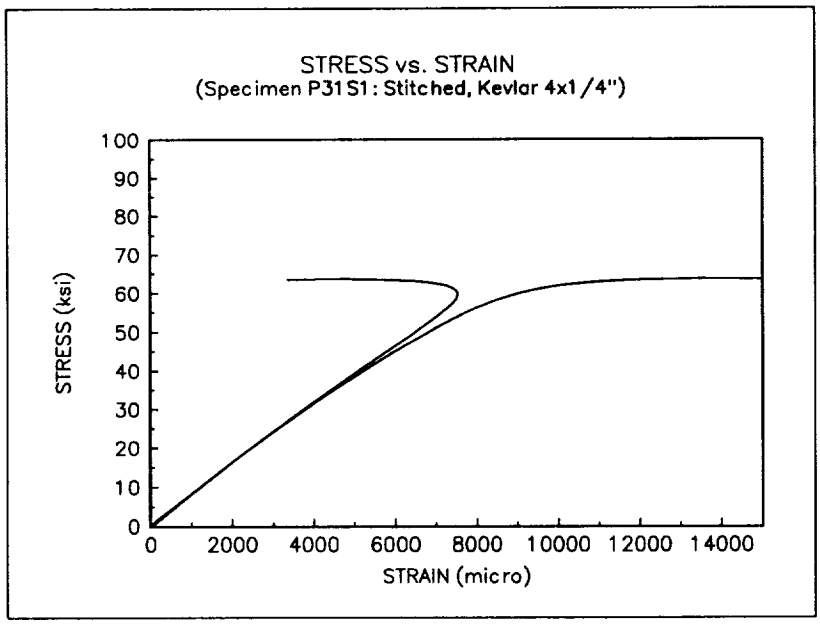

Figure 2-4: A typical stress-strain response for a stitched laminate.

Example to calculate the scale factor to convert 2.9" gage length CAI strength to 2.4" gage length CAI strength for Plate #31:

Plate#31; Stitched: Kevlar 2790 yds/lb., 4×1/4", gage Length = 2.9", no teflon

CAI strength of specimens #P31S1 to #P31S3 (refer Table A-2) = 63.15 ksi

Plate#31; Stitched: Kevlar 2790 yds/lb., 4×1/4", gage Length = 2.4", no teflon

CAI strength of specimens #P31S4 to #P31S6 (refer Table A-2) = 72.88 ksi

therefore,

Scale Factor to normalize CAI strength of 2.9" gage length

to CAI strength of 2.4" gage length = (72.880/63.149) = 1.154

Similarly, scale factors were calculated for other plates. All are listed below:

Plate #31; Stitched: Kevlar 2790, 4×1/4"	=	1.154
Plate #32; Stitched: Kevlar 2790, 8×1/8"	=	1.104
Plate #33; Stitched: Glass 1250, 4×1/4"	=	1.183
Plate #34; Stitched: Glass 1250, 8×1/8"	=	1.119
Plate #35; Stitched: Glass 750, 4×1/4"	=	1.142
Plate #36; Stitched: Glass 750, 8×1/8"	=	1.090
Plate #37; Unstitched	=	1.274

The average values of CAI strength normalized for 2.4" gage length are given in Table 2-1. The variation in CAI strength data did not exceed 5% in 90 specimens out of the total 126 tests and it did not exceed 10% in the remaining specimens which indicates good consistency in test results. CAI strengths of different damage types for the unstitched laminates are plotted in Fig. 2-5. The CAI strength drops significantly with

increasing delaminations for the unstitched laminates. The effect of stitching with different yarns of 4×1/4" stitch density is shown in Fig. 2-6. The effect of increased stitch density 8×1/8" can be observed from Fig. 2-7. It is clear from the CAI strength data and the above mentioned graphs that all three stitch yarns seem to improve the CAI strength to about same extent when their stitch densities are equal. This may be due to the fact that any through-the-thickness stitch yarn with sufficient breaking strength and stiffness is able to restrain buckling of the sublaminates by holding them together. More evidence of this is discussed in the next section on the sublaminate buckling failure mode.

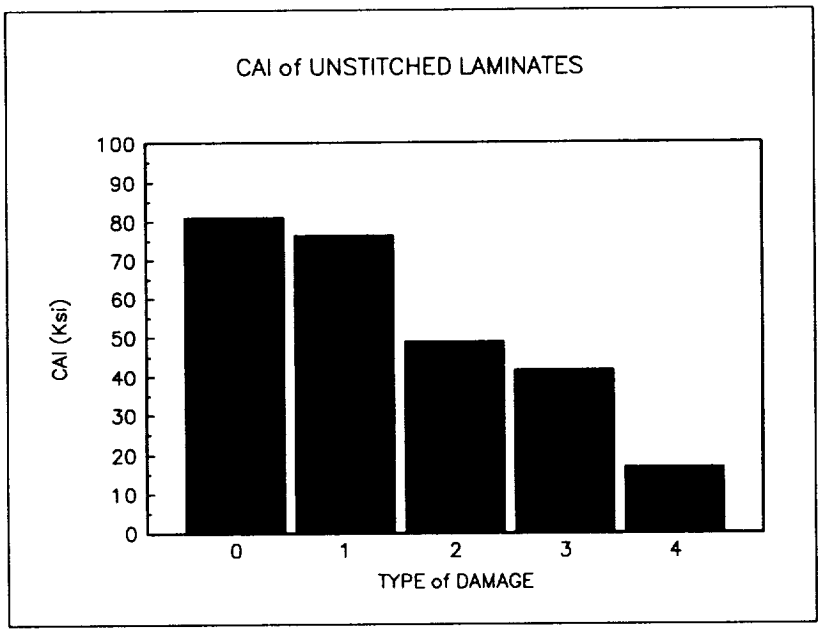

Figure 2-5: Drop of compression strength in unstitched laminates with different types of damages.

Table 2-1: Effect of Stitch Yarn and Stitch Density on CAI strength

Type of Damage†	CAI (ksi) Plate #31, Stitched: Kevlar 2790,4x1/4	CAI (ksi) Plate #32, Stitched: Kevlar 2790,8x1/8	CAI (ksi) Plate #33, Stitched: Glass 1250,4x1/4	CAI (ksi) Plate #34, Stitched: Glass 1250,8x1/8	CAI (ksi) Plate #35, Stitched: Glass 750,4x1/4	CAI (ksi) Plate #36, Stitched: Glass 750, 8x1/8	CAI (ksi) Plate #37, Un-stitched
Zero (No Damage)	72.88	69.24	75.04	69.72	73.53	71.53	80.92
1	71.28	68.79	68.33	60.51	66.58	58.77	76.36
2	54.44	63.96	56.86	69.51	54.68	62.91	48.76
3	43.27	65.11	47.65	62.22	45.71	57.24	41.7
4	33.37	60.04	39.46	69.54	38.82	64.01	16.9

† Damage Type #1 = 3 teflon film inserts, each of 0.5" height running through the entire width of the specimen and located at $[A/A/T/A/A/\underline{T}]_s$ where A = $(45/0/45)_s$ and T is a teflon insert. Thickness of teflon film in all cases was 0.0005".
Damage Type #2 = same as Damage Type #1 but the teflon film inserts are of 1.0" height each.
Damage type #3 = 7 teflon film inserts, each of 0.5" height and located at $[(A/T)_3 /A/\underline{T}]_s$.
Damage Type #4 = same as Damage Type #3 but the teflon film inserts were of 1.0" height each.

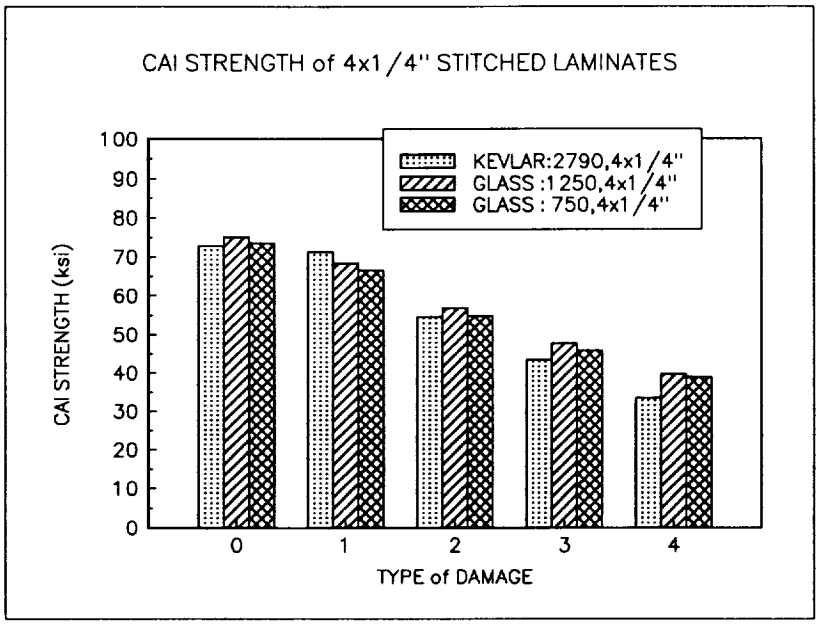

Figure 2-6: Effect of 4×1/4" stitch density yarns on CAI strength

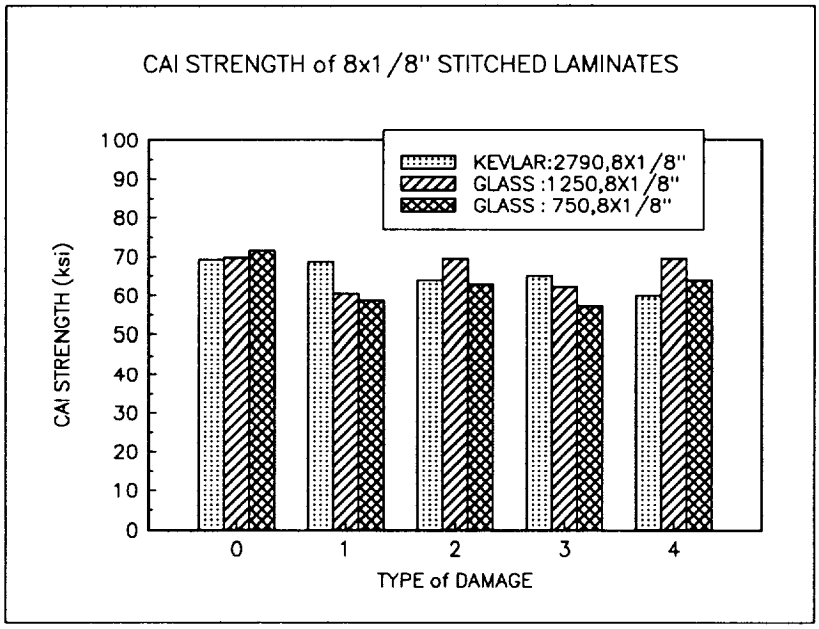

Figure 2-7: Effect of 8×1/8" stitch density yarns on CAI strength

Apparent loss of initial compressive strength . There seems to be a slight loss of initial compressive strength due to stitching in case of undamaged specimens (about 6% for 4×1/4" stitch density and about 12% for 8×1/8" stitch density). This compares well with earlier studies like [16] but we consider this loss as apparent due to the increased thickness of stitched laminates. The nominal increase in thickness of 4×1/4" stitch density laminates was 7% and for the 8×1/8" laminates was about 14%. It is to be noted that the stitch yarns are not in the compressive load bearing direction. The added thickness due to stitch yarn gives an impression as if stitching degrades in-plane compressive properties. Therefore, this loss of initial compressive strength has to be considered with care. The penalty for stitching is the added thickness of the structure and not reduced compressive strength. The apparent initial drop in the compressive strength is plotted for all types of stitch yarns in Fig.2-8.

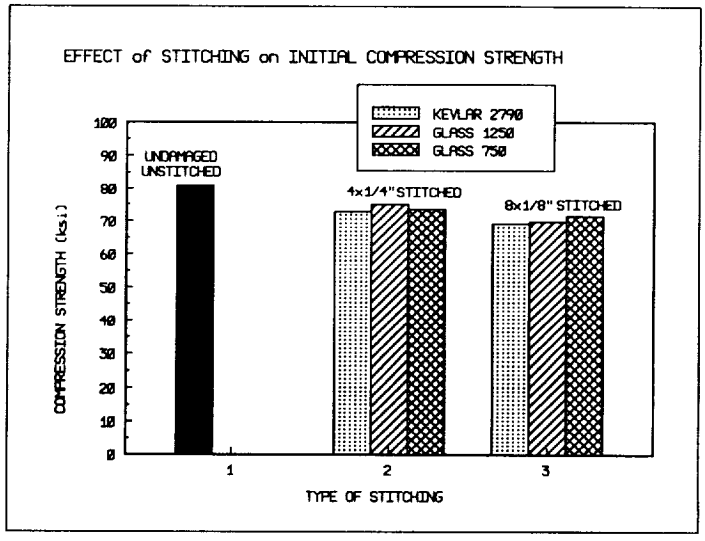

Figure 2-8: Initial compression strength appears to drop by 12% due to stitching.

Effect of stitch density

Apart from the initial apparent loss of the compressive strength, the CAI strength of delaminated stitched laminates showed excellent improvement over the delaminated unstitched laminates. The improvement in the case of the worst delaminated specimens (Damage type #4) with high stitch density (8×1/8") was as much as 400% over the unstitched laminates. To study a comparative trend of the improvement in CAI strength data due to stitch density, the data were curve fitted using a locally weighted linear regression (Axum software) and the curves are plotted in Fig 2-9. Here, it was assumed that the different delaminated states (i.e., Damage types #Zero to 4) simulate impact damage of an increasing order.

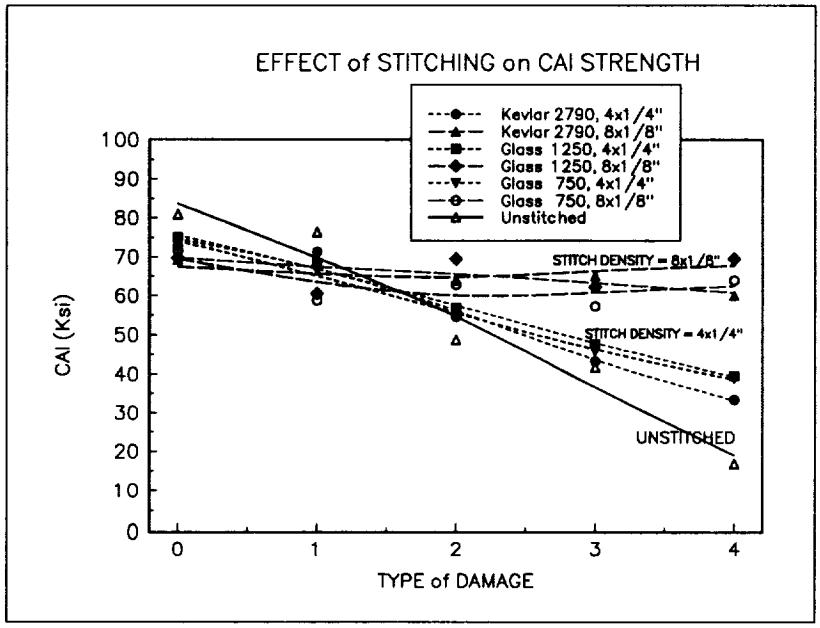

Figure 2-9: A trend of the effect of stitch density on CAI strength

Effect of stitching on failure mode

It was observed that the damaged unstitched laminates tend to fail by buckling of the sublaminates. This could be seen from the white painted side edge surfaces. The painted surface opens up at the teflon inserted interplies and the laminate buckles, but the laminate regains its geometry after the unloading. This failure mode is sketched in Fig. 2-10. However, stitching tends to hold the sublaminates together thus prevent buckling. The stitch yarns will be subjected to tensile loading in the process of trying to restraint sublaminate buckling. Therefore, stitching changes the failure mode from sublaminate buckling to typical small kink zone formation and subsequent fiber fracture. This also explains the impressive gains in strength due to 8×1/8" stitch density as compared to 4×1/4" density. This type of failure is schematically shown in Fig. 2-11. A typical strain gage behavior observed in most of the specimens is shown in Fig. 2-12.

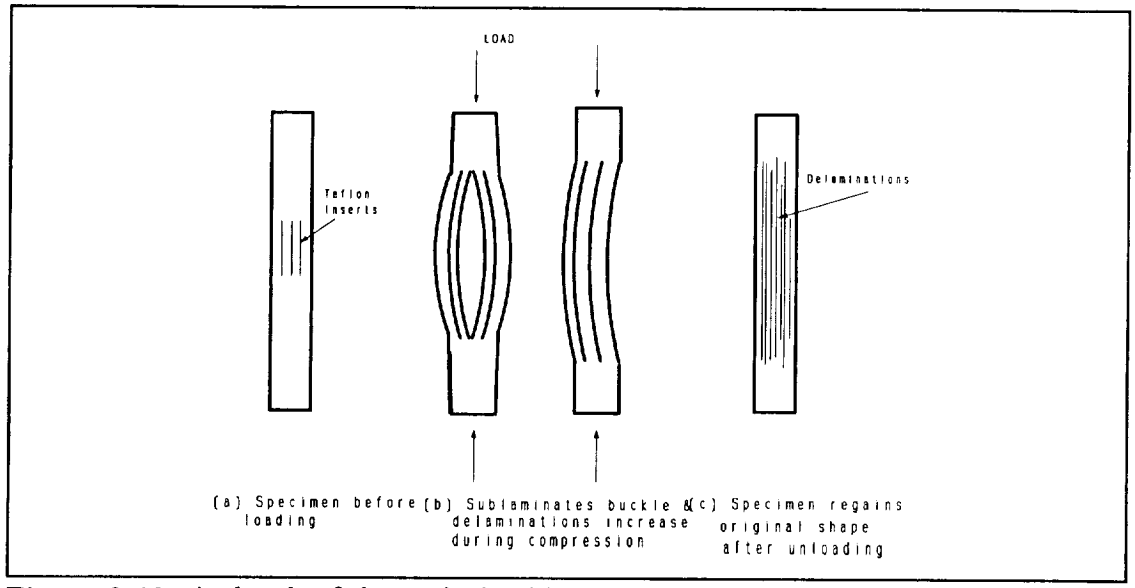

Figure 2-10: A sketch of the typical sublaminate buckling failure mode of delaminated unstitched specimens

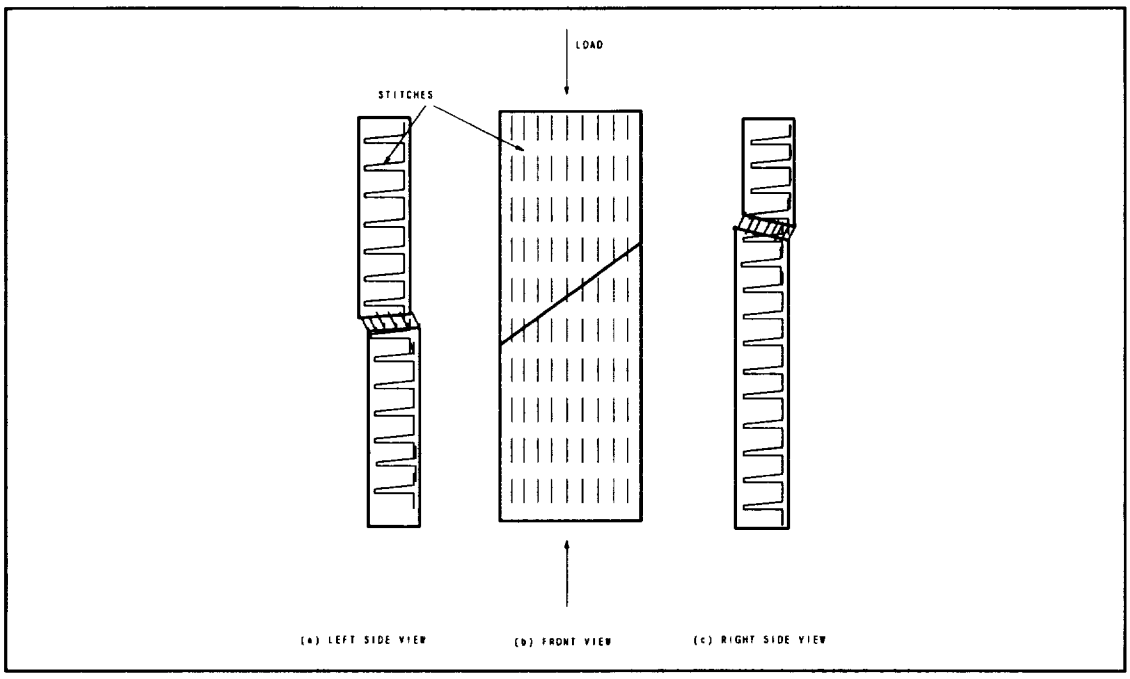

Figure 2-11: A sketch of a typical stitched sublaminate buckling failure mode

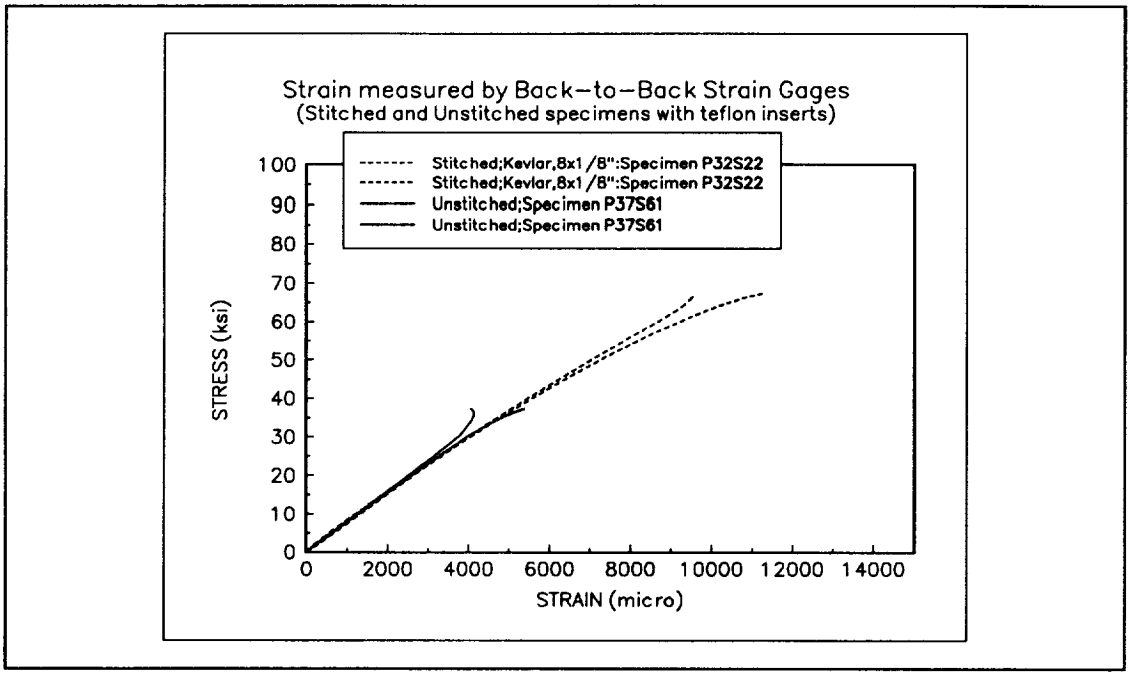

Figure 2-12: A typical strain gage reading curve for a delaminated unstitched and a stitched laminate.

An empirical relation for optimum stitch density

As observed earlier, the effect of different stitch yarns is insignificant if the selected stitch density is equal and the yarn has sufficient breaking strength and stiffness (e.g., Kevlar, Glass, Carbon or equivalent). Therefore, the average strength of the stitched laminates, regardless of the type of stitch yarn used, can be used as an empirical guide for determining optimum stitch density for a desired strength. The overall average strength data of stitched laminates for the worst case scenario (Damage type #4) is shown in Table 2-2.

Table 2-2: Increase in residual compression strength due to stitch density

STITCH DENSITY (Stitches/ in^2)	CAI STRENGTH OF UNDAMAGED LAMINATES (ksi)	CAI STRENGTH OF DAMAGED (TYPE #4) LAMINATES (ksi)	% OF RESIDUAL COMPRESSION STRENGTH
0 (UNSTITCHED)	81	17	21
16 (4x1/4")	73	37	46
64 (8x1/8")	70	65	80

The empirical variation of residual compression strength with stitch density is plotted in Fig. 2-13. As can be inferred from this graph, the strength improves with stitch density and reaches a peak when the stitch density is high. As an example, to ensure a minimum residual compression strength of 60 ksi (i.e., 75% of original compression strength) in a wing box structure of an aircraft using the material system studied in this report, a designer may select a stitch density of about 45 stitches/in^2 from the above

empirical relation. Further improvement of strength for a stitch density of more than 45 stitches/in^2 is insignificant as the curve tends to reach its peak. However, a higher than 45 stitches/in^2 stitch density may be selected if higher impact damage states than the one investigated in this study are considered.

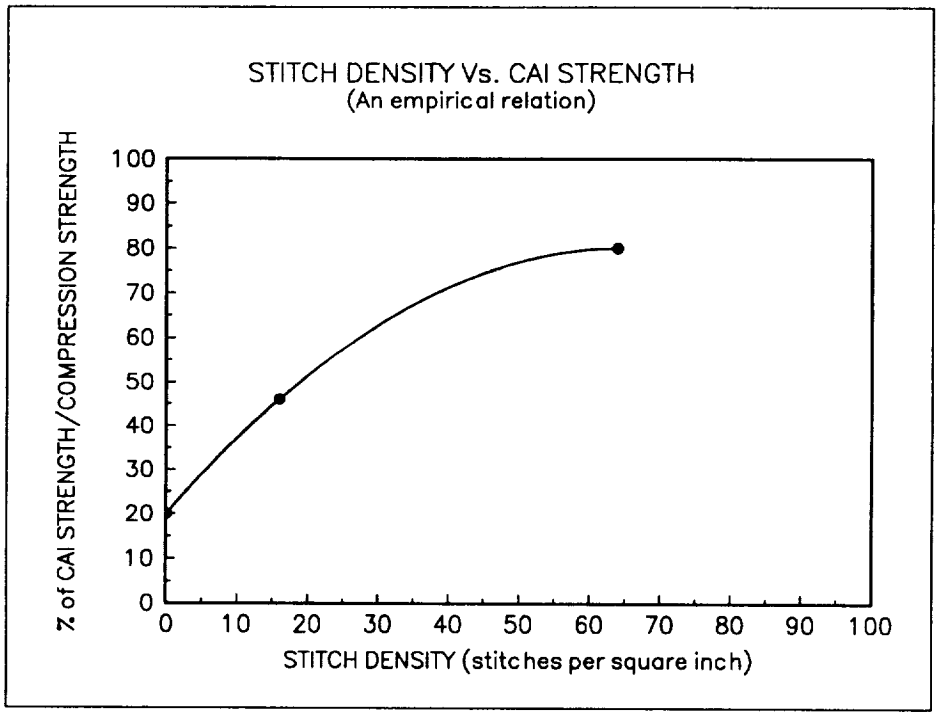

Figure 2-13: An empirical relation between stitch density and CAI strength

CHAPTER 3
MODE I FRACTURE TOUGHNESS TEST

Test Approach

In order to measure Mode I fracture toughness of unstitched and stitched uniweave laminates Double-Cantilever-Beam (DCB) tests were conducted following guidelines by Carlsson [23]. Preliminary tests indicated intermittent and dynamic crack propagation as the stitches break during loading. It is difficult to contain crack propagation between two successive stitches to record the critical load for crack propagation. The crack front moves ahead of unbroken stitches during the loading. Hence, the energy-area approach was chosen to calculate an effective critical strain energy release rate (G_{Ic}) rather than using the load at which crack propagates. It was considered that the approach would give a better average estimate of effective G_{Ic} as the stitched laminates can not be strictly treated in accordance with beam theory formulation due to partially broken stitches remaining in the wake of the crack front. Stitch damage mechanism were studied using Photomicrography and Scanning Electron Microscopy. A more economical and efficient method of installing hinges for preparation of specimens was also explored.

Test Variables and Specimen Preparation

Specimen geometry

Nominal dimensions of a typical specimen cut from the RTMed plate are shown in Fig. 3-1 The side edges of the specimen were painted white with a thin layer of paint to enhance crack detection. A natural starter crack extending up to the first stitch beyond the teflon film was carefully created using a sharp surgical knife. A few initial tests with increased starter crack length of 2" revealed large curvature and deflections of the beam during the DCB test. Therefore, the initial starter crack length was kept nominally at one inch. Special attention was paid to ensure uniform stitch density among a particular set of specimens. The geometry of the specimen meets the design considerations required to keep the test in the linear regime [16].

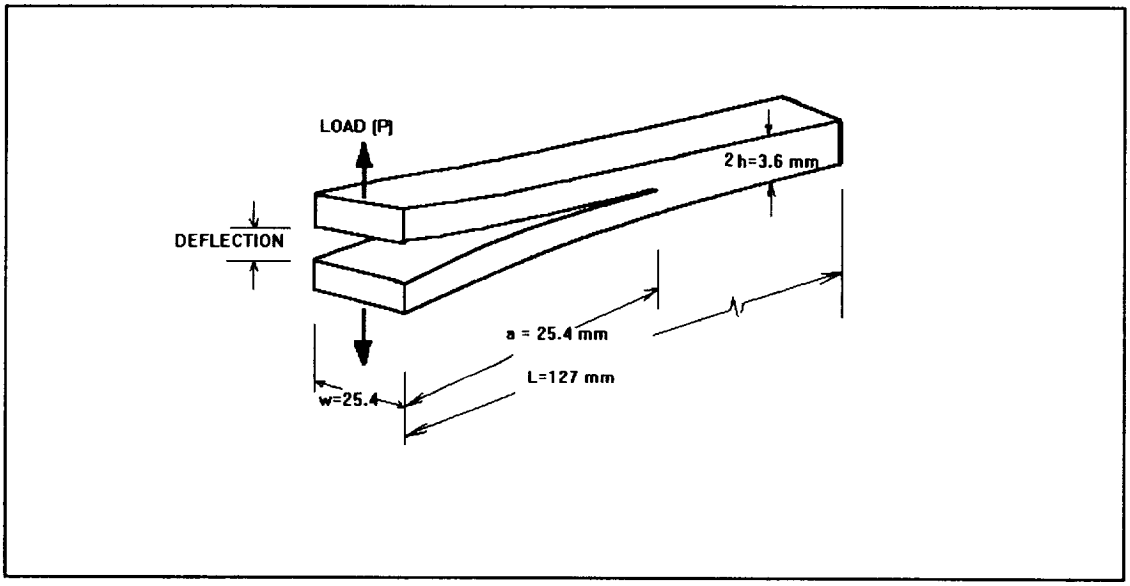

Figure 3-1: A schematic diagram of a DCB specimen cut from the RTMed plates

Hinge installation on unstitched and 4×1/4" stitched specimens

Adhesively bonded and/or mechanically fastened hinges have been tried by researchers in past. Most adhesives used need high temperature curing (250 -350 ^{0} F) to make a strong and noncompliant bond (e.g., 3M AF163-2K-06 or HYSOL 398). These adhesives are expensive. Mechanical means to install hinges cause damage to the specimens, are labor intensive, and use expensive special cutting tools. A survey of various new engineering products revealed that new "Third generation" epoxies [24] may meet the DCB test requirements. One such product DP-460 epoxy was successfully tried out. This adhesive is inexpensive, room temperature curable and easy to use with its manufacturer supplied applicator and mixing nozzles. Surface preparation methods as per standard engineering practices for application of adhesives were followed. Care was taken to align the hinges using a locally fabricated fixture as suggested by Carlsson [23]. Single leaf hinges of 1" length (Fig. 3-2a) were suitable for unstitched laminates and Double leaf hinges of 2" length (Fig. 3-2b) were suitable for all 4×1/4" stitched laminates.

Hinge installation on 8×1/8" stitched specimens

Six different hinges schematically shown in Fig. 3-2a through Fig. 3-2d were evaluated. The difficulties encountered are presented in the chronological order of evolution. The 1" and 2" Single or Double leaf hinges failed due to insufficient adhesive bond area or stress concentration at hinge pivots. Hence, it was decided to integrally machine the hinges out of a solid block of aluminum alloy as shown in Fig. 3-2c. A provision to connect the hoisting clevis through a pin was made. These hinges worked

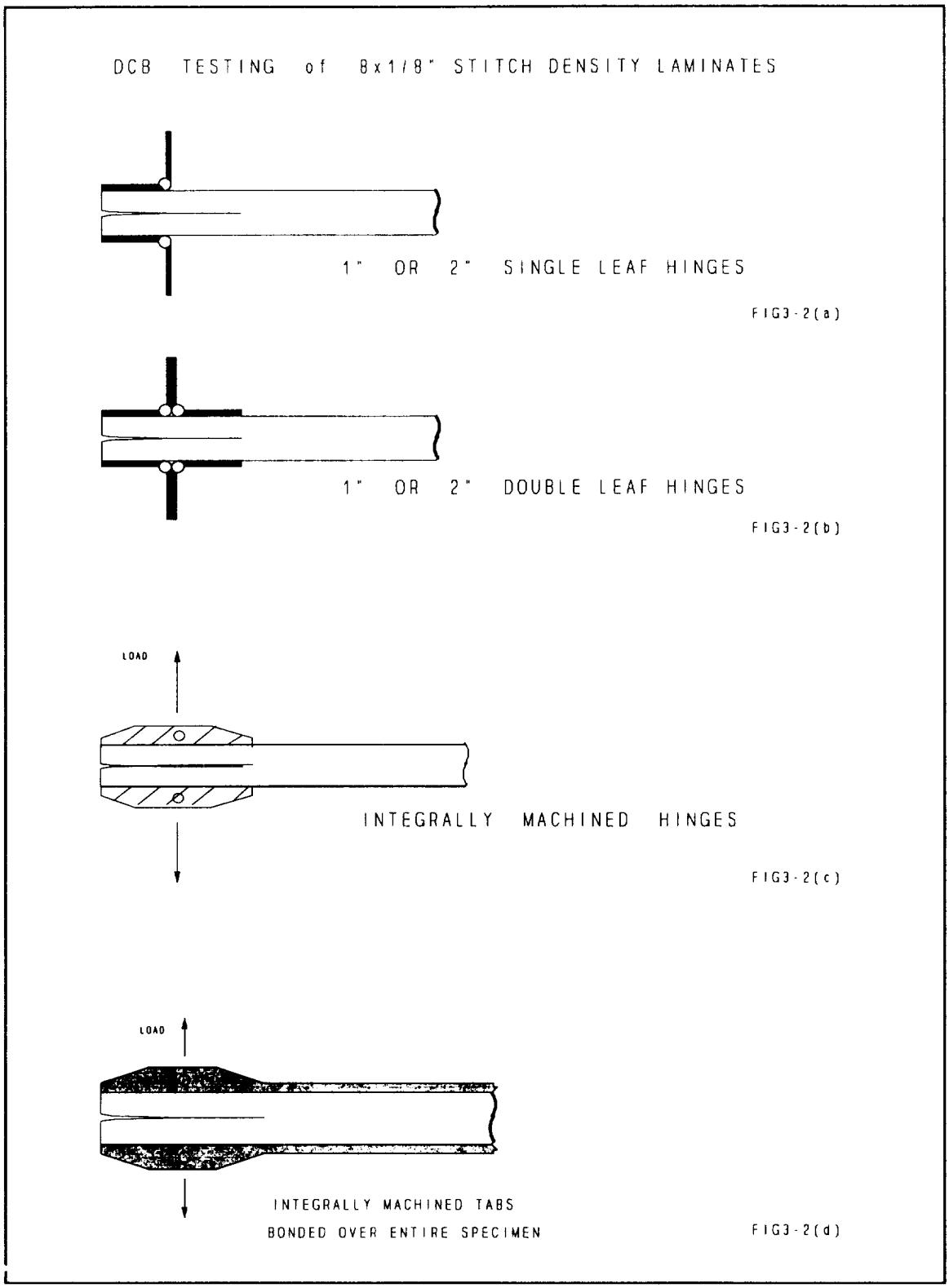

Figure 3-2: Various types of hinges/tabbing methods experimented for 8×1/8" stitched laminates. The hinge shown in Fig. 3-2 (c) did not fail but the specimen failed.

well as far as bond strength was concerned but the fracture toughness of 8×1/8" stitched specimens was found to be so high that the specimen failed in bending about 1/4" away from the initial starter crack front line. In order to strengthen the specimen, new integrally machined tabs of steel as shown in Fig. 3-2d were bonded over the entire surface of the specimen. Guenon [25] has studied Mode I interlaminar fracture toughness of 3-D woven composites using a "tabbed specimen" which is similar to the one in Fig.3-2d. However, it was found that this type of tabbing is not suitable for stitched laminates due to the nature of stitch failure mechanisms as explained in the following section. Therefore, it was not possible to experimentally determine G_{Ic} for 8×1/8" stitched specimens of this study using this type of DCB test. The specimens would have to be made thick enough to prevent bending failure.

Test Procedures and Data Reduction

The DCB tests were conducted in stroke control mode using a 12 kips screw driven Tinius-Olsen machine at the Center for Studies of Advanced Structural Composites, University of Florida. The load and deflection real time signals were acquired using a calibrated load cell and a Linear Variable Differential Transformer (LVDT) output into a Nicolet digital oscilloscope 4094 with XF-44 recorder. The crack propagation was observed using a magnification lens (×5) and crack growth was allowed to increment about 1/2" before commencement of unloading. This 1/2" propagation of the crack invariably extended over about two stitches. Whenever the crack front on both sides of the specimen was observed to be different, an average was taken to get the incremental

crack growth (Δa). As the energy-area approach is being used for calculating G_{Ic}, each crack propagation is equivalent to testing a new specimen with an increased initial crack length. The crack was allowed to propagate for 5-6 increments in each specimen. The critical strain energy release rate is given by:

$$G_{Ic} = \frac{\Delta W}{\Delta A} \tag{3-1}$$

where ΔW is the work done during the incremental crack propagation and ΔA is the new incremental crack surface area created. The work done was reduced from the area under the P-δ curve using a spreadsheet software (Quattro Pro), and the crack surface area was obtained by multiplying the width of the specimen by the incremental crack propagation measured on the side edge of the specimen. It was assumed that the crack front follows a near straight line path and propagates in a self-similar manner. The results of the calculation for the critical strain energy release rate are given in Table B-1 through Table B-7 in Appendix-B. A set of representative P-δ curves for an unstitched and a stitched laminate are shown in Fig. 3-3 and Fig. 3-4 respectively. The roughness of acquired load and displacement signals is attributable to noise in the machine circuitry.

Results and Discussions

G_{Ic} of unstitched and the 4×1/4" stitched laminates

The reduced data shows about 7% variation for the unstitched and up to about 25% in the 4×1/4" stitched laminates in the obtained G_{Ic} values. The Mode I critical strain energy release rates for various laminates are compared in Fig. 3-5.

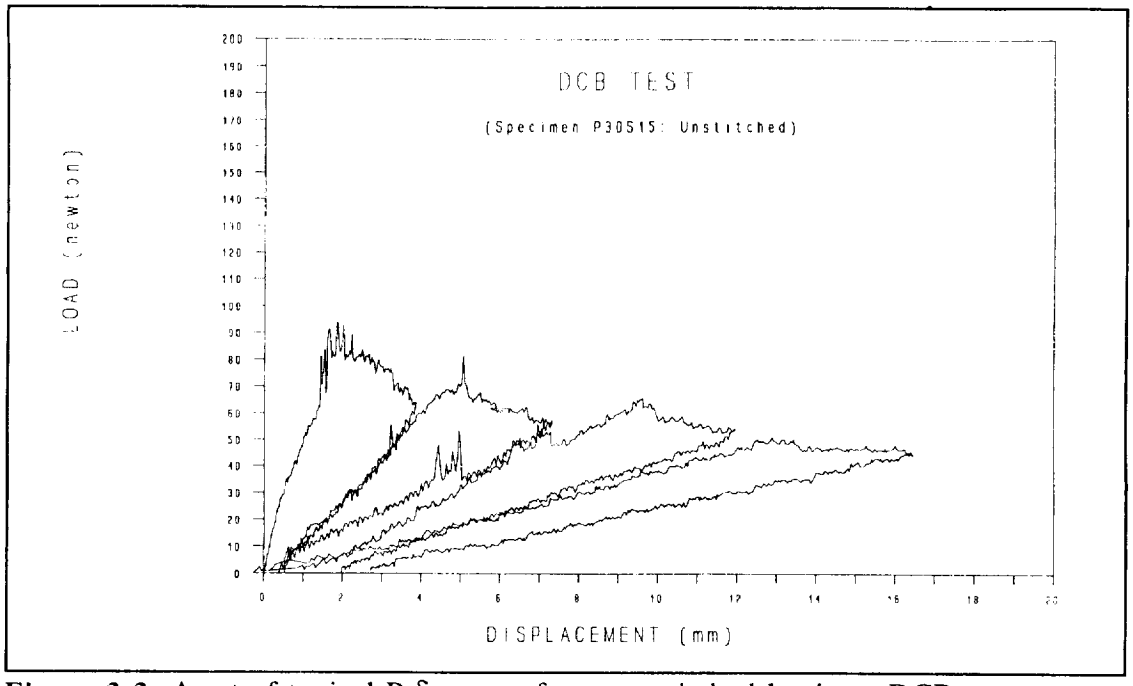

Figure 3-3: A set of typical P-δ curves for an unstitched laminate DCB test

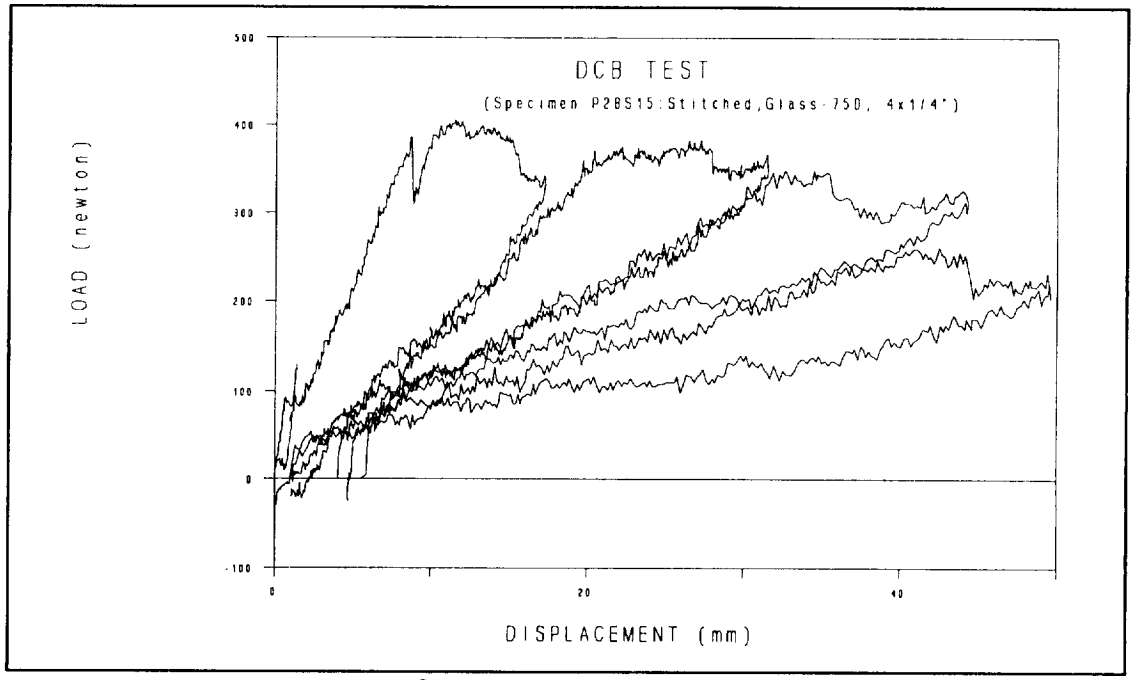

Figure 3-4: A set of typical P-δ curves for a stitched laminate DCB test

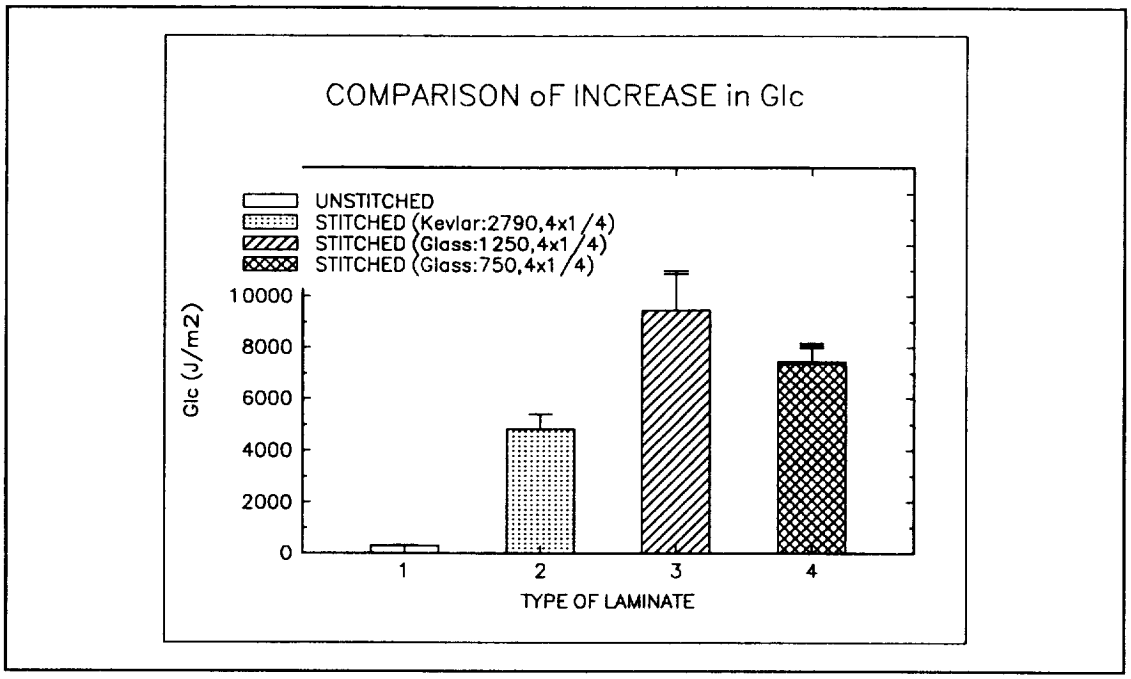

Figure 3-5: Stitching increases Mode I fracture toughness by 15-30 times for 4×1/4" stitch density laminates.

Stitching significantly increases the Mode I fracture toughness. The average increase in Mode I fracture toughness due to stitching is at least an order higher than the unstitched laminates. The use of Kevlar-2790 as stitching yarn improved the fracture toughness by about 15 times, the Glass-1250 improved it by about 30 times, and the Glass-750 increased the toughness by about 21 times. The G_{Ic} value for the unstitched laminates was 302.6 J/m^2. The variation in G_{Ic} with crack length is shown in Figs. 3-6 through 3-8 for Kevlar-2790, Glass-1250 and Glass-750 stitched specimens respectively. The values of all the specimens were curve fitted using a polynomial curve fit. It appears that, except for the first one or two crack increments, the energy required to propagate the crack remains constant with increasing crack length. The first initiation of crack

propagation seems to occur at lower energy requirements. This could be due to manufacturing flaws such as the first stitch line not being perfectly straight. Subsequently, the critical energy release rate appears to stabilize as the crack starts propagating in a self similar manner. The first low value of G_{Ic} introduces a variation of up to 25% in the data for the stitched laminates. Overall, the variation in the G_{Ic} does not seem to be significant as the crack grows. The fracture toughness reaches a fairly steady value soon after the onset of crack propagation. This also brings out the importance of ensuring that the first stitch line is straight.

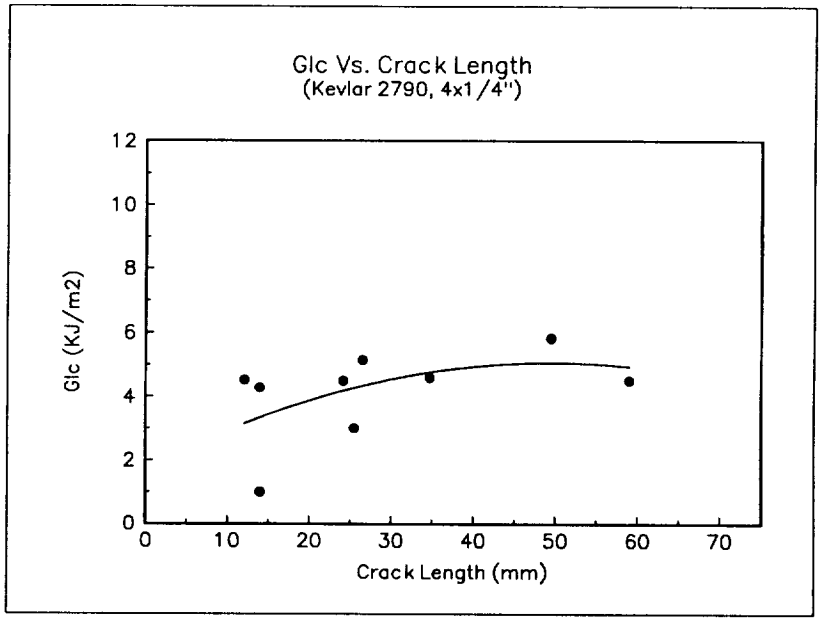

Figure 3-6: G_{Ic} vs. Crack length for Kevlar-2790, 4x1/4" stitched laminate

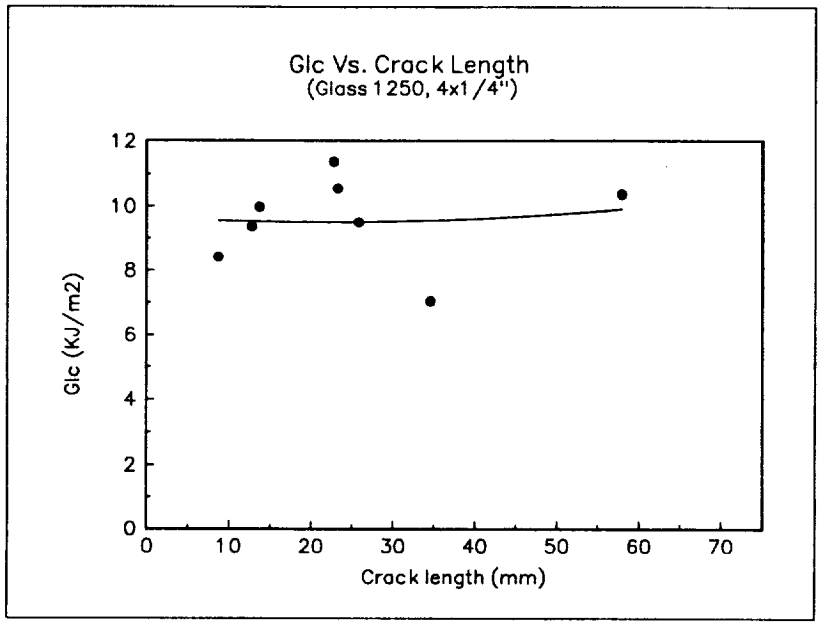

Figure 3-7: G_{Ic} vs. Crack length for Glass-1250, 4×1/4" stitched laminates

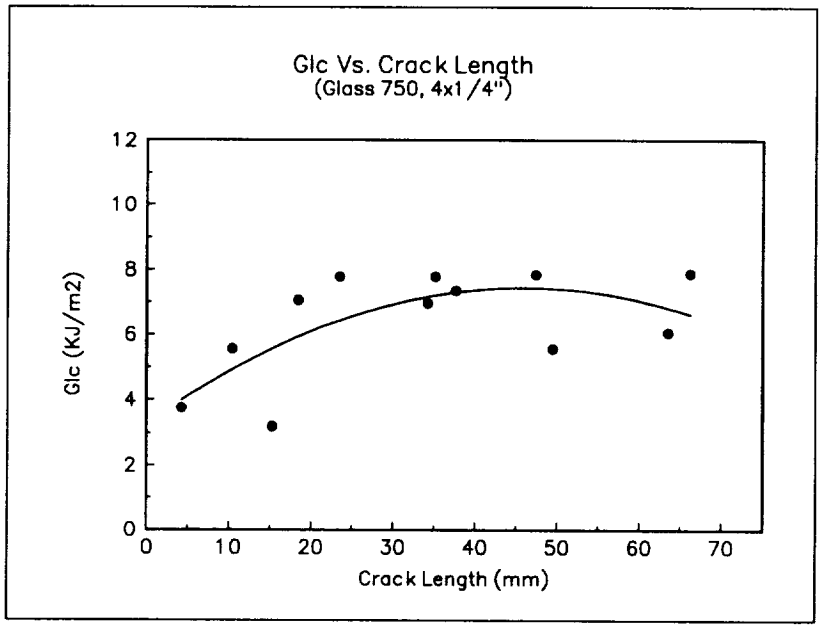

Figure 3-8: G_{Ic} vs. Crack length for Glass-750, 4×1/4" stitched laminates

Stitch Failure Mechanism and Crack Propagation

The crack propagation for the unstitched laminates was gradual and steady, while the crack propagation for the stitched followed an intermittent and dynamic pattern. A step-by-step scenario of crack propagation and stitch breaking is described in Figs. 3-9a through 3-9e for a complete DCB test. The sequence and pattern of this mechanism was observed to be same for all three types of stitching yarns. However, the precise location of stitch failure varied in the case of Glass-750 as explained later in this section.

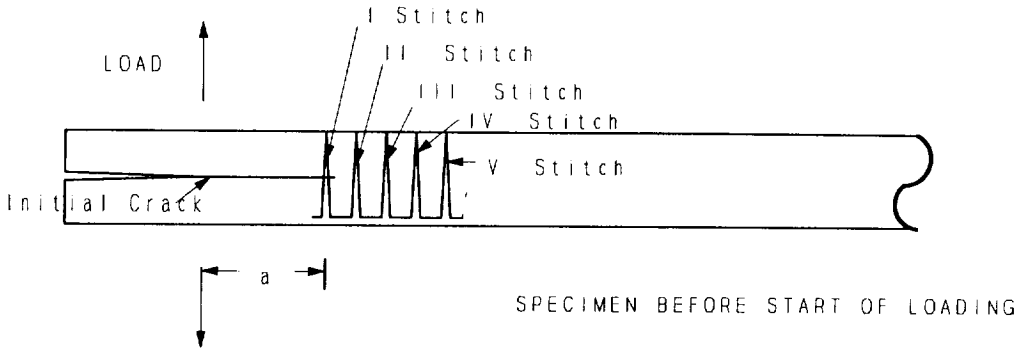

Figure 3-9 (a): The specimen before loading in the DCB test. The starter crack length is close to the first stitch line. Status of the first five stitches is shown.

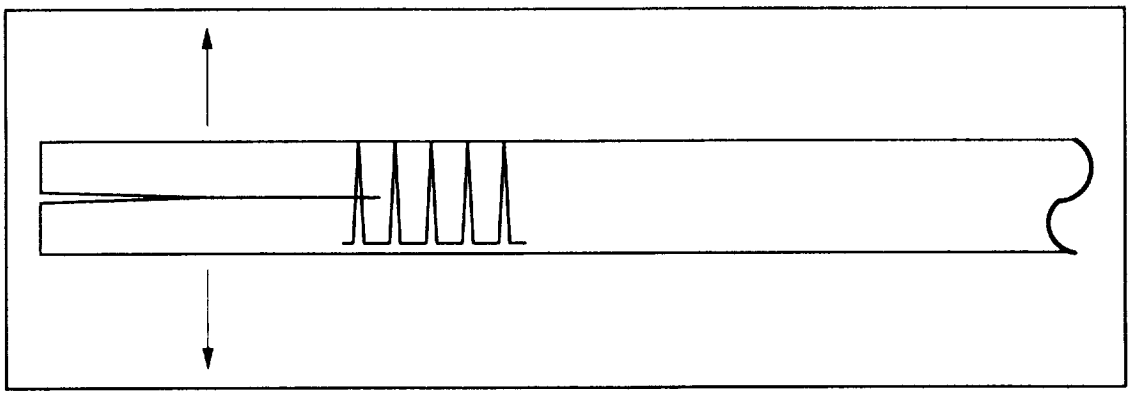

Figure 3-9 (b): Load and deflection start to rise on the Nicolet oscilloscope screen. Both increase linearly. Crack starts to slightly propagate (not more than 1/4", close to second stitch) without any perceptible drop in load.

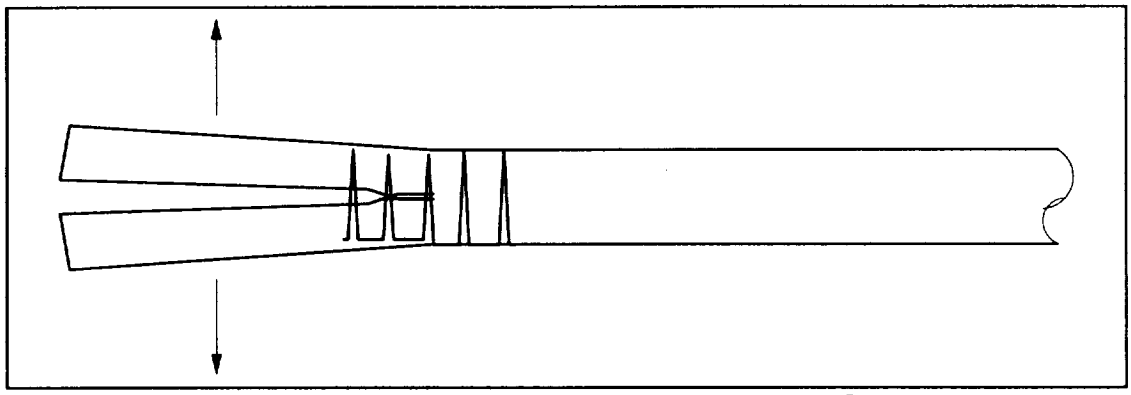

Figure 3-9 (c): For some time no further crack propagation. P-δ continue to rise. Then, cracking sounds are heard, crack extends to third stitch, first debonded stitch can be seen, load drop observed. Second appears bonded.

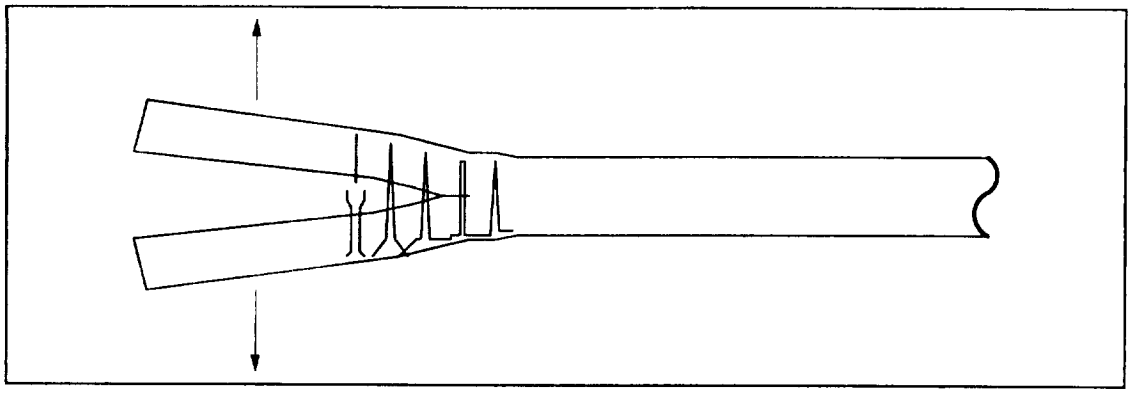

Figure 3-9(d): A little more loading breaks the first stitch. No perceptible load drop is observed at this point. Crack propagates up to the 4th stitch. Second partially debonded stitch can be seen. Third appears bonded.

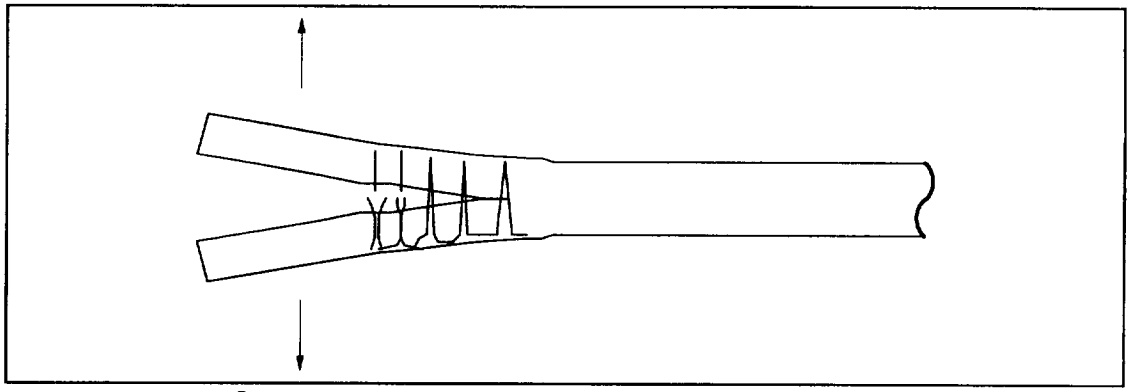

Figure 3-9(e): P-δ continue to rise. After some time crackling sounds heard again. Crack extends to fifth stitch. Second stitch fails completely. Third partially debonded can be seen. Fourth appears bonded.

A photograph of a crack surface with bobbin yarn failure close to the stitch lock position is shown in Fig.3-10. This pattern was observed for Kevlar-2790 stitched laminates. The nature and location of Glass-1250 stitch yarn failure was strikingly similar to that of the Kevlar. It appears that once the bobbin yarn has debonded/sheared from the matrix, the stitch lock provides the necessary stress concentration for the yarns to fail at that location. Glass-750 yarns failed in the same sequence but showed different damage. In this case, the bobbin yarns after getting debonded from the matrix, did not fail by splitting at the stitch lock, instead they broke the needle yarn, thereby creating a free surface on top (i.e., a hole on top surface of the laminate). It is to be noted that the Glass-750 yarns have a higher strength than the Kevlar or Glass-1250. It may be interesting to see the effect of variation of needle yarn denier on the fracture toughness. This variation was not studied in this program. The failure of the stitch yarn (bobbin or needle) always at the stitch lock position brings out the critical importance of this position to fracture toughness. In this context, the need to incorporate a suitable tension setting/sensing mechanism in the sewing machines which will not allow inadvertent small changes in the position of the stitch lock during stitching process becomes important. Further, it is recalled that the creation of the holes in the top surface is also the cause for unsuitability of the integrally machined tabs shown in Fig. 3-2d. Despite the tab being bonded to the entire surface of the specimen, the adhesive bond fails due to a number of holes created on the specimen surface. A photograph of the intact Glass-750 bobbin yarn and a photomicrograph of the top surface of the laminate showing a hole caused by the failure of needle yarn are shown in Figs. 3-11 and 3-12 respectively.

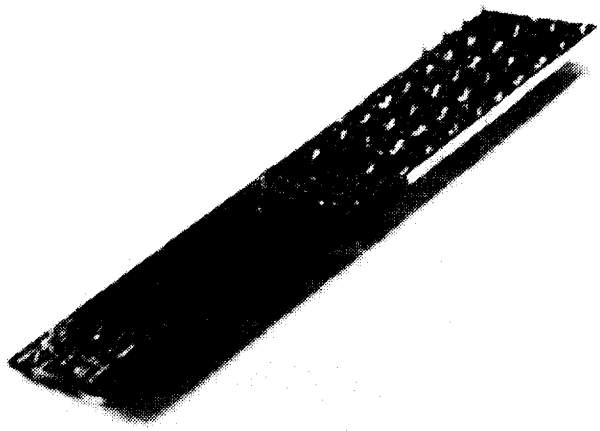

Fig. 3-10: A photograph of failed Kevlar -2790 bobbin yarns at needle yarn interlock

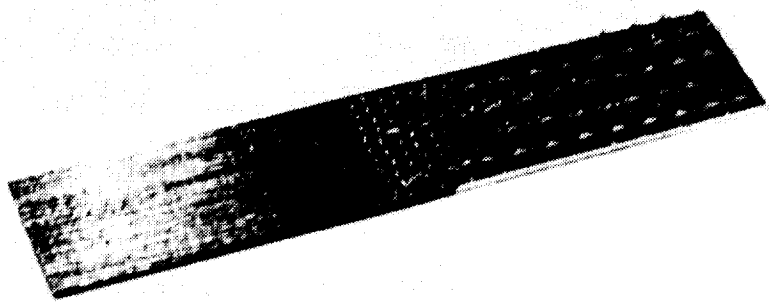

Fig. 3-11: A photograph of failed Glass-750 bobbin yarn crack surface

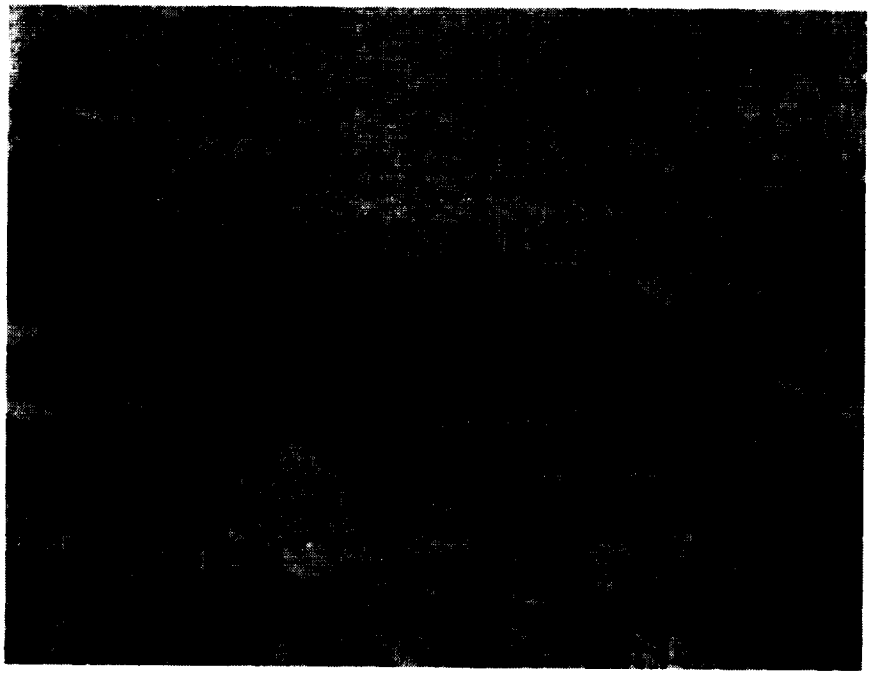

Fig. 3-12: A photograph of a hole created on the top surface by the Glass-750 bobbin yarn breaking the needle yarn

Compressive Load Observed during Unloading in DCB Tests

During unloading of the specimen the top sublaminate starts bearing against the protruding broken stitch stems. Thus the specimen exerted a slight compressive load near the end of the loading curve. This observation is sketched in Fig.3-13 and can also be noted in the typical P-δ curve of a stitched laminate (Fig.3-4). The work done to overcome this resisting force is not significant and does not qualitatively change the results obtained using the area of the P-δ curve. The opened crack surfaces do not fully close after the unloading due to this phenomenon in the stitched laminates. This phenomenon was observed during the initial two or three crack increments and diminishes with increasing crack length due to increased length of cracked beam. This type of unloading curve is peculiar to stitched laminates only and is not observed in the unstitched laminates.

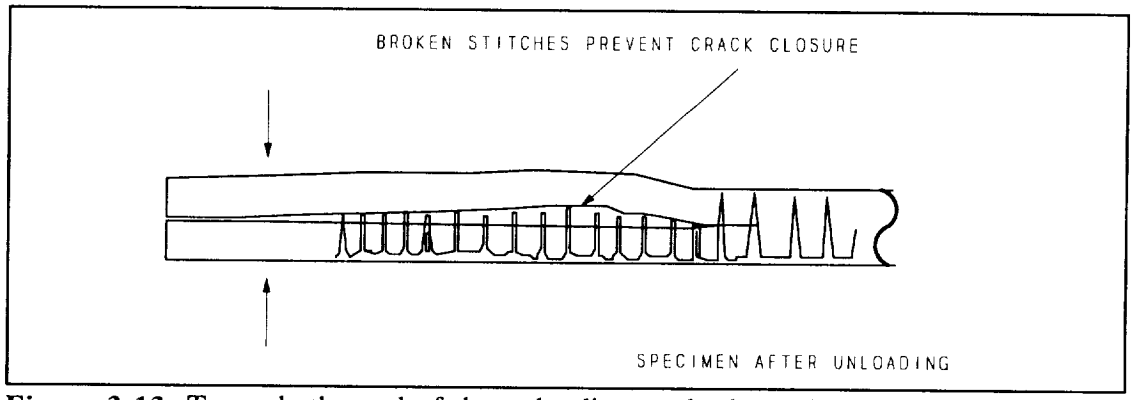

Figure 3-13: Towards the end of the unloading cycle the stubs of the broken bobbin yarn prevent the crack from closing completely. This tends to exert a small compressive force as seen in a typical P-δ curve.

Matrix Deformation and Stitch Surface Morphology

In order to gain insight into debonding, stitch failure and the role of stitch-matrix interaction during the crack opening phase, Scanning Electron Microscopy was conducted on the top surface of a failed stitch and the adjoining matrix area. A stitch that was not compressed during the unloading phase of the test was selected for this study. Some of these photographs are shown in the Figs. 3-14 through 3-17. These studies indicate that the stitch yarn movement is resisted by the matrix surrounding it. Though the stitch yarn in a DCB test is assumed to fail in tension, it does deform the adjoining matrix as the yarn tends to bend when the crack openings grow. The resistance offered by the matrix adds to the toughness brought about by the yarn tensile strength. The texture of the plastically deformed matrix appears to be like that of "ploughing" of earth. The matrix appears "ploughed" by the stitch as seen in the Fig. 3-15.

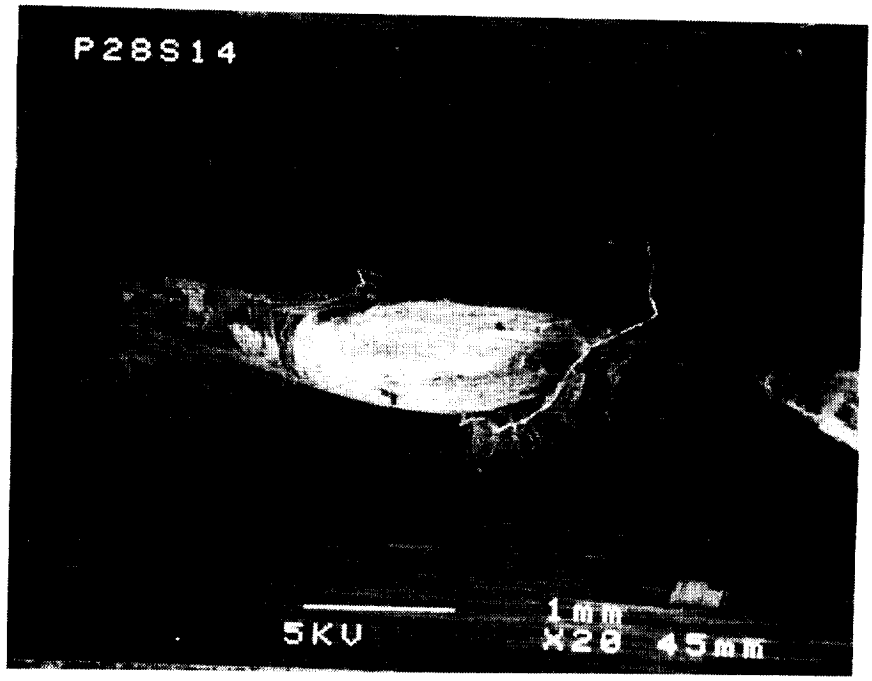

Fig. 3-14: Glass-750 stitch yarn top surface after failure

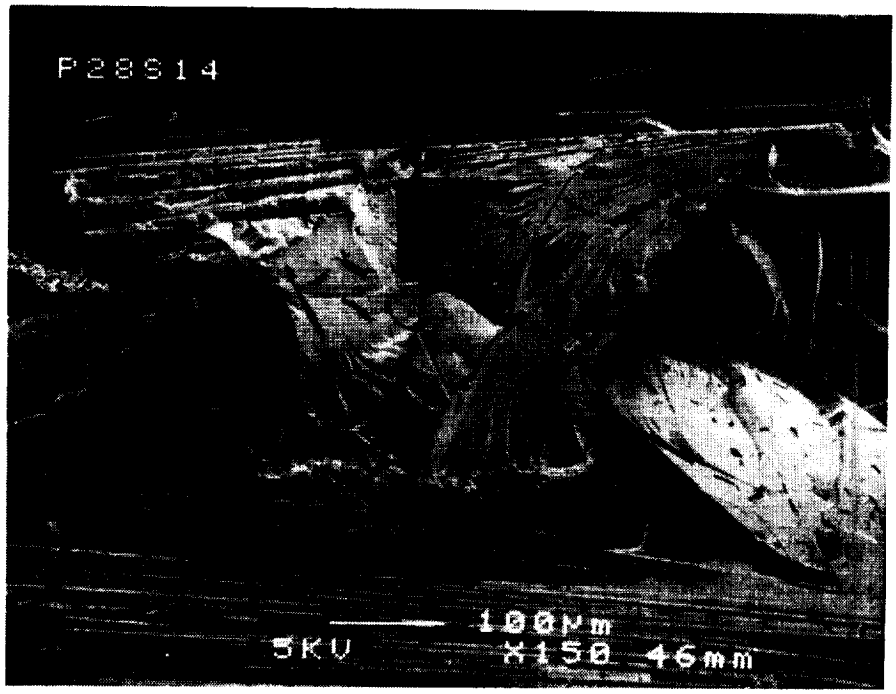

Figure 3-15: Matrix in the adjoining area of the Glass -750 stitch appears "ploughed"

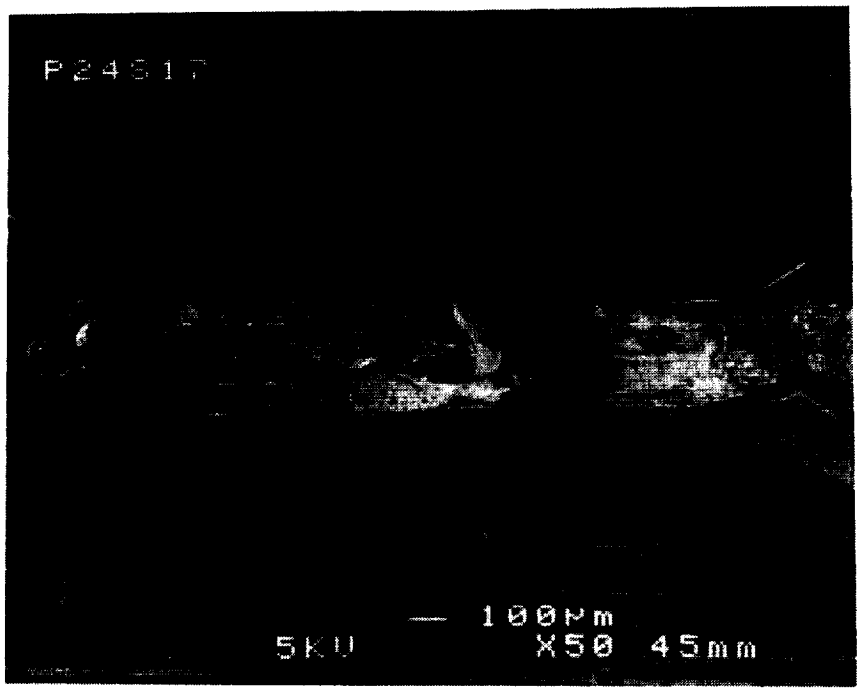

Figure 3-16: Kevlar-2790 stitch yarn split at the needle yarn interlock

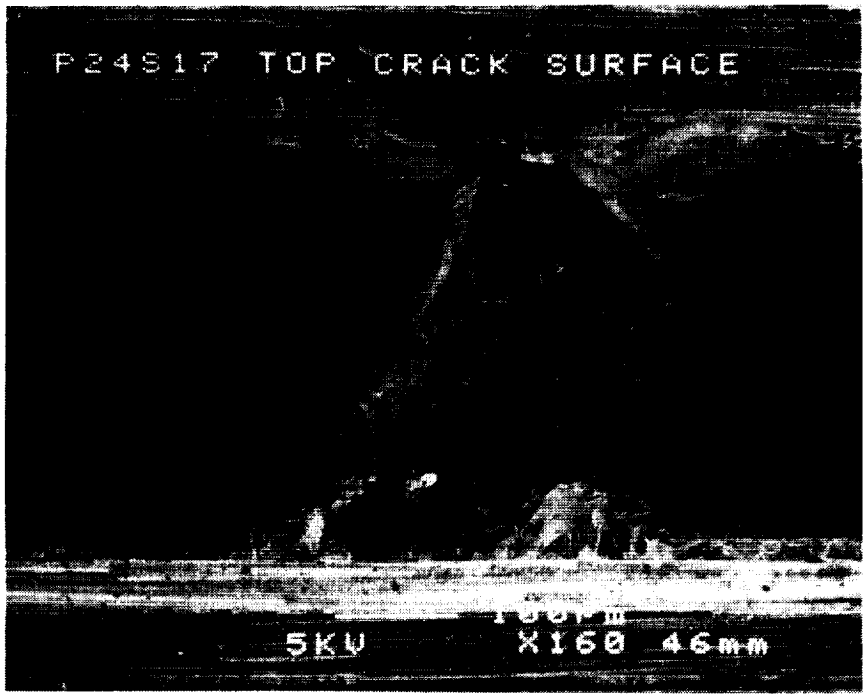

Figure 3-17: Top crack surface of the failed Kevlar-2790 stitch shown in Fig.3-16

CHAPTER 4
MODE II FRACTURE TOUGHNESS TEST

Test Approach and Test Variables

End-Notched-Flexure (ENF) tests were conducted to measure Mode II fracture toughness of the uniweave laminates following guidelines by Carlsson [23]. The behavior of crack propagation in the unstitched and the stitched laminates was studied. Limitations of calculating critical strain energy release rate (G_{IIc}) of stitched composites using existing standard beam theory formulation were studied. New methods to determine the G_{IIc} for stitched composites have been explored. Photomicrography, X-Radiography and Ultrasonic C-Scanning were used to identify the extent of crack propagation. The contribution of the stitching yarn on the effective G_{IIc} values has been investigated. The effects of crack surface friction and roller pin contact friction were studied. The effects of the following variables were investigated: starter crack length (a_0), length of specimen ($2L$), type of stitching yarn and stitch density, frictional effects and unstitched length (defined as the distance between the starter crack and the first stitch). A schematic of the loading conditions and the specimen geometry are shown in Fig. 4-1. The specimens were machined from the same plates as those for the DCB testing. A test matrix is shown in Table 4-1.

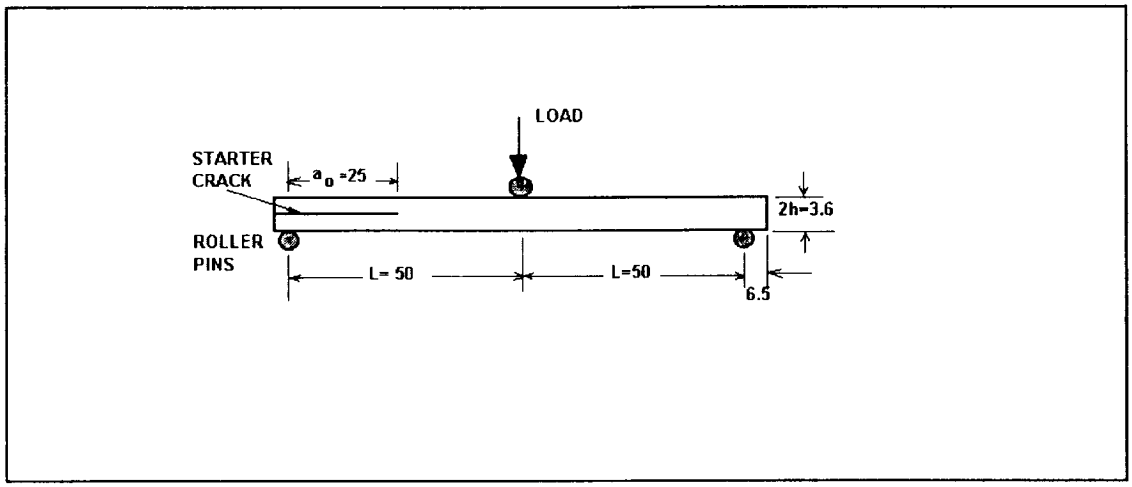

Figure 4-1: A schematic diagram of an ENF specimen. All dimensions are in mm.

Table 4-1: ENF Test matrix

UNSTITCHED LAMINATES			
CRACK LENGTH (a_0)	(L)	LUBRICATION	# OF SPECIMENS
1.0"	2.0"	No	9
1.5"	2.5"	Yes	3
2.0"	3.0"	No	3

STITCHED LAMINATES (L=2.0" & CRACK LENGTH =1.0")			
STITCH YARN	DENIER	STITCH DENSITY	# OF SPECIMENS
Kevlar-2790	1600	4×1/4"	7
Kevlar-2790	1600	8×1/8"	7
Glass-1250	3570	4×1/4"	6
Glass-1250	3570	8×1/8"	6
Glass-750	5952	4×1/4"	6
Glass-750	5952	8×1/8"	6

Test Procedures and Data Reduction

The testing was conducted in stroke control mode using the 12 kips screw driven Tinius-Olsen testing machine. The load and displacement were measured by acquiring the load cell and LVDT signal into the Nicolet digital oscilloscope. The loading rate was 0.02 inch per minute. Crack propagation was observed with the help of a magnifying lens (×5) during the test. Unlike the DCB testing, a thin layer of white paint did not help in the detection of crack propagation during ENF tests. Therefore, it was subsequently not used. First, a set of 6 specimens each of unstitched and stitched (Kevlar-2790, 4×1/4") laminates were loaded and unloaded to increasing peak loads to understand the load-displacement pattern. During these tests, the crack front extended incrementally as the load increased. These specimens were subsequently used to investigate crack propagation and stitch failure mechanisms using Photomicrography and Ultrasonic C-Scanning. Having established a scheme, the remaining sets of 6 specimens each were loaded up to a point where the crack front approximately extended up to about the center line. A P-δ curve for each test was plotted. A representative load-displacement curve for an unstitched and a stitched laminate is shown in Fig. 4-2. For the unstitched laminates, the critical load (P_c) to initiate crack propagation was noted, using the compliance (C) from the P-δ curve and other dimensions of the specimen, the critical strain energy release rate was calculated using existing elastic beam theory formula as described in the following section. A typical P-δ curve for intermediate stages of crack propagation for a stitched laminate is also shown at Fig. 4-3.

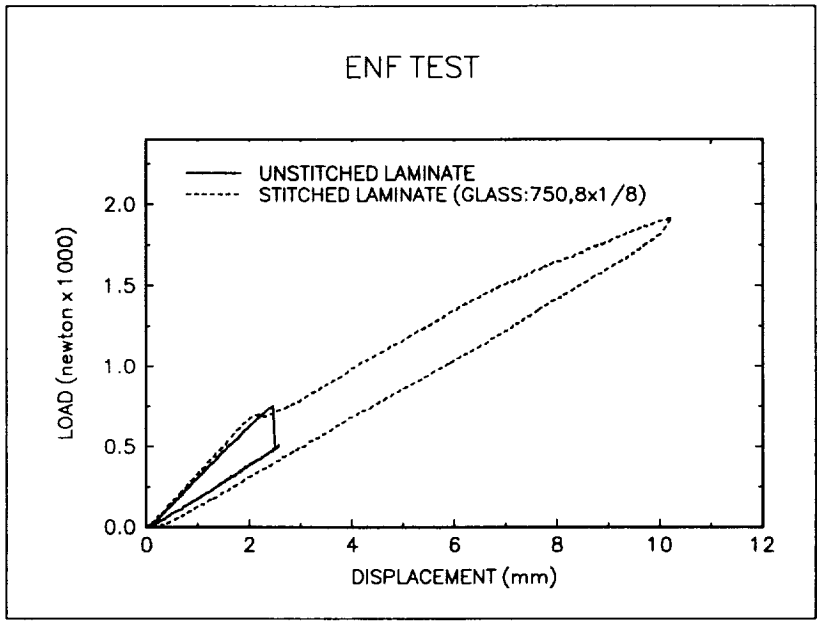

Figure 4-2: A typical P-δ curve for an unstitched and stitched laminate ENF test

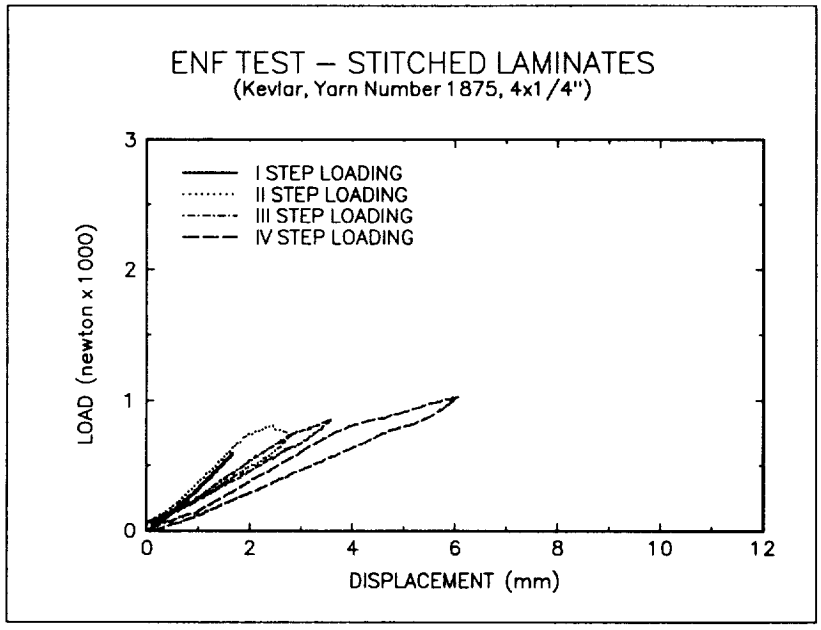

Figure 4-3: A typical set of P-δ curves for intermediate steps of crack propagation

Methods to Determine Effective G_{IIc} of Stitched Laminates

Existing method using beam theory formula and its applicability to stitched laminates

The existing literature uses the well known formula to calculate the critical strain energy release rate[16,23]for a conventional unstitched laminate:

$$G_{IIc}=\frac{9P^2Ca^2}{2w(2L^3+2a^3)} \qquad (4\text{-}1)$$

where, w is the width of the specimen and P is the critical load at the time of crack propagation. The average value for the unstitched laminates obtained by this method was 670.72 J/m^2. Energy-area approach similar to the one used for calculation of G_{Ic} was also used to compare the G_{IIc} values obtained from the formula. An average G_{IIc} of 672.77 J/m^2 was obtained indicating excellent correlation between the two approaches.

While the crack propagation in an unstitched laminate is unsteady as is indicated by the sudden drop in load on the P-δ curve, the crack propagation in the stitched specimens was observed to be steady. The P-δ curves for all the stitched laminates were observed to follow the same nonlinear pattern during the loading. There is no sudden drop in load as the crack starts propagating. Compliance of the specimen gradually changes as the crack propagates. Therefore, the use of beam theory formula using nonlinear P_c and linear C as suggested by Ogo [16] will not give a correct estimate of G_{IIc} in the case of stitched laminates. Two new methods to calculate G_{IIc} for the stitched

laminates are presented in the following section. Preliminary photomicrographic studies of tested stitched specimens suggest that the crack length can not be measured accurately from the visual inspection of the side edge. X-Radiography of the crack surface was tried as discussed later. Then, C-Scans were taken and it was found that actual crack propagation was much more than visually observed. Hence, the values of crack propagation measured by C-Scans were used in computations for the first of the two new methods presented.

New methods to determine G_{IIc} of stitched laminates

(1) Area method using C-Scan

(2) Equivalent area method using compliance of unloading curve

Area method using C-Scan

STEPS:

- Ensure starter crack at first stitch line
- Ensure crack propagates to at least few stitches during test
- Calculate work done (ΔW) from P-δ curve
- Find area of crack surface (ΔA) using C-scan
- $G_{IIc} = (\Delta W)/(\Delta A)$

Equivalent area method using compliance of unloading curve

STEPS:

- Calculate EI from linear compliance (C) of the loading curve
- Calculate compliance of unloading curve (C') at 500 N line (i.e., a

20% less load than the P_c of linear loading curve)

- Calculate effective crack length (a_{eff}) using C' and the following formulae:

For $a < L$

$$C' = \frac{(2L^3 + 3a_{eff}^3)}{96EI} \qquad (4\text{-}2)$$

For $a > L$

$$C' = \frac{-(2L - a_{eff})^3}{32EI} + \frac{L^3}{12EI} \qquad (4\text{-}3)$$

- Select appropriate a_{eff} out of the two calculated above
- Calculate crack surface area (ΔA) using the selected a_{eff}
- $G_{IIc} = (\Delta W)/(\Delta A)$

Results and Discussions

Effect of different stitch yarns and stitch density on G_{IIc}

The G_{IIc} values using all three methods described above (i.e., Beam theory formula, Area method using C-Scan and the Equivalent area method using compliance of the unloading curve) were calculated and are tabulated in Tables C-1, C-2 and C-3 respectively in Appendix-C. A bar chart of the average values of the data is given in Fig. 4-4 showing the comparison of G_{IIc} values using beam theory formula and the two new methods presented above. It is recalled that the crack had propagated up to about

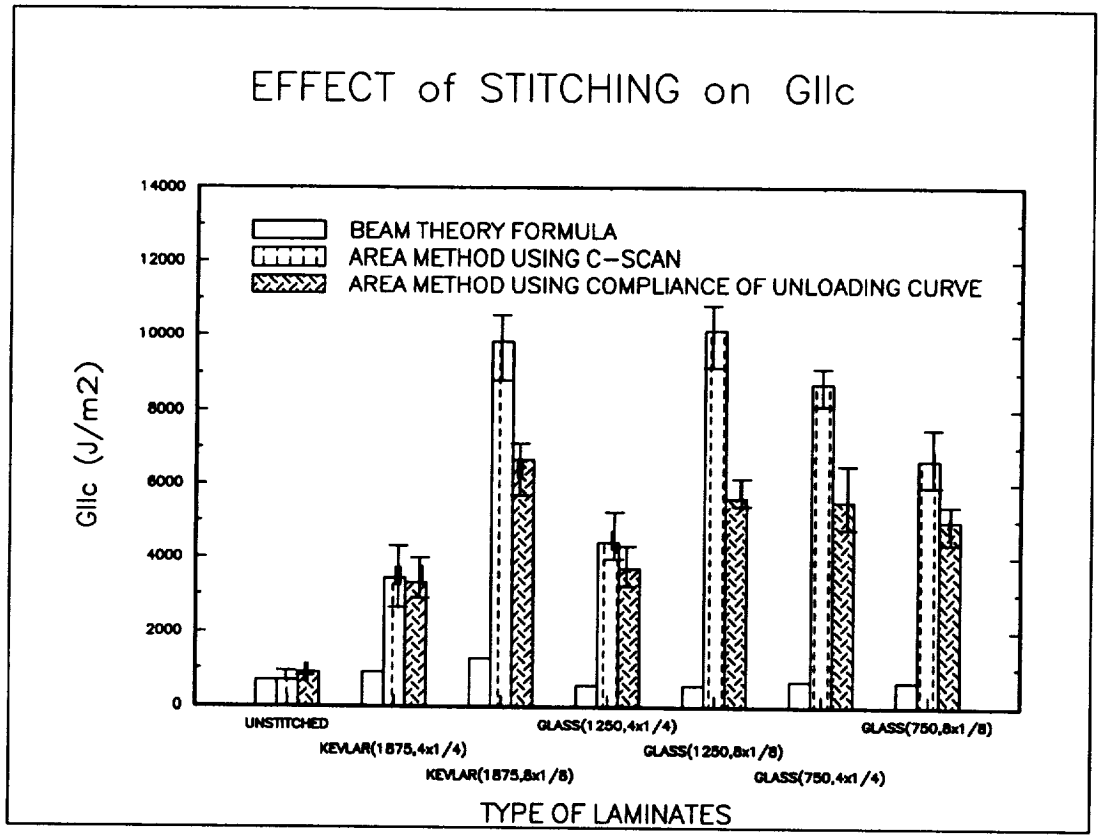

Figure 4-4: Effect of stitching on G_{IIc}. The crack propagated up to about center line ($\Delta a=0.5\times L$) in all cases.

the center line in all these tests as found by the C-Scans. As expected, the values of G_{IIc} obtained using beam theory formulation do not show any appreciable increase, indicating that the intrinsic Mode II critical strain energy release rate of the material remains same. However, the stitching does significantly improve the effective or apparent G_{IIc} as indicated by the values obtained using both the new area methods. The energy required to propagate the crack is apparently more due to the stitches. This is because not all the imparted energy during the test directly goes to the crack front, a good amount of the energy is also being used in other stitch damage mechanisms. The stitched laminate appears to behave more like a structure.

The Area method using C-Scans seems to be the upper bound G_{IIc} while the Equivalent area method using compliance of the unloading curve gives the lower bound values. The increase in apparent G_{IIc} values is very impressive regardless of the stitch yarn. It is about 5-15 times that of the unstitched laminates using the conservative lower bound values. It appears that the crack length detected by the C-Scanning is smaller than the effective crack propagation length. For each stitch material the apparent G_{IIc} increases with increasing stitch density except for the Glass-750 where the change is insignificant due to increased stitch density. Thus, it can be concluded that stitching significantly improves the Mode II fracture toughness. The possible damage mechanisms observed are discussed in the following section which further explains the rise in G_{IIc}.

Stitch failure mechanism and Contribution of the stitch yarn

The crack is very narrow in the ENF tests of these laminates and visual resolution is much less than the actual extent of crack front propagation. Therefore, the technique of painting side edges with white paint does not work accurately. X-Radiography of crack surface was attempted. X-Ray opaque fluid solutions of Zinc Iodide, Barium Chloride and Conray® were tried in varying concentrations. The capillary action does not seem to be adequate to obtain good contrast. Variations in X-Ray intensity were also conducted using the facilities at the University's Medical Center. Changes in the distance to the specimen, soaking time for capillary action, X-Ray exposure times, and different photographic films were tried without satisfactory results. The primary problem appears to be the inability of the X-ray opaque dye to penetrate into the extremely narrow crack space. Ultrasonic C-Scanning did reveal the crack length but, as we have seen in the preceding section, that technique also measures less than the actual crack length. Future experimental work may explore a more accurate method. However, physically cutting the specimens in small incremental steps starting from the undamaged end confirmed that even the first stitch line did not break although the crack had propagated at least up to about the center line of the specimen.

The stitch yarn contribution towards increasing Mode II fracture toughness and the associated deformation mechanisms were investigated. It was observed during physical cutting of the tested specimens that it is not possible to split open any of the specimens and reveal the cracked surface specimens even though the C-Scan showed the crack front had grown as much as half of its total length or more. The type of stitches used in this

study generally did not break. The first one or two stitches, however, may have partially broken. The crack front appears to have travelled around the stitch yarn. Due to the uniweave architecture of the fabric there was no additional resistance except that of the matrix and the glass fill yarn (2.5%) typically used in the uniweave cloth during fabric manufacture. The stitch yarn "ploughed" through the matrix. To study this effect, the specimens were gradually wedged open but the process of wedging damages the crack surface by opening it in Mode I. However, a hint of the matrix deformation can be seen in the SEM photograph (Fig. 3-15). The "ploughing" represents plastic or elastic-plastic deformation of the matrix. This explains the similar fracture toughness increases by the Kevlar-2790 and Glass-1250 which are close to each other in diameter. The Glass-750, being the thicker yarn, gives a larger increase in fracture toughness for the 4×1/4" stitch density. Thicker yarn more would greater deform of the matrix. Also the fracture toughness increases with increasing stitch density (except for Glass-750) which indicates increased matrix deformation. In the case of the 8×1/8" Glass-750, the fracture toughness drops down compared to 4×1/4" Glass-750, this may be due to the high density of thick yarns making the available matrix volume easier to "plough." This also indicates that there is a possible optimum stitch density for the desired fracture toughness and design loading requirements.

Variation of G_{IIc} with increase in crack length

The slope of the nonlinear part of the P-δ curve can be very useful in predicting some of the material properties. This curve represents gradually changing compliance as the crack length increases. Variation in G_{IIc} as the crack propagates was investigated using this part of the curve. Mode II fracture toughness at each data point of the acquired signal was calculated using the energy area method ($\Delta W/\Delta A$). The ΔW is work done from the P-δ curve to propagate the crack length by a total increment of Δa. The total increment of propagated crack length is a_{eff} minus the initial starter crack length a_o. The a_{eff} at each point was computed by using Equ. 4-2, where C' would be the nonlinear compliance at that point. A typical variation of G_{IIc} with the crack length for all the stitch yarns used in this study is shown in Fig. 4-5. The effect of stitching on Mode II fracture toughness can be studied from this curve. Initially, there is very little effect of the stitches and the value of G_{IIc} is about the same as that of an unstitched laminate. As the crack starts propagating, more and more stitches start becoming effective in improving the fracture toughness by "ploughing" the matrix thereby making the material system tougher. The rate of increase in the G_{IIc} for all the 4×1/4" stitch density is less than 8×1/8" density laminates. A sample calculation is given in Table C-4 in Appendix-C.

The variation of G_{IIc} was also studied by calculating the ΔW for the two successive load increments and dividing this incremental work done by the corresponding incremental increase of ΔA between those two successive points. A typical curve for Glass-750 is shown in Fig.4-6 and represents the instantaneous variation of G_{IIc} with crack length.

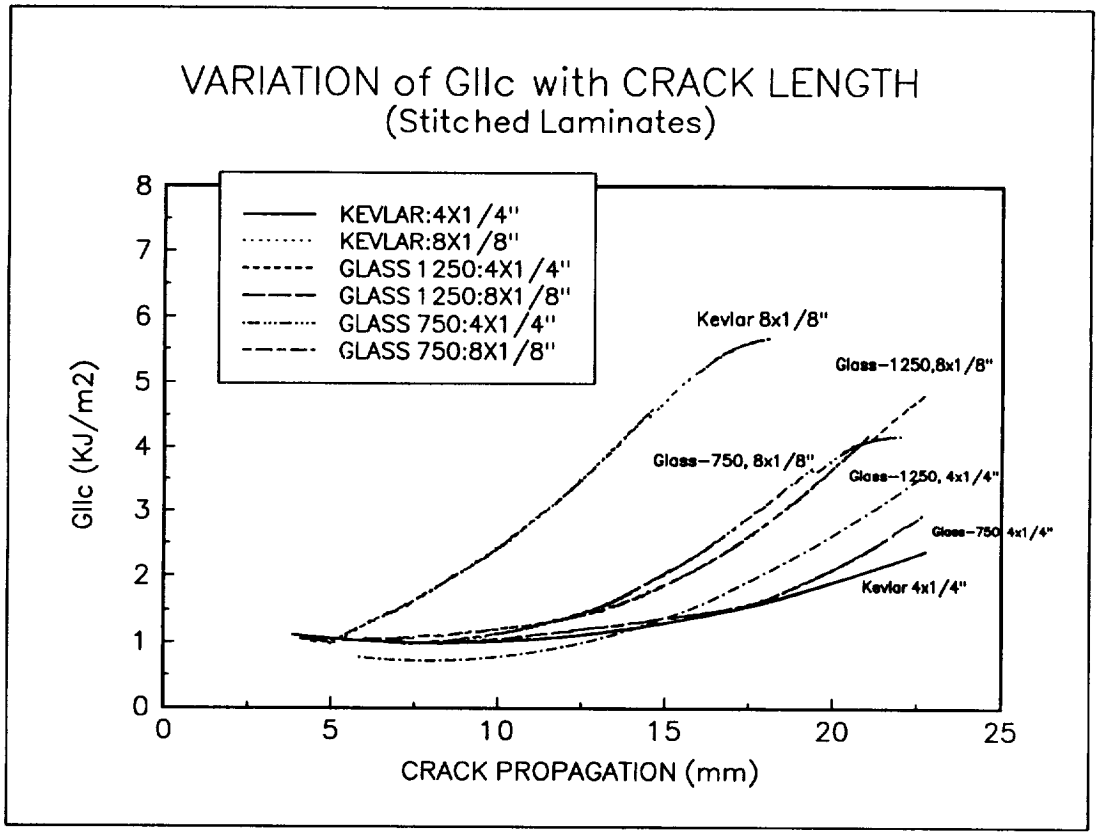

Figure 4-5: Variation in G_{IIc} with increase in crack length of stitched laminates

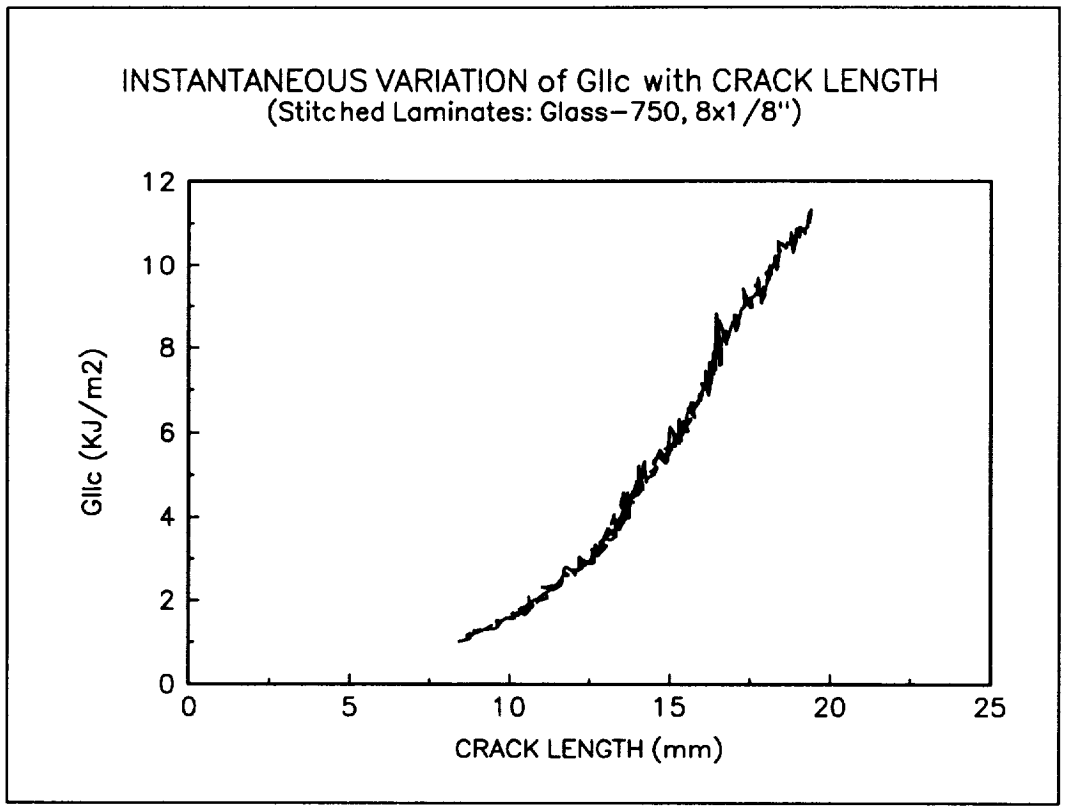

Figure 4-6: A typical variation of G_{IIc} at each time interval (instantaneous) with increase in crack length of stitched laminates.

Effect of friction on G_{IIc}

Tests were conducted in which the specimen was loaded well within the elastic range and then unloaded. The test was repeated after applying lubricating oil between the crack surface. The work done as calculated from the area under the curve represented frictional losses at the support roller pins, loading pin and the initial crack surface with or without lubrication. One typical response of such a test is shown in Fig. 4-7. The total losses in this elastic range were calculated to be about 2-3%. This matches with results reported earlier [26].

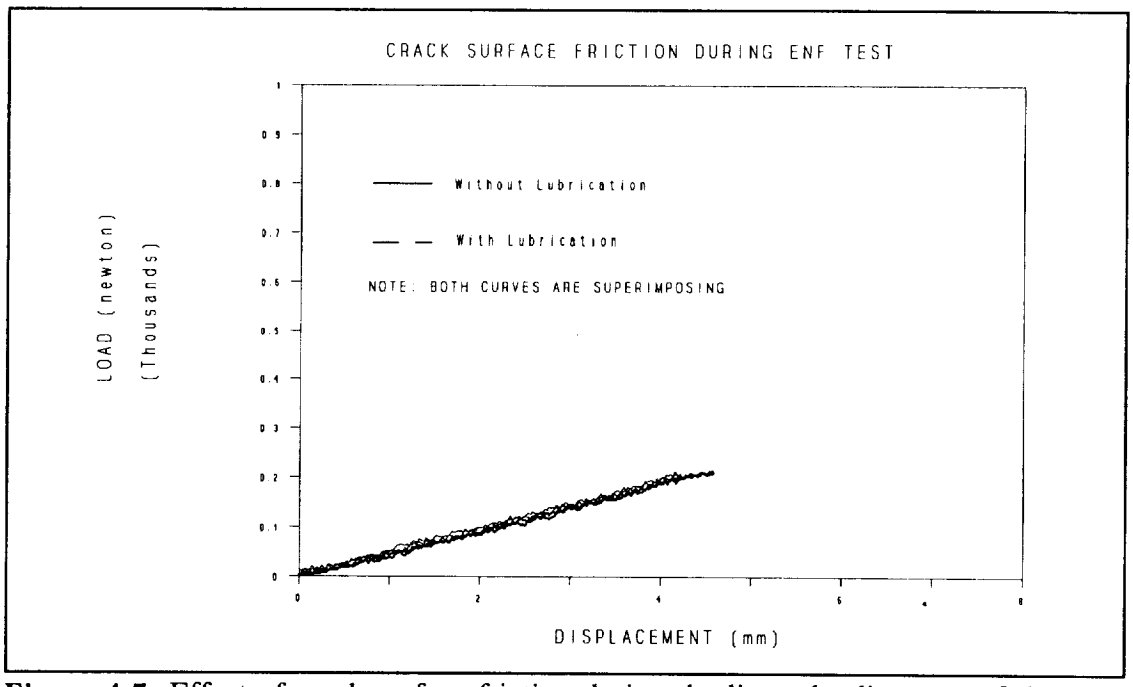

Figure 4-7: Effect of crack surface friction during the linear loading part of the test.

The frictional losses in the nonlinear region can be high. This type of frictional effect can be inferred from the P-δ curve of the stitched laminates shown in Figs. 4-2 and 4-3. In most of the load-displacement curves a small but sudden drop in load can be observed immediately on the commencement of the unloading cycle. It is believed that this is due to contact friction at the point of maximum deflection and the support roller pins. As this drop is observed only when the test is well into the nonlinear region its affect can be ignored in the initial part of the test. However, for later regimes this load drop will give a larger work done (area under the curve) during the test. Therefore, values of G_{IIc} obtained from new methods should be reduced accordingly. On an average, a study of 48 P-δ curves in this study suggested a 20% reduction in the peak G_{IIc} values obtained by the Equivalent area method which gives a conservative lower bound for G_{IIc} values. The data regarding frictional effect of work done in the nonlinear regime is given in Table C-5 in Appendix-C. It may be noted that the contribution of stitching to improve Mode II fracture toughness still remains significant.

CHAPTER - 5
STATIC INDENTATION-FLEXURE (SIF) AND COMPRESSION-AFTER-IMPACT (CAI) TESTS OF PLAIN WEAVE LAMINATES

Approach to Study of Impact Damage Resistance and Damage Tolerance of Thin Plain Weave Laminates

The static indentation-flexure (SIF) test can be used to study impact damage response due to impact of large masses at very low velocities [6,27]. These tests simulate quasi-static impact conditions. In addition, they offer greater opportunity to study progressive damage propagation during the impact event. These tests were conducted on unstitched and stitched 16 ply plain weave graphite fabric/epoxy (Hercules A193-P/ 3501-6) laminates. The processing of the plates for the specimens was done at Center for Studies of Advanced Structural Composites, University of Florida. The specimens were 3.6 mm (0.140") nominally thick square plates i.e., about half the thickness of the uniweave laminates studied in Chapter-2. These were simply supported on circular support rings of different diameters. The specimens were statically indented and unloaded at three different contact force levels in order to assess damage progression. Load-displacement data was gathered. The effect of stitching on indentation damage area for a given contact force, damage propagation and residual compression strength were studied. Ultrasonic C-Scans were taken to assess damage area. The effect of varying support ring diameters was also studied.

Processing of the Stitched Plain Weave Laminates

A preform of 16 plies [0_{16}] of 12"×12" size plain weave graphite fabric (Hercules A193-P) was stitched using an industrial sewing machine. An out-of-balance stitch lock using Kevlar®29 (1600 denier) bobbin yarn and Kevlar®29 (400 denier) needle yarn was used. This type of stitch lock is similar to the modified stitch lock used on the uniweave laminates but the position of the lock tends to be slightly inside of the top surface rather than on the top of it. The stitched preform was sandwiched between two equal quantity of film resin (3501-6) and a vacuum bag lay-up was prepared as shown in Fig. 5-1. The lay-up was cured in an autoclave following the manufacturer's recommended curing cycle.

Stitching the preform The speed of stitching has to be steadily maintained to achieve consistent product quality. Variation in stitching speed leads to frequent breaking/entanglement of stitch yarns (needle or bobbin or both). This may lead to non-continuous stitching in the laminates which may affect desired properties. Therefore, stitching speed should be automatically controlled in the sewing machines designed for composite preform stitching. Another problem area is the possibility of small and gradual changes in bobbin or needle yarn tensions during the stitching process. The tension is adjusted by the operator before the start of stitching and should be checked frequently to ensure it does not change. The tension setting determines the stitch lock position. Deviation in stitch lock position will lead to varying stitch lock stress concentrations in the laminate. Therefore, a suitable mechanism to ensure preset tensions do not change or

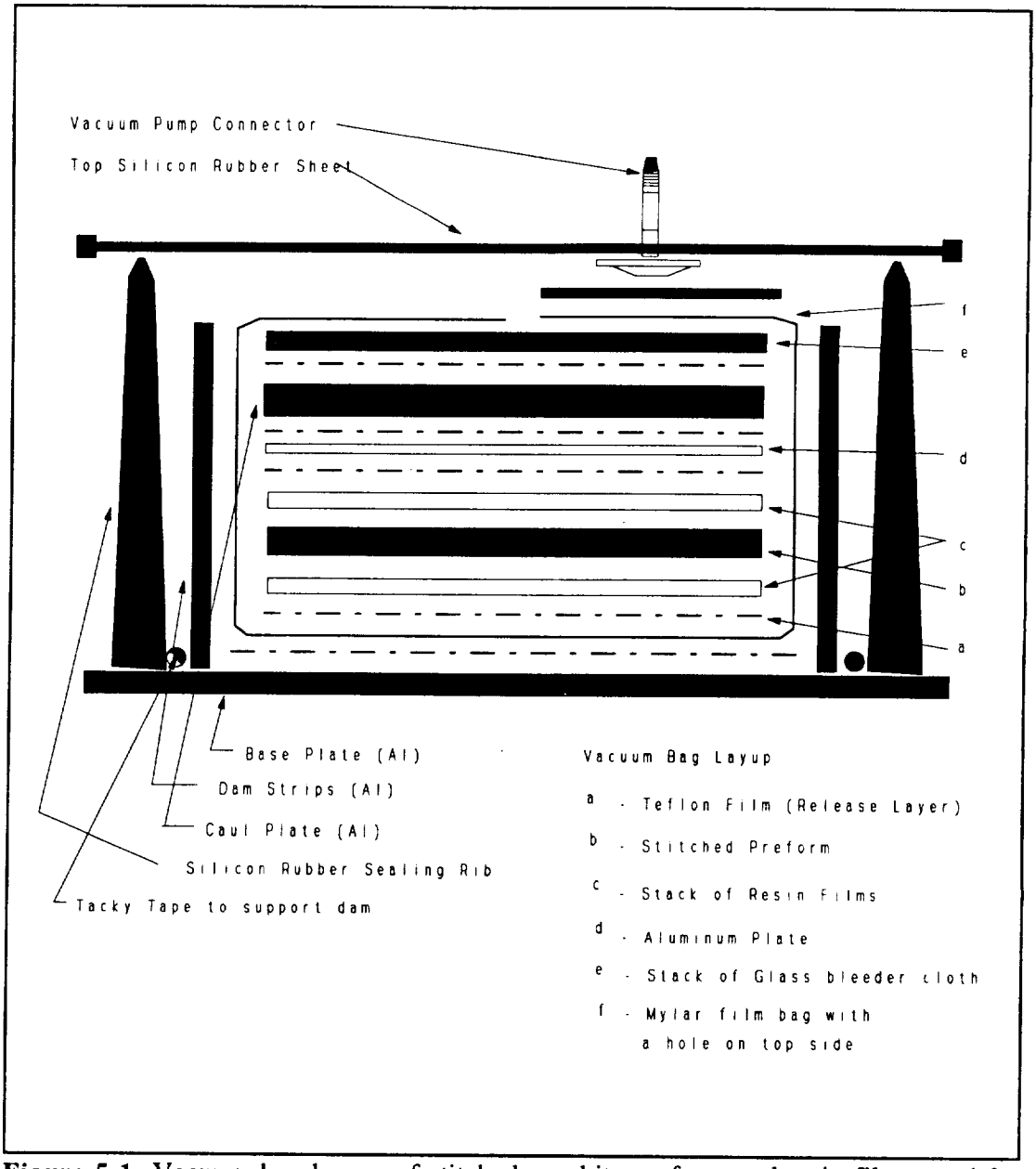

Figure 5-1: Vacuum bag lay-up of stitched graphite preform and resin films used for autoclave processing of the stitched laminates at the Center for Studies of Advanced Structural Composites.

sensors for any inadvertent changes in the preset tension need to be incorporated in the sewing machines for composites manufacture. Nylon, Glass and Kevlar® yarns were considered for their suitability to stitch a 16 ply preform. Rounded stitching needle #160 was used in the machine to minimize damage to textile fabric warp and fill yarns. Nylon and Kevlar yarns were found satisfactory for their stitchability while the Glass yarn was observed to break frequently. Kevlar®29, the stronger of the two satisfactory yarns, was selected for stitching the laminates. Two stitch densities for the plain weave specimens studied were: 8×1/4" (= 32 stitches/in^2) and 5×1/4" (= 20 stitches/in^2). A paper template marked with the desired stitch pattern was used as a guide on top of the preform to assist straight line movement of the preform between the dog and the feed as shown in Fig. 5-2. The paper template was carefully removed after stitching using tweezers.

Vacuum bag lay up and autoclave curing. The vacuum bag mold was cured following the cycle shown in Fig. 5-3. Two equal stacks of film resin on either side of the preform allow the infusion of the film resin during the curing cycle. The specimens were ultrasonically C-Scanned for void content. About 25% percent of the production was rejected due to high porosity. The volume fraction of fiber (V_f) was 60%. The thickness of the stitched and the unstitched composite plates were 0.140" and 0.135" respectively. The cured 12"×12" composite plates were cut into different size square laminates using a dressing machine with a diamond-impregnated cutting wheel.

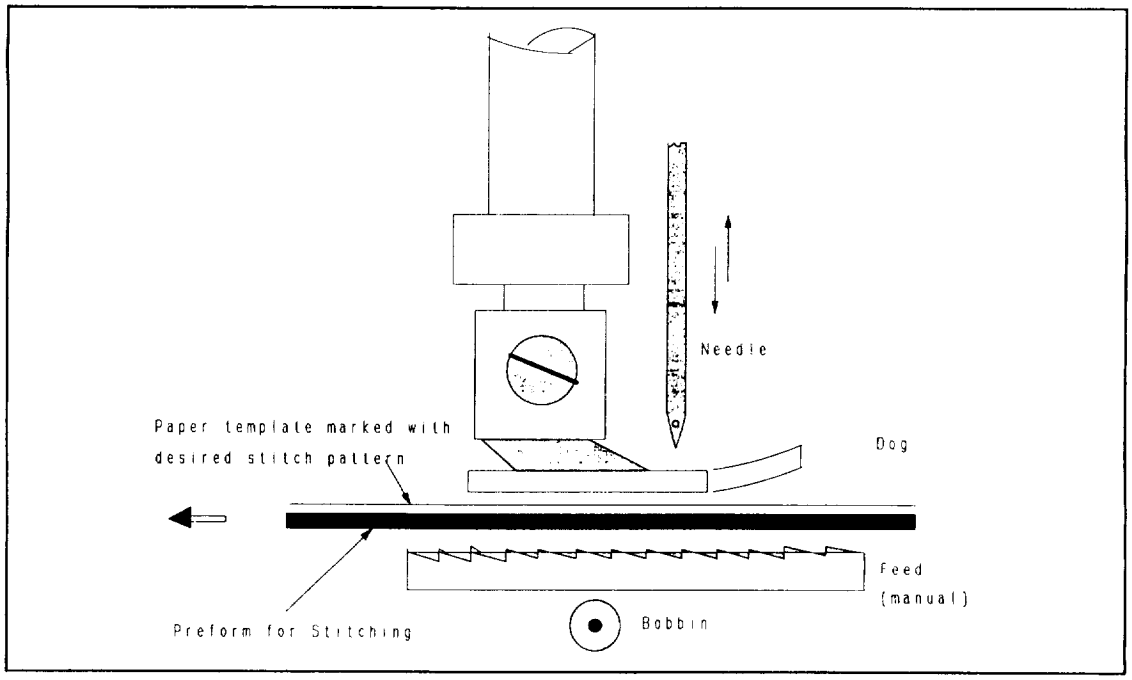

Figure 5-2: Use of a paper template to assist straight movement between the dog and the feed.

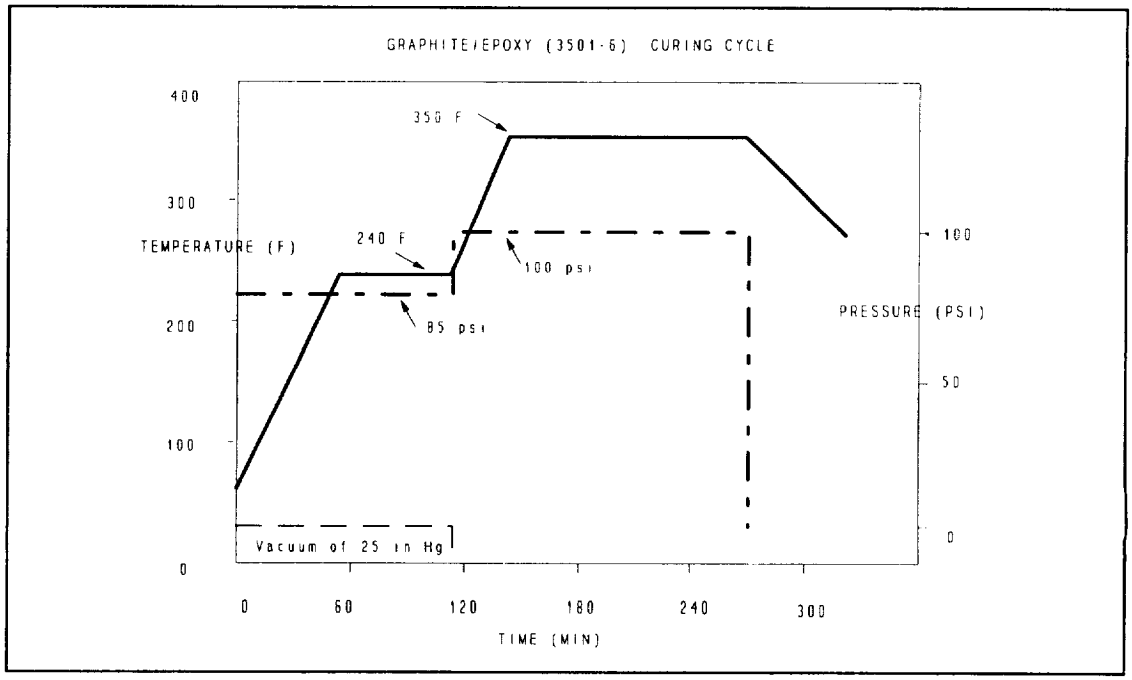

Figure 5-3: Curing cycle of graphite/epoxy laminate (Hercules A193-P/3501-6)

Static Indentation-Flexure (SIF) Test

Test variables and procedures

A one-half inch diameter hemispherical shaped steel indenter was used to indent the simply supported plate specimens. A schematic diagram of the test set-up is shown in Fig. 5-4. The support ring diameters selected for study were 2", 3" and 4". The specimens were cut to ensure at least 0.5" overhang on all sides beyond the support ring. The diameter/thickness ratio was 15 to 30 conforming to thin plate analysis assumptions. A test matrix is shown in Table 5-1.

Table 5-1: Test Matrix of SIF and CAI Tests

TYPE OF TEST	STITCH DENSITY	SUPPORT RING DIAMETER	# OF SPECIMENS
SIF and CAI Test	Zero (Unstitched)	2"	3 each
		3"	3 each
		4"	3 each
	8 × 1/4"	2"	3 each
		3"	3 each
		4"	3 each
	5 × 1/4"	3"	12 each

The tests were conducted under stroke control on a 12 kips Tinius-Olsen machine at a rate of 0.05 in/min. The load and indenter displacement were recorded using

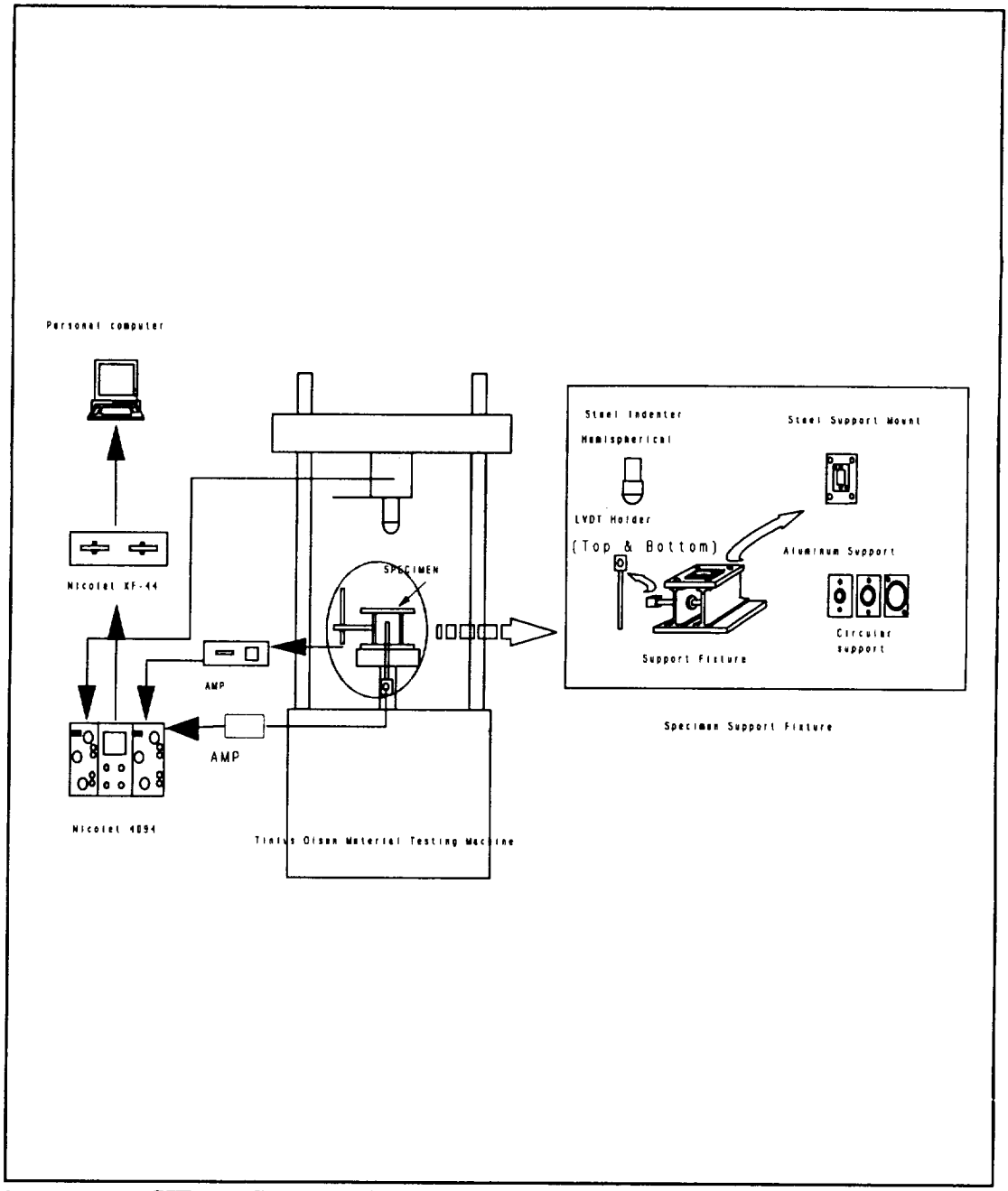

Figure 5-4: SIF test fixture and a schematic diagram of the test set-up

a calibrated load cell and a LVDT respectively into the Nicolet digital oscilloscope 4094 with XF-44 recorder. The displacement of the specimen was measured using a separate LVDT positioned at the bottom surface. The difference in both displacements gives the indentation. As a first step, 8×1/4" specimens were loaded and unloaded within the linear region of the P-δ curve. A few crackling sounds typical of matrix cracking could be heard near the peak of the linear region. The damage was assessed using Ultrasonic C-Scan. Subsequently, in the second and third steps, other specimens were loaded well into the nonlinear region. The damaged specimens were C-Scanned to calculate damage areas. Having studied the effect of variation in support ring diameter, the 5×1/4" specimens were tested similarly up to the same level in the nonlinear region of the P-δ curve for each specimen using the 3" diameter ring only.

SIF Test Results and Discussions

Textile laminates vs. Unidirectional laminates

A representative P-δ curve for the unstitched and a 8×1/4" stitched laminate are shown in Fig. 5-5 and Fig. 5-6 respectively. The onset of damage initiation in the case of stitched textile composite laminates is not marked by a sudden and pronounced drop in the load as happens in the case of an unstitched or a unidirectional laminate [6]. Instead, it is smooth and the damage progression in stitched textile laminates is similar to yielding in ductile materials. A similar behavior was observed with $\pi/8$ laminates [6].

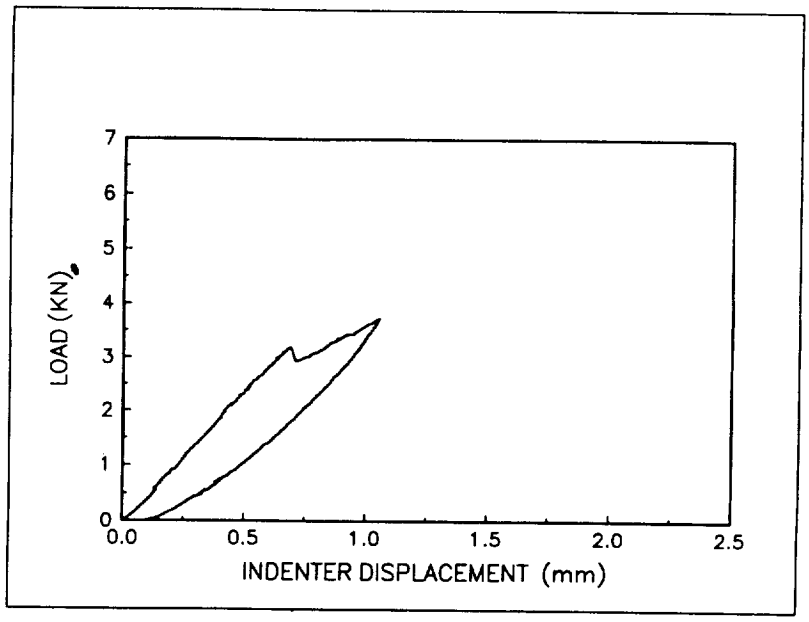

Figure 5-5: A typical P-δ curve for unstitched laminates.

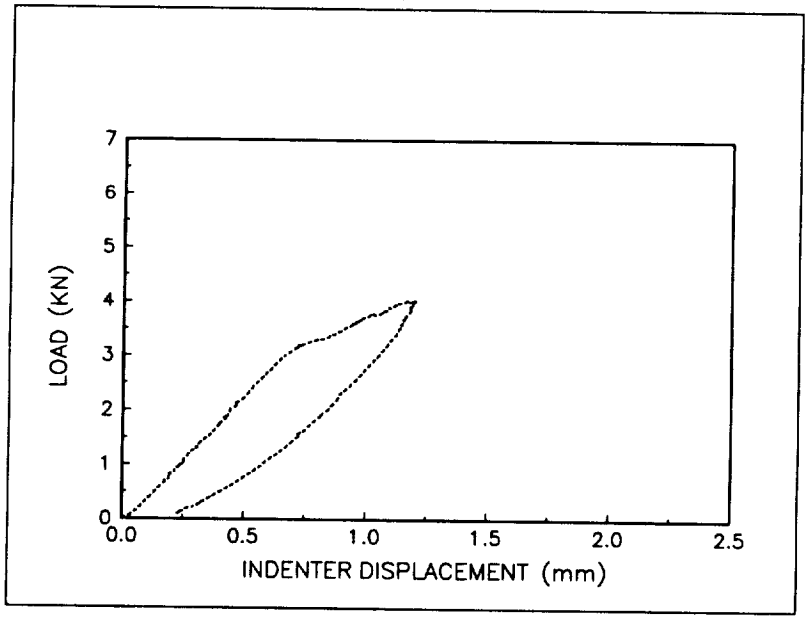

Figure 5-6: A typical P-δ curve for stitched laminates

Impact damage resistance of the thin unstitched and the stitched laminates as characterized by impact force

A comparison of the low velocity impact damage response as simulated through static indentation tests for the 8×1/4" stitched and the unstitched laminates at different loading steps and with different support ring diameters can be seen in Figs. 5-7, 5-8 and 5-9. It is noted that there is no significant difference in the contact force required to initiate damage in the stitched and unstitched plates which indicates that the stitching does not affect this impact response in these plates. Apparently, the through-the-thickness reinforcement does not become very effective in these cases. There is a slight increase in the ultimate load in the stitched plates which could be due to the increased thickness also. This insignificant affect of stitching on the impact damage resistance of thin laminates is consistent with the findings of Poe, et al [28] who reported an increase in improvement of the impact resistance of the stitched laminates as the thickness of laminate was increased. An increase in support ring diameter decreased the maximum failure load.

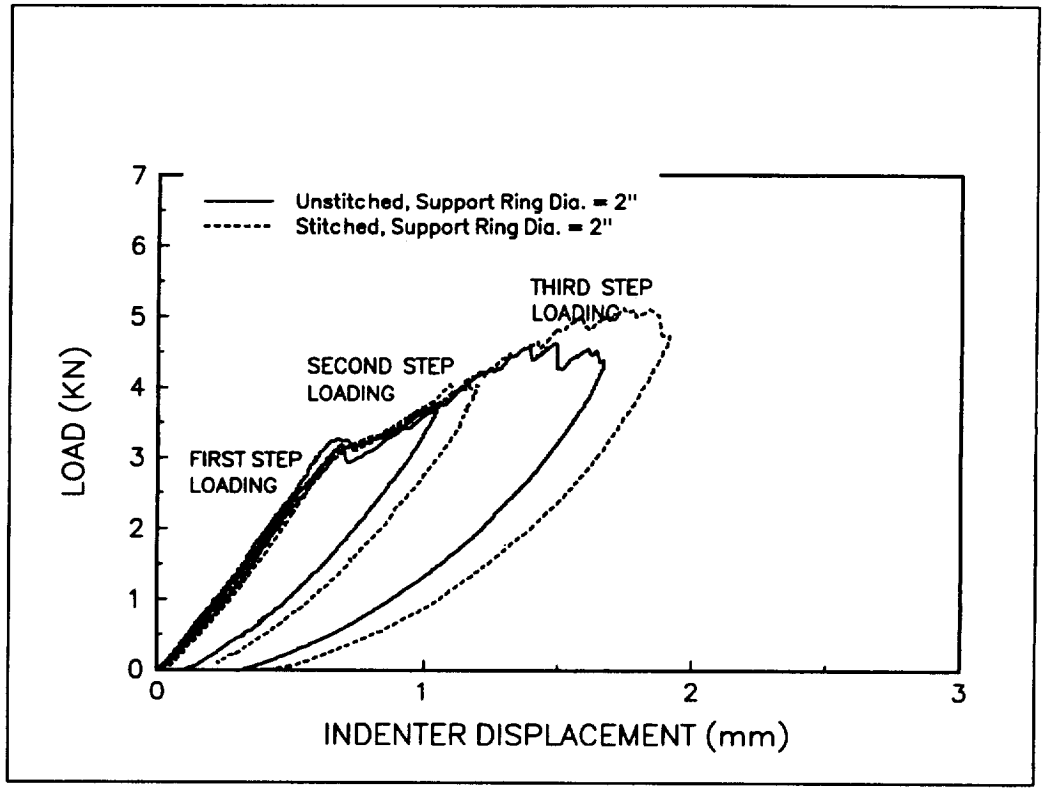

Figure 5-7: Indentation response; 2" support ring diameter

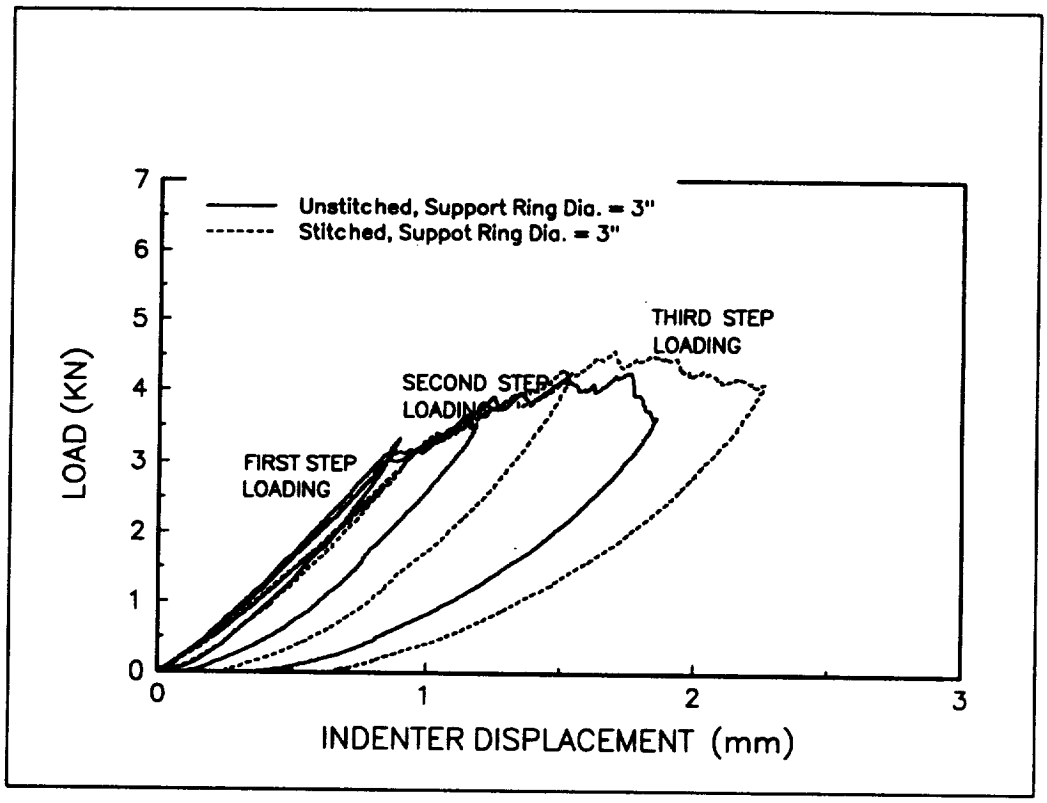

Figure 5-8: Indentation response; 3" support ring diameter

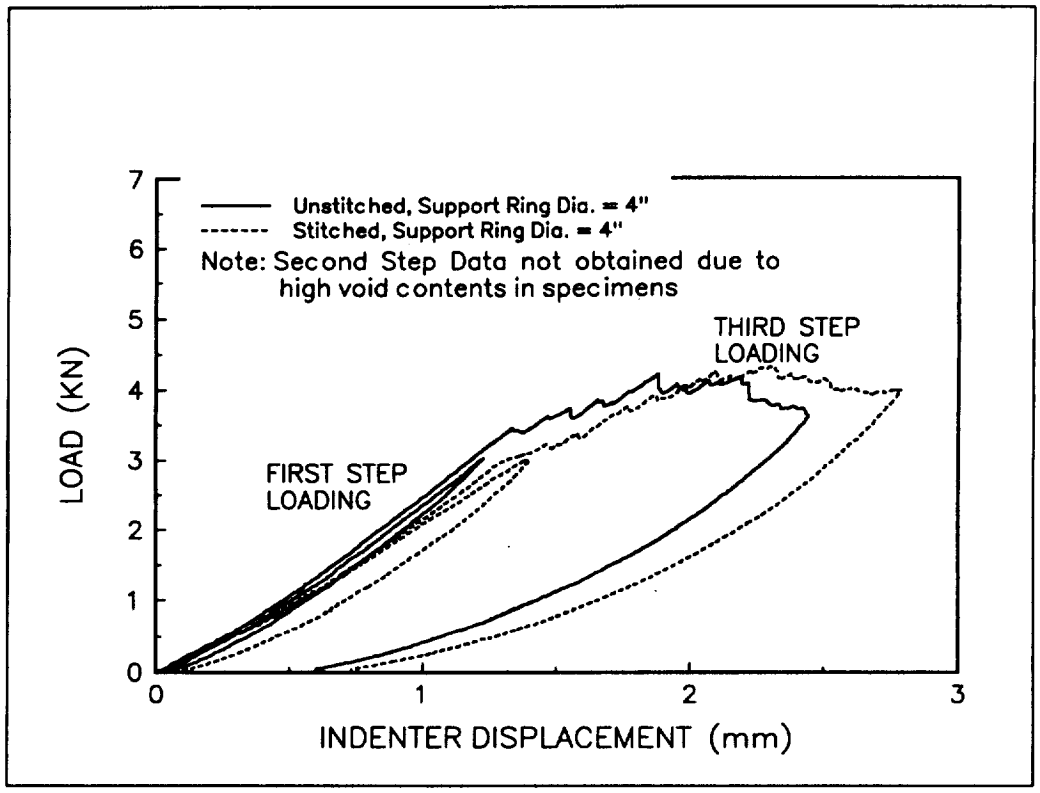

Figure 5-9: Indentation response; 4" support ring diameter

Impact damage resistance of the unstitched and the stitched laminates as characterized by impact damage area

The damage area is smaller for a given force for increasing support ring diameters for both the unstitched and the 8×1/4" stitched laminates as seen in Fig. 5-10. However, 8×1/4" stitching seems to not affect the impact damage area, only three specimens of each type were tested. It was therefore decided to fabricate and test 12 of the 5×1/4" specimens to get a more statistically reliable data. Loading/unloading levels were the same at each step. Support ring diameter was also kept constant (3") for all these specimens. Fig. 5-11 shows impact damage area versus impact force for the unstitched and the 5×1/4" stitched laminates. The stitched specimens demonstrated about 40% less damage area compared to unstitched specimens for the same load. Thus, impact damage resistance improved significantly due to stitching. Fig. 5-12 shows two representative C-scans taken to measure damage area for the unstitched and the stitched laminates. Thus it can be inferred that the damage initiation for the unstitched and the thin stitched laminates is likely to occur at the same load, further propagation of the damage can be significantly restricted by stitching.

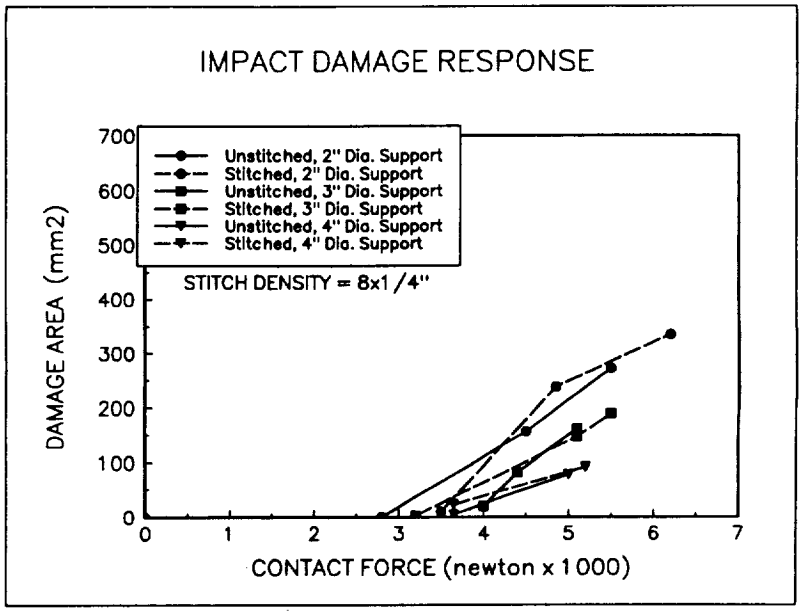

Figure 5-10: Impact Damage Area (C-Scan) vs. Contact Force for the unstitched and 8×1/4" stitched laminates with variation in support ring diameter.

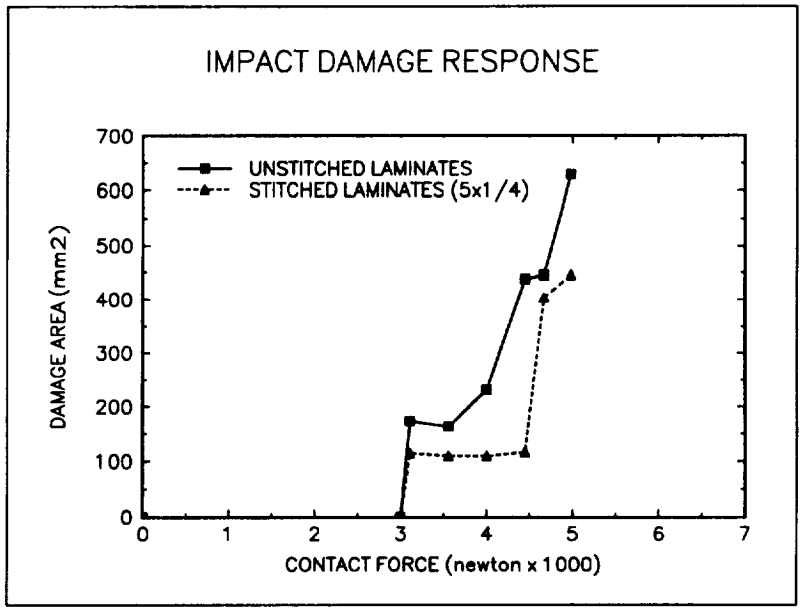

Figure 5-11: Impact Damage Area (C-Scan) vs. Contact Force for the unstitched and 5×1/4" stitched laminates with 3" support ring diameter.

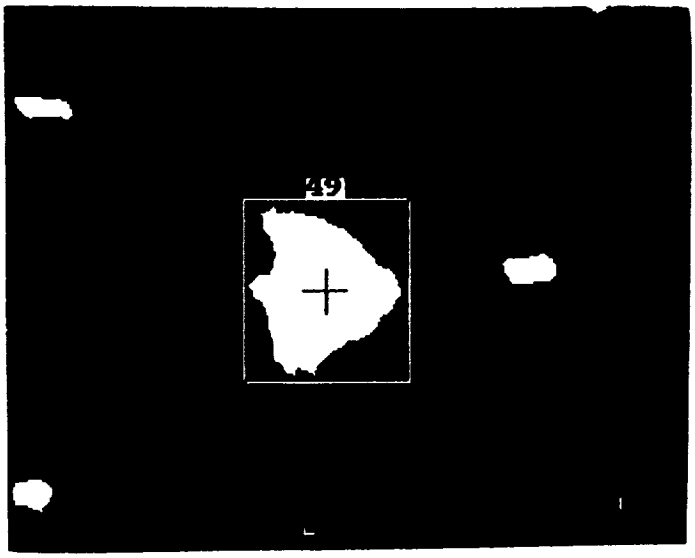

(a) Unstitched Specimen # USSI-15: C-Scan Damage Area = 629 mm^2

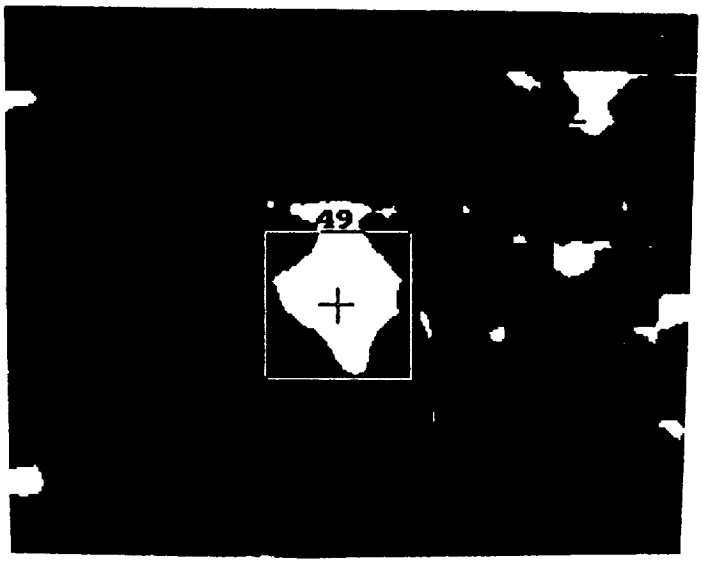

(b) Stitched Specimen #STSI-15: C-Scan Damage Area = 446 mm^2

Figure 5-12: C-Scans showing damage areas of the Unstitched and Stitched laminates created by same indentation load.

Compression-After-Impact Test

Test variables and procedures

The residual post-impact strength for the statically indented unstitched and stitched textile laminates was characterized by measuring compressive failure strength. It may be recalled that the SIF tests of the unstitched and 8×1/4" stitched laminates were conducted on 2", 3" and 4" diameter support rings, and the 5×1/4" stitched laminates were conducted on a 3" diameter support ring. Thus the plates that were indented on 2", 3" and 4" diameter rings were 3", 4" and 5" tall respectively. The UF-CAI fixture (Appendix- A) was used to conduct CAI tests. The tests were conducted in stroke control mode on a calibrated 20 kips capacity hydraulic-powered MTS testing machine using a digital controller (Type 455) and a dedicated computerized (PDP-11) remote control system at the Center for Studies of Advanced Structural Composites. The total travel of the top crosshead was programmed not to exceed the unsupported height of the specimen in the fixture. The rate of loading was 0.02 mm/s. The compression failure was detected by observing the sudden drop in the load signal and was read from the memory of the control panel indicator. The failure was preceded by crackling sounds in quick succession ending with a loud bang noise. The load signal was also recorded on the Nicolet digital oscilloscope for later comparison and reference. The specimen loading was stopped immediately after compressive failure occurred. The specimens were examined for the type of failure.

CAI test results and discussions

The residual compressive strength was calculated by using the peak load and dividing it by the average cross-sectional area of the specimen. The average thickness was calculated using thicknesses measured at ten points on the coupon. The failed specimens were again C-scanned to study the progression of damage during the CAI test. The reduced CAI load data and C-scans for all the specimens tested are given in Appendix-D.

The compressive strength is known to increase with a reduction in gage length [22]. The 8×1/4" stitched specimens were primarily manufactured to study stitching, processing and impact damage with varying support ring diameters (meaning different gage lengths in a CAI test). Consequently, their numbers in each category were insufficient to study the CAI data to observe the effect of stitching with other variables remaining constant. Therefore, the effect of stitching for 5×1/4" stitched specimens (all of them had the same gage length = 2.4") is presented. The residual post-impact strength is plotted against the impact force in Fig. 5-13. The stitched specimens showed about 25% higher CAI strength than the unstitched laminates for the maximum damage area. However, it should be noted that the CAI strength for low impact force are similar. This trend is similar to the one observed in the Sublaminate Buckling Tests described in Chapter-2, although the plain weave laminates were much thinner than the uniweave laminates. The effect of stitch density was not studied in the plain weave laminates. The CAI tested specimens were C-scanned to see progression of damage. A typical C-scan is shown in Fig. 5-14. The damage invariably progressed on either side of the center line

of impact damage area, the laminate being weakest in those regions. In the case of the control specimens, the failure occurred at the well known 45^0 angle shear band at the mid-section.

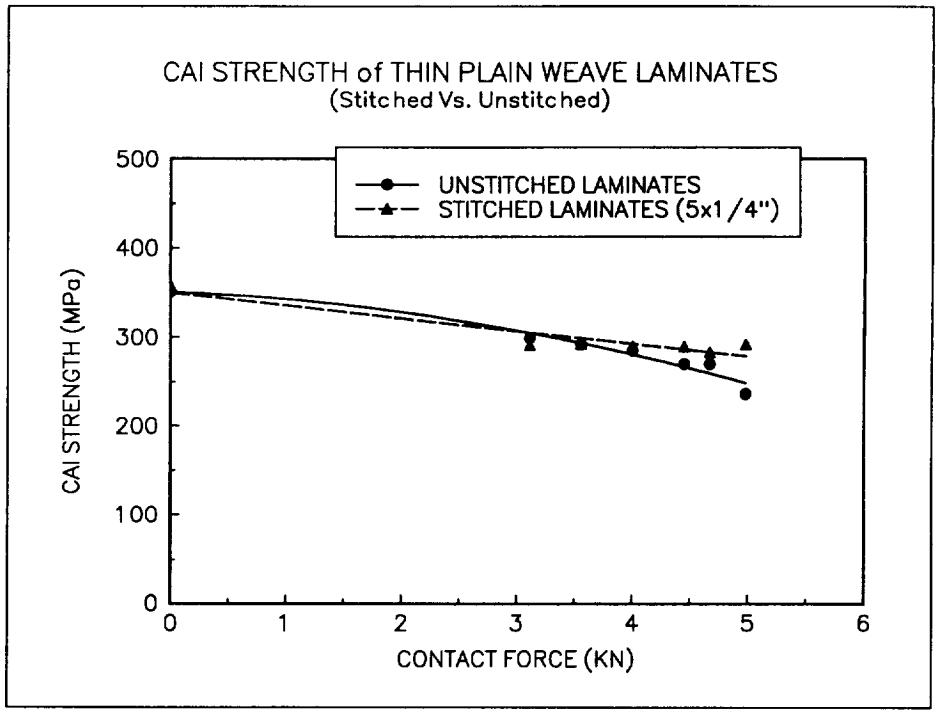

Figure 5-13: Stitching improves the CAI strength of thin plain weave laminates by about 25% for the maximum contact force applied.

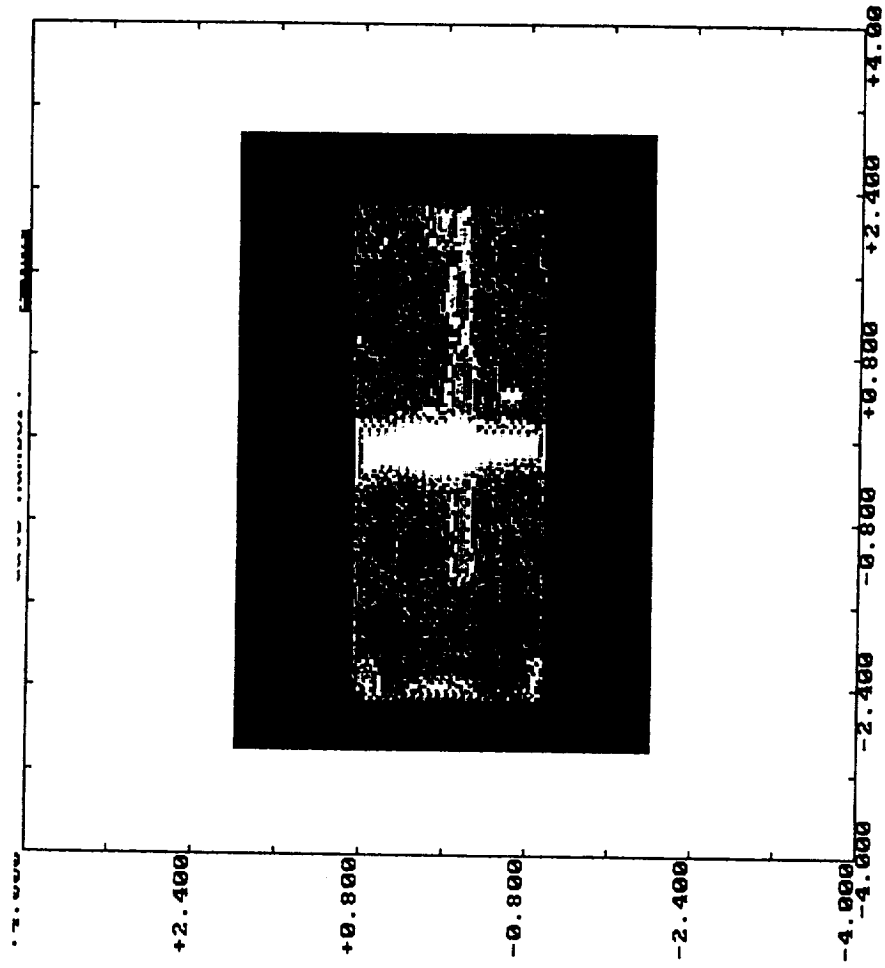

Figure 5-14: A typical C-scan showing damage progression during CAI test on either side of the initial impact damage area in the center.

CHAPTER 6
CONCLUSIONS

These studies show that through-the-thickness stitching of textile graphite/epoxy laminates significantly improves low velocity impact damage resistance, impact damage tolerance, Mode I fracture toughness and Mode II fracture toughness. Therefore, combined with mass production advantages of the well established textile technologies, stitched textile structural composites emerge as a potentially superior alternative material system for high performance needs at lower costs. Salient observations made during the study and the conclusions drawn thereof are summarized below. The chapters for reference of complete details are mentioned against each conclusion.

Uniweave Laminates
(AS4 uniweave fabric/3501-6 resin/Kevlar or Glass stitched/RTM processed)

Effect of stitching on sublaminate buckling strength . . (Refer to Chapter-2 for details)

1. Stitching was observed to effectively restrict sublaminate buckling failure of uniweave laminates with teflon implanted delaminations. The improvement in the sublaminate buckling strength of stitched laminates with 8×1/8" stitch density was as high as 400% compared to the unstitched laminates for the worst case of delamination studied.

2. The sublaminate buckling strength increases rapidly with increasing stitch

density. It reaches a peak CAI strength that is very close to the original compression strength of the material. For the highest stitch density studied i.e., 8×1/8", the CAI strength of the stitched uniweave laminates for the worst damage case was about 65 ksi as compared to about 70 ksi of the undamaged stitched control specimens.

3. The effect of the different types of stitch yarn is not noticeable. All the stitch yarns investigated demonstrated very close performance in improving the CAI strength. It appears that any stitch yarn with adequate breaking strength and stiffness successfully restricts sublaminate buckling.

Effect on Mode I fracture toughness . . . . . (Refer to Chapter-3 for details)

1. Stitching increases the Mode I fracture toughness (G_{Ic}) increases by at least an order of magnitude. In case of 4×1/4" stitch density, Kevlar-2790 (1600 denier) stitch yarn increased G_{Ic} by about 15 times, Glass-1250 (3570 denier) by about 30 times and Glass-750 (5952 denier) by about 21 times. The Mode I critical strain energy release rate for the unstitched lamnates was 302.6 J/m^2.

2. The Mode I fracture toughness of 8×1/8" stitch density laminates could not be measured experimentally as the specimen failed in bending before the crack could propagate any distance. In order to find the G_{Ic} for these high stitch density laminates, thicker specimens are required. This illustrates the impressive increase in Mode I fracture toughness due to stitching.

3. The G_{Ic} increases rapidly with increasing crack length but stabilizes at a peak value as the crack increments start following a self-similar pattern.The initial low value

of G_{Ic} for the first increment is probably due to manufacturing imperfections like misalignment of the first stitch of each stitch row. A stabilized G_{Ic} value is observed once the crack starts progressing in a self-similar manner.

4. The crack propagation in unstitched laminates is gradual and steady. The crack propagation in the stitched laminates is intermittent and unsteady. The stitches first debond from the matrix after the crack front passes ahead. The stitches always fail at or near the stitch lock. The bobbin yarns failed with Kevlar-2790 and Glass-1250 stitch yarns, the needle yarn failed with the stronger bobbin Glass-750 yarn. This indicates the role a needle yarn may play in further improving G_{Ic}. In general, both bobbin and needle yarns may be of approximate equal strengths to avoid a weaker linkage.

5. The SEM studies of crack surface morphology hint at matrix "ploughing" by the stitch yarn in a uniweave architecture.

Effect on Mode II fracture toughness . . . . . (Refer to Chapter-4 for details)

1. Stitching significantly improves Mode II fracture toughness. The increase in apparent G_{IIc} was 5 to 15 times when the crack was allowed to propagate up to about midspan of the ENF beams.

2. The crack surfaces do not open during the ENF test and hence it is difficult to estimate the crack length by any method such as visual, X-radiography or Ultrasonic C-Scan. The Ultrasonic C-Scan underestimates it. Two new methods to calculate apparent G_{IIc} have been developed: one using work done from the P-δ curve and the C-Scan area of the crack surface; the second method uses compliance of the unloading curve.

3. The critical strain energy release rate increases with increasing crack length. This is because not all energy imparted to the laminate goes directly to the crack front. Part of it is used in stitch and other matrix failure mechanisms as more stitches become effective as the crack propagates. The stitched laminate seems to behave more like a structure rather than a material.

4. The stitches did not break during these tests. The stitch yarn seemed to plough through the matrix causing elastic and elastic-plastic deformation. Therefore, as the crack starts propagating, the ploughing resistance increased resulting in more Mode II fracture toughness.

5.The effect of crack surface friction was found to be 2-3% on the G_{IIc} , while the effect of support roller pins and loading pin contact friction should not be neglected when the P-δ loading curve reaches well into nonlinear region.

Thin Plain Weave Laminates
(Hercules A193-P graphite fabric/3501-6 resin/Kevlar stitched/autoclave cured)

Observations on processing of stitched laminates . . . . . (Refer Chapter-5)

1. The location of stitch lock within the laminate is critical to all the properties investigated in this study. This location is sensitive to stitching speed and bobbin and needle tensions. To achieve consistent quality, automated speed control and a suitable mechanism to ensure preset bobbin and needle tensions are considered essential.

2. Kevlar is easy to stitch with while the Glass yarn is not. Though the Mode I, Mode II fracture toughness and CAI strength of Glass-1250 stitched laminates are slightly

better than Kevlar-2790 stitched laminates, the additional care, time, and wastage due to frequent breaking of Glass stitch yarns may offset the processing cost advantages that textile structural composites offer.

Low Velocity Impact damage resistance and damage tolerance of thin Plain Weave Laminates . . . . . (Refer Chapter-5 for details)

1. Low velocity impact damage resistance was studied by conducting static indentation tests. The damage progression during a static indentation test in stitched textile laminates is similar to yielding in ductile materials. This is unlike most unstitched laminates where a delamination initiates suddenly during a static indentation test.

2. In the case of the thin laminates, the force where delaminations initiated did not change significantly. The impact damage area for the stitched laminates, however, was about 40% less compared to that of the unstitched laminates. These results match well with other studies where improvement in impact damage resistance increases with increase in the thickness of laminates. It may be that through-the-thickness reinforcement is not fully effective in thin laminates.The CAI strength of stitched laminates (5×1/4") was about 25% higher than the unstitched laminates for the largest impact force but was the same for the smaller impact force.

APPENDIX - A
THE UNIVERSITY OF FLORIDA COMPRESSION-AFTER-IMPACT (UF-CAI) TEST FIXTURE AND SUBLAMINATE BUCKLING TEST DATA

The UF-CAI Test Fixture

Limitations of existing CAI test fixtures

A study to select a suitable CAI fixture that will allow specimens of 3", 4" and 5" height to be tested was made. It is to be noted that the static indentation-flexure (SIF) tests on the thin plain weave laminates described in Chapter 5 were planned on 2", 3" and 4" diameter support rings. Thus the plates that were indented on 2" diameter support ring were 3" tall (0.5" overhang was allowed on all sides during the SIF test) and the plates that were indented on 3" and 4" support ring diameters were 4" and 5" tall respectively. The Center for Studies of Advanced Composites has an existing NASA post impact compression fatigue test fixture shown in Fig. A-1 [29]. Preliminary tests with this fixture revealed that the test fixture was not suitable to meet the requirements of this program for two reasons: the height of specimen is fixed, and global buckling is prevented by knife-edge supports. The knife-edge supports tend to cut into the side edges of the specimen which may fail from the cut area.

A study of a variety of existing CAI fixtures including NASA linear bearing fixture, ASTM, Celanese, IITRI, Wyoming modified IITRI and ELSS, Short block

compression, UDRI and Boeing was carried out. Though a few of these fixtures could be used for the purposes of this program with little modifications, the existing NASA post impact compressive fatigue test fixture was modified for reasons of economy as well as to adequately meet the specific design considerations listed below. During the course of development this fixture has undergone extensive fundamental changes and has been christened the "UF-CAI Test Fixture". Top and bottom platens along with the top and bottom side support plates of the existing fixture are interchangeable with the new UF-CAI fixture.

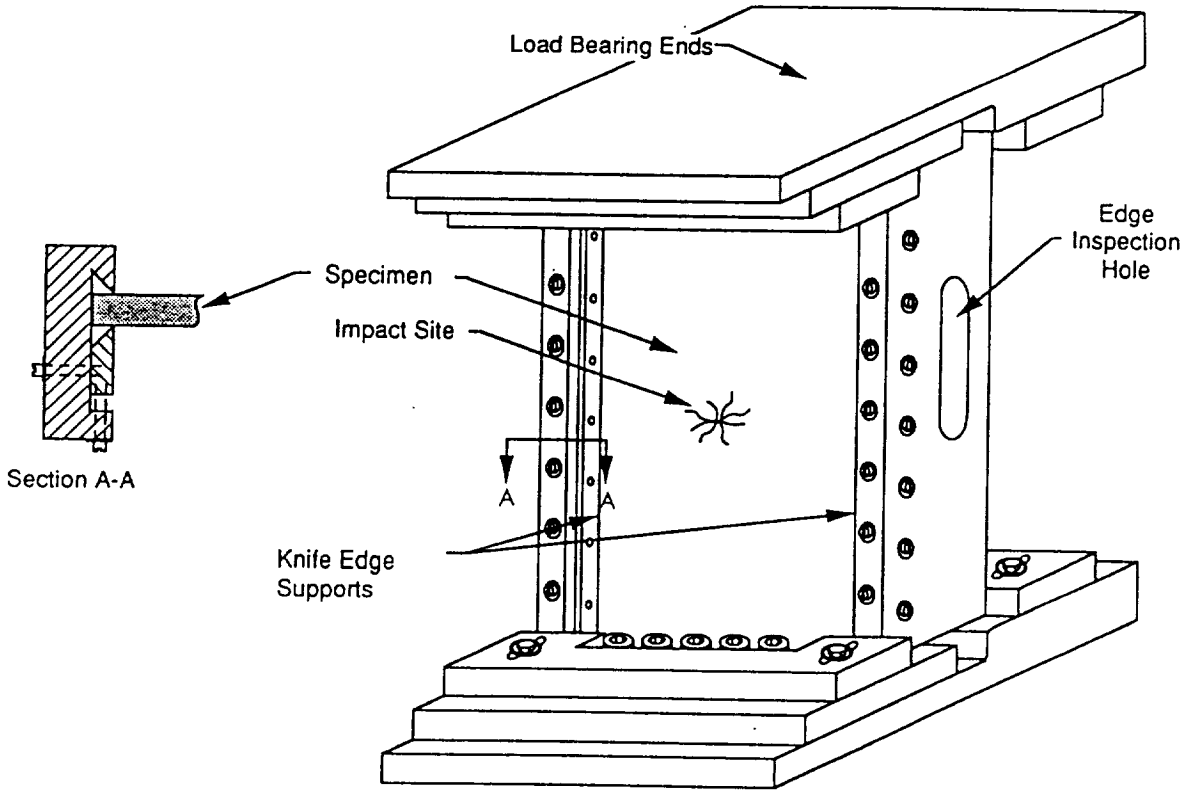

Figure A-1: Existing NASA post impact compressive fatigue test fixture [29]

Design considerations for the UF-CAI Test Fixture

The following were considered during the development of the UF-CAI test fixture;

1. It should be compatible with test specimens of different heights of 3", 4" & 5" and be flexible enough to test taller specimens with necessary modifications later.
2. It must not constrain the damage progression in any way during the compression test.
3. It should uniformly apply compressive end loading, and be easily aligned with load axis.
4. It should be able compatible with laminates of any thickness.
5. It should give repeatable results.

A schematic diagram of the UF-CAI test fixture is shown in Fig. 2-1, Chapter 2. Two photographs showing an isometric view and an end view with a graphite/epoxy specimen of 5" height are shown in Fig. A-2.

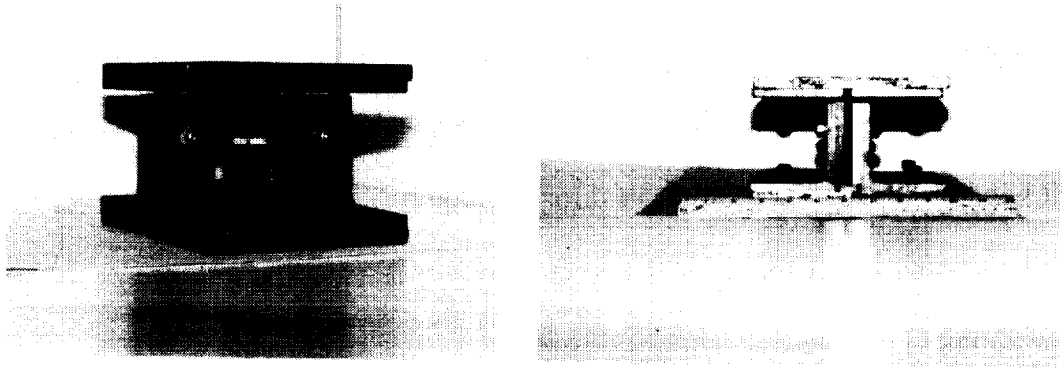

(a) (b)

Figure A-2: Photographs of the UF-CAI test fixture with 5" tall specimen
(a). Assembled isometric view (b). End view

Basic construction and operation of the UF-CAI test fixture

The UF-CAI fixture uses two L-shaped steel brackets to support the specimen from top and bottom side surfaces. The L-shaped brackets are secured in the bottom plate with 3 bolts each during the test. The L-shaped brackets have window-cutouts that allow the damage progression without any constrains. The shape and markings on the brackets allow quick and accurate alignment. The specimen is end loaded and side-supported. The brackets also prevent global buckling. In addition, two anti-buckling plates of different heights in conjunction with a matching bottom distance piece are used to allow testing of different heights of specimens. The anti-buckling plates also have corresponding window cutouts. The openings of the window cut-outs are also used for back-to-back strain gage mounting and for observing the nature of failure during the test.

Fabrication

A drawing of the UF-CAI Fixture is shown in Fig. A-3. The top and bottom platens and the side support plates have been used from the existing NASA fixture. Unsupported height of the specimen is 0.2" to permit end shortening of specimen.. Aluminum alloy and hot-rolled low carbon steel angle plates of different sizes and different window cutouts were investigated for the prototype development. The steel one was finally adopted after experimental validation of test results. The total weight of the fixture is 12 lbs.

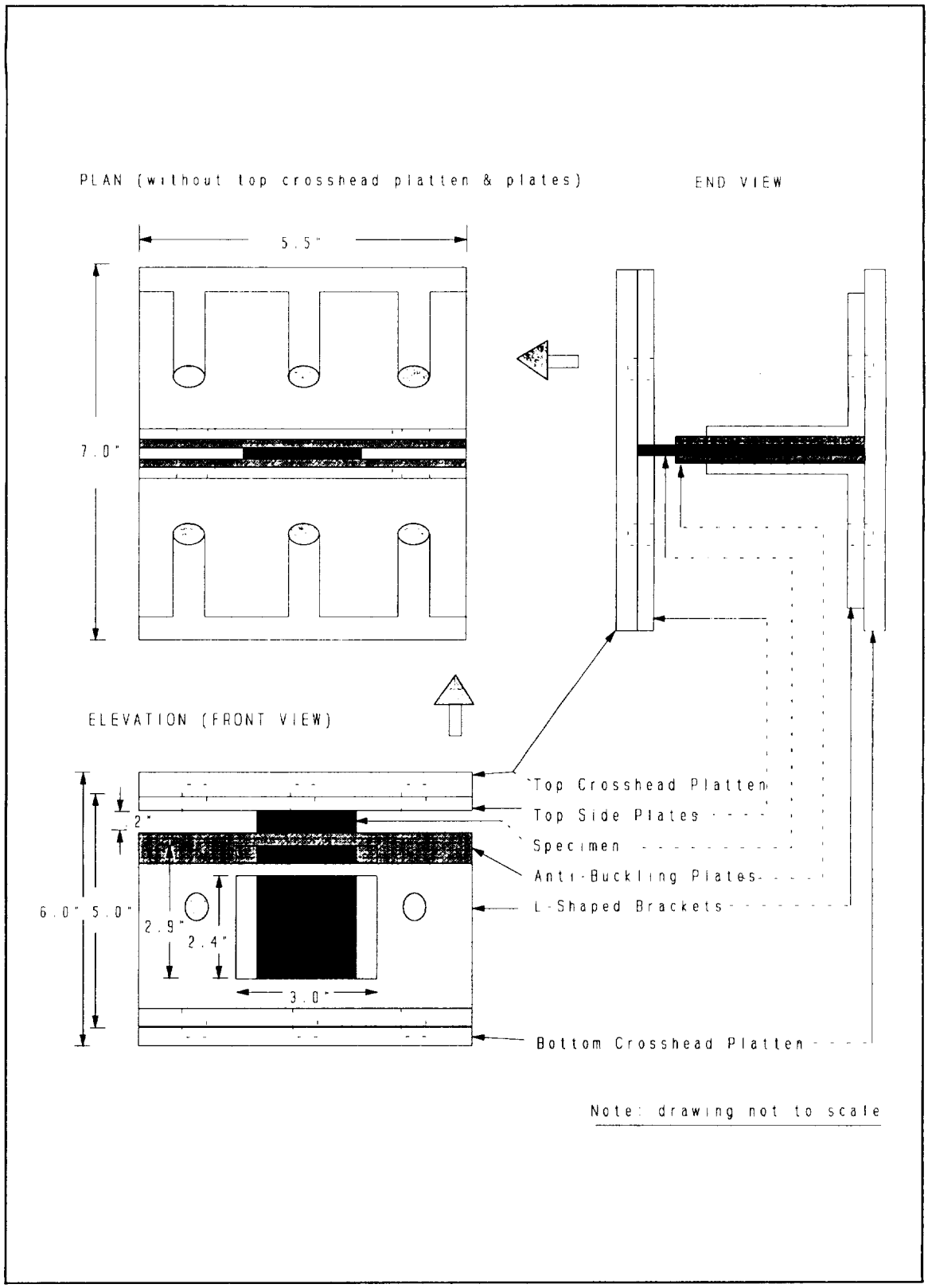

Figure A-3: Key dimensions of the UF-CAI test fixture shown for a 5" tall specimen

Validation of the UF-CAI test fixture

Compression tests were conducted on 12 three-dimensional braided graphite/epoxy composite laminates to compare the performance of UF-CAI fixture with available compressive failure strength data in the literature [30]. It was found that the UF-CAI fixture gave results within 10% of the values cited in the literature. The fixture was used for Sublaminate Buckling Tests on 131 specimens as described in Chapter-2, the results again being consistent with the compressive strength data in [22]. The fixture also met other design considerations satisfactorily.

Advantages and limitations of the UF-CAI fixture

1. The impact damage area is allowed to grow without constraints due to the window cutouts in the L-shaped brackets and the anti-buckling plates. This is considered better than the knife-edge supports which tend to pinch the specimen during buckling. This design seems to work well for materials of moderate strength e.g., composites of up to about 100 ksi strength. For higher strength materials it may be strengthened with thicker anti-buckling plates.

2. It allows three different heights of specimens for testing. Any other size of anti-buckling plates can be added to the fixture to adapt it to another specimen height. However, a NASA linear bearing fixture may be more suitable if the gage lengths are more than 4" or 5".

3. This fixture was found suitable for thin as well as thick plates, was easy to align and light weight for easy handling.

Detailed CAI Strength Test Data of Sublaminate Buckling Test

Table A-1: Compression strength data for the unstitched laminates (Plate #37)

			PLATE	#37				
Specimen	Height	Gage	Thickness	Width	PeakLoad	Strength	Av Str.	Damage
(Label)	(inch)	Length	(mm)	(mm)	(lbs)	(Ksi)	(Ksi)	Type
P37S1	5	2.9	7	38.7	27072	64.47		
P37S2	5	2.9	6.95	38.6	25800	62.05	63.51	No
P37S3	5	2.9	6.95	38.85	26791	64.01		Damage
P37S40	5	2.9	6.6	38.05	14746	37.88		
P37S41	5	2.9	6.6	38.05	15231	39.13	38.27	#2
P37S42	5	2.9	6.6	38.1	14734	37.8		
P37S80	5	2.9	6.8	38.3	5100	12.63		
P37S81	5	2.9	6.75	38.5	5500	13.65	13.27	#4
P37S82	5	2.9	6.8	38.6	5500	13.52		
P37S4	4	2.4	6.9	38.75	32629	78.73		
P37S5	4	2.4	7	38.8	35748	84.92	80.92	No
P37S6	4	2.4	6.9	38.65	32700	79.11		Damage
P37S20	4	2.4	6.65	38	31888	81.41		
P37S21	4	2.4	6.75	37.9	29239	73.74	76.36	#1
P37S22	4	2.4	6.7	37.85	29056	73.92		
P37S60	4	2.4	6.55	38	15179	39.35		
P37S61	4	2.4	6.6	38.05	15552	39.95	41.7	#3
P37S62	4	2.4	6.85	39.9	19406	45.8		

Table A-2: Compression strength data for Kevlar-2790, 4×1/4" stitched laminates (Plate #31)

		PLATE	#31					
Specimen	Height	Gage	Thickness	Width	Peak Load	Strength	Av Str.	Damage
(Label)	(inch)	Length	(mm)	(mm)	(lbs)	(Ksi)	(Ksi)	Type
P31S1	5	2.9	6.8	39.25	26260	63.47659		
P31S2	5	2.9	7	39.05	27496	64.89599	63.14872	No
P31S3	5	2.9	6.9	39.05	25586	61.2632		Damage
P31S40	5	2.9	6.95	39	20105	47.85442		
P31S41	5	2.9	7.05	39	19015	44.61799	47.17918	#2
P31S42	5	2.9	7	38	20288	49.20679		
P31S80	5	2.9	6.85	39	13031	31.46951		
P31S81	5	2.9	7	38.9	13220	31.32213	28.92002	#4
P31S82	5	2.9	7.05	39.1	10278	24.05527		
P31S4	4	2.4	6.85	39.1	30426	73.29004		
P31S5	4	2.4	6.85	38.8	30563	74.18927	72.88039	No
P31S6	4	2.4	6.8	41.2	30997	71.38073		Damage
P31S20	4	2.4	7	39.1	30298	71.41782		
P31S21/2	4	2.4	6.9	38.7	28572	69.03161	71.28318	#1
P31S22	4	2.4	6.9	39.15	30823	73.61418		
P31S63	4	2.4	6.95	38.9	18561	44.29293		
P31S64	4	2.4	7	38.9	17334	41.06942	43.27054	#3
P31S65	4	2.4	6.95	39.05	18753	44.57921		

Table A-3: Compression strength data for the Kevlar-2790, 8×1/8" stitched laminates (Plate #32)

		PLATE	#32					
Specimen	Height	Gage	Thickness	Width	PeakLoad	Strength	Av Str.	Damage
(Label)	(inch)	Length	(mm)	(mm)	(lbs)	(Ksi)	(Ksi)	Type
P32S1	5	2.9	7.25	37.5	28769	68.2689		
P32S2	5	2.9	7.25	37.25	25714	61.42891	62.75044	No
P32S3	5	2.9	7.2	37.4	24518	58.74195		Damage
P32S40	5	2.9	7.3	37.5	23981	56.51719		
P32S41	5	2.9	7.3	37.5	24524	57.79691	57.96171	#2
P32S42	5	2.9	7.25	37.5	25177	59.74508		
P32S80	5	2.9	7.3	37.6	23386	54.96835		
P32S81	5	2.9	7.3	37.75	22748	53.25628	54.4149	#4
P32S82	5	2.9	7.15	37.85	23148	55.18347		
P32S4	4	2.4	7.15	37.1	28186	68.55213		
P32S5	4	2.4	7.2	37.4	29187	69.92827	69.24296	No
P32S6	4	2.4	7.2	37	28680	69.45641		Damage
P32S20	4	2.4	7.4	37.95	29083	66.81333		
P32S21	4	2.4	7.25	37.9	30829	72.38518	68.78964	#1
P32S22	4	2.4	7.25	37.9	28696	67.37699		
P32S63/6	4	2.4	7.3	37.6	26556	62.41937		
P32S64/6	4	2.4	7.25	37.65	26120	61.73588	65.11166	#3
P32S65	4	2.4	7.3	37.7	30447	71.37526		

Table A-4: Compression strength data for the Glass-1250, 4×1/4" stitched laminates (Plate #33)

		PLATE	#33					
Specimen	Height	Gage	Thickness	Width	Peak Load	Strength	Av Str.	Damge
(Label)	(inch)	Length	(mm)	(mm)	(lbs)	(Ksi)	(Ksi)	Type
P33S1	5	2.9	6.8	36.9	24997	64.27174		
P33S2	5	2.9	6.9	39.4	26645	63.23213	63.41362	No
P33S3	5	2.9	6.9	39.2	26382	62.92743		Damage
P33S40	5	2.9	7.1	39.25	23434	54.25201		
P33S41	5	2.9	7.05	39.4	19482	45.24969	48.0516	#2
P33S42	5	2.9	7.1	39.55	19498	44.79738		
P33S80	5	2.9	6.9	39.05	13889	33.25587		
P33S81	5	2.9	6.95	38.8	13574	32.47572	33.3425	#4
P33S82	5	2.9	6.9	38.9	14310	34.39603		
P33S4	4	2.4	6.95	39.4	31543	74.31721		
P33S5	4	2.4	6.9	39.5	30746	72.77963	75.04288	No
P33S6	4	2.4	6.9	39.5	33060	78.25716		Damage
P33S20	4	2.4	7.05	39.2	29929	69.86899		
P33S21	4	2.4	7	36.55	25958	65.45657	68.32748	#1
P33S22	4	2.4	7	39.6	30017	69.86208		
P33S60	4	2.4	7	39.05	20374	48.08666		
P33S61	4	2.4	7.05	39.3	21936	51.0791	47.65282	#3
P33S63	4	2.4	6.95	39.1	18506	43.93579		

Table A-5: Compression strength data for the Glass-1250, 8×1/8" stitched laminates

Specimen (Label)	Height (inch)	PLATE Gage Length	#34 Thickness (mm)	Width (mm)	Peak Load (lbs)	Strength (Ksi)	Av Str. (Ksi)	Damage Type
P34S1	5	2.9	7.2	37.15	24826	59.88015		
P34S2	5	2.9	7.35	38.9	28287	63.8289	62.29714	No
P34S3	5	2.9	7.35	38.7	27939	63.36946		Damage
P34S40	5	2.9	7.3	34.5	25195	64.54162		
P34S41	5	2.9	7.45	37.5	26385	60.93082	62.61404	#2
P34S42	5	2.9	7.3	38	26898	62.55773		
P34S80	5	2.9	7.35	38.8	25656	58.04132		
P34S81	5	2.9	7.45	34	24414	62.18293	62.14375	#4
P34S82	5	2.9	7.4	34.5	26273	66.39361		
P34S4	4	2.4	7.2	39.25	30035	68.56823		
P34S5	4	2.4	7.2	34.7	27573	71.20156	69.71764	No
P34S6	4	2.4	7.2	38.85	30173	69.59249		Damage
P34S20	4	2.4	7.25	39.7	27554	61.76232		
P34S21	4	2.4	7.35	39.85	26196	57.70145	60.50514	#1
P34S22	4	2.4	7.45	39	28027	62.23335		
P34S60	4	2.4	7.35	36.1	26205	63.71725		
P34S61	4	2.4	7.5	38.75	29050	64.48825	62.22356	#3
P34S63	4	2.4	7.35	39.05	26093	58.65203		

Table A-6: Compression strength data for Glass-750, 4×1/4" stitched laminates (Plate #35)

		PLATE	#35					
Specimen	Height	Gage	Thickness	Width	Peak Loac	Strength	Av Str.	Damage
(Label)	(inch)	Length	(mm)	(mm)	(lbs)	(Ksi)	(Ksi)	Type
P35S1	5	2.9	6.9	40.75	29492	67.66981		
P35S2	5	2.9	6.9	38.8	25375	61.14947	64.40964	No
P35S3	5	2.9	6.85	39.4	-----	0		Damage
P35S40	5	2.9	6.9	38.9	20218	48.59672		
P35S41	5	2.9	6.9	39.3	19922	47.39786	47.89638	#2
P35S42	5	2.9	6.9	39.2	20056	47.83839		
P35S80	5	2.9	6.85	39.15	16208	38.99191		
P35S81	5	2.9	6.9	39.2	12988	30.97951	33.99981	#4
P35S82	5	2.9	6.95	39.2	13568	32.13012		
P35S4	4	2.4	6.85	38.5	29538	72.25988		
P35S5	4	2.4	6.85	38.8	30692	74.50241	73.53313	No
P35S6	4	2.4	6.85	38.5	30273	74.05793		Damage
P35S20	4	2.4	6.9	37.95	27570	67.92714		
P35S21	4	2.4	6.9	38.2	27045	66.19756	66.5844	#1
P35S22	4	2.4	6.9	38.15	26859	65.82845		
P35S60	4	2.4	6.85	38.1	18100	44.74355		
P35S61	4	2.4	6.9	38.6	18381	44.52462	45.69936	#3
P35S63	4	2.4	6.95	38.5	19894	47.96716		

Table A-7: Compression strength data for Glass-750, 8×1/8" stitched laminates (Plate #36)

		PLATE	#36					
Specimen	Height	Gage	Thickness	Width	Peak Load	Strength	Av Str.	Damage
(Label)	(inch)	Length	(mm)	(mm)	(lbs)	(Ksi)	(Ksi)	Type
P36S1	5	2.9	7.3	39.1	26898	60.79779		
P36S2	5	2.9	7.3	39.15	31293	70.64152	65.6543	No
P36S3	5	2.9	7.2	38.75	28421	65.72076		Damage
P36S40	5	2.9	7.4	39.85	26584	58.16044		
P36S41	5	2.9	7.45	39.1	24274	53.76204	57.74025	#2
P36S42	5	2.9	7.45	38.8	27542	61.47166		
P36S80	5	2.9	7.4	38.9	24673	55.29783		
P36S81	5	2.9	7.4	39.15	26794	59.668	58.74451	#4
P36S82	5	2.9	7.5	39.05	27893	61.44412		
P36S4	4	2.4	7.4	39.1	32813	73.16526		
P36S5	4	2.4	7.1	36	27911	70.45016	71.53023	No
P36S6	4	2.4	7.25	39.25	31400	71.19007		Damage
P36S20	4	2.4	7.45	39.1	24567	54.41098		
P36S21	4	2.4	7.5	39.1	24442	53.77323	58.76492	#1
P36S22	4	2.4	7.45	39.2	30911	68.28702		
P36S60	4	2.4	7.4	38.15	21735	49.67076		
P36S61	4	2.4	7.5	39.15	25641	56.33903	57.24064	#3
P36S63	4	2.4	7.35	39.3	29498	65.88402		

APPENDIX B

MODE I FRACTURE TOUGHNESS TEST DATA

Table B-1: DCB test data and G_{Ic} for unstitched laminates (Plate #30)

Specimen Type & #	Width w(mm)	DCB Test #	Starter Crack(a0)	Crack Incre(mm)	Work Don W(N.mm)	Area A(mm^2)	Glc J/m^2	Crack Length	Type of Hinge	
P30S13 Unstitched	25.7	P30S13-1	Nominal	Invalid					1" Single	
		P30s13-2	2.0"	Invalid						
		P30S13-3		Invalid						
		P30S13-4		9.5	71.54	244.15	293.0166	9.5		
		P30S13-5		13	102.52	334.1	306.8542	22.5		
		P30S13-6		18	120.81	462.6	261.1543	40.5		Overall Average Glc= 302.63
P30S14 Unstitched	25.02	P30S14-1	Nominal	Invalid					1" Single	
		P30S14-2	2.0"	17	115.7	425.34	272.0177	17		
		P30S14-3		20.5	170.52	512.91	332.456	37.5		
P30S15 Unstitched	24.75	P30S15-1	Nominal	20.25	140.47	501.1875	280.2743	20.25	1" Single	
		P30s15-2	1.0"	12	112.85	297	379.9663	32.25		
		P30S15-3		10.55	76.37	261.1125	292.4793	42.8		
		P30S15-4		12.95	96.48	320.5125	301.0179	55.75		
		P30S15-5		13.15	99.72	325.4625	306.3947			
		P30S15-6		Invalid						

Table B-2: DCB test data for Kevlar-2790, 4×1/4" stitched laminates (Plate #24)

Specimen Type & #	Width w(mm)	DCB Test #	Starter Crack(a0)	Crack Incre(mm)	WorkDone W(N.mm)	Area A(mm^2)	Glc J/m^2	Crack Length	Type of Hinges	
P24S13 Stitched Kevlar 4x1/4"	26.16	P24S13-1	Nominal 2.0"	Invalid	LVDT bottoms out				1" Single	
P24S14 Stitched Kevlar 4x1/4"	25.65	P24S14-1 P24S14-2	Nominal 2.0"	6.5 Invalid	268.5 LVDT bottoms out	166.725	1610.436		1" Single	
P24S15 Stitched Kevlar 4x1/4"	25.75	P24S15-1 P24S15-2 P24S15-3 P24S15-4 P24S15-5	Nominal 1.0"	13.95 11.5 Invalid 13.5 Invalid	239.53 891.25 2032.38	359.2125 296.125 347.63	666.8198 3009.709 5846.47	13.95 25.45 52	1" Single	
P24S16 Stitched Kevlar 4x1/4"	27.6	P24S16-1 P24S16-2 P24S16-3 P24S16-4 P24S16-5	Nominal 1.0"	9.65 11.15 Invalid 11 11.5	672.48 1493.33 740.289 818.272	266.34 307.74 303.6 317.4	2524.893 4852.57 2438.37 2578.047		2" Double -hinge overlaps crack	Overall Average Glc= 4563.81
P24S17 Stitched Kevlar 4x1/4"	26	P24S17-1 P24S17-2 P24S17-3 P24S17-4 P24S17-5	Nominal 1.0"	13.925 12.54 Invalid Invalid 9.1	1551 1681.46 1069.97		4283.94 5157.2 4522.27	13.925 26.465 58.665	2" Double -One end trimmed	
P24S18 Stitched Kevlar 4x1/4"	24.4	P24S18-1 P24S18-2 P24S18-3	Nominal 1.0"	12.05 34.65 Invalid	1330.75 3889.98	294.02 845.46	4526.05 4601.02	12.05 46.7	2" Double -One end trimmed	
							For Graph of Glc & crack			length
							3009.709 5846.47	25.5 52		
							4283.94 5157.2 4522.27	13.925 26.465 58.665		
							4526.05 4601.02	12.05 46.7		

Table B-3: DCB test data for Kevlar-2790, 8×1/8" stitched laminates (Plate #25)
Note: The G_{Ic} could not be computed as the specimens failed in bending.

Specimen Type & #	Width w(mm)	DCB Test #	Starter Crack(a0)	Crack Incre(mm)	Work Don W(N.mm)	Area A(mm^2)	GIIc J/m^2	Type of Hinges
P25S13 Stitched Kevlar 8x1/8"	26	P25S13-1	Nominal 2.0"	Invalid	Hinge bond failed			1" Single
P25S14 Stitched Kevlar 8x1/8"	27.6	P25S14-1	Nominal 1.0"	Invalid	Hinge bond failed			2" Double
P25S15 Stitched Kevlar 8x1/8"	27.55	P25S15-1	Nominal 1.0"	13	Bond failed	Integral machined hinge failed due to clevis fouling with hinge		
P25S16 Stitched Kevlar 8x1/8"	24.95	P25S16-1	Nominal 1.0"	9.75	bottom sub--laminate failed in bending (750 N)			

Table B-4: DCB test data for Glass-1250, 4×1/4" stitched laminates (Plate #26)

Specimen Type & #	Width w(mm)	DCB Test #	Starter Crack(a0)	Crack Incre(mm)	Work Don W(N.mm)	Area A(mm^2)	GIIc J/m^2	Crack Length	Type of Hinges	
P26S13 Stitched Glass (1250) 4x1/4"	25.7	P25S13-1	Nominal 2.0"	Invalid	Hinge bond failed				1" Hinge	
P26S14 Stitched Glass (1250) 4x1/4"	27.6	P26S14-1 P26S14-2 P26S14-3 P26S14-4 P26S14-5 P26S14-6	Nominal 1.0"	0 8.675 11.425 11.325 14.5 12.9	Invalid 2016.1 3324.36 2199.6 Invalid Invalid	239.43 315.33 312.57	8420.415 10542.48 7037.144	11.825 23.25 34.575	2" Double -One end cut	Overall Average Glc= 9121.33
P26S15 Stitched Glass (1250) 4x1/4"	25	P26S15-1 P26S15-2 P26S15-3 P26S15-4 P26S15-5	Nominal 1.0"	12.75 10 10.05 13.9 11.2	2982.97 2842.8 558.68 1222.06 1888.14	318.75 250 Invalid Invalid 280	9358.34 11370 6743.36	12.75 22.75 57.9		
P26S16 Stitched Glass (1250) 4x1/4"	25.1	P26S16-1 P26S16-2 P26S16-3	Nominal 1.0"	13.7 12.1 Invalid	3428.4 2883.09	343.87 303.71	9970 9492.9	13.7 25.8		
							For graph	of Glc	vs. a	
							8420.42	8.675		
							10542.5	20.1		
							7037.2	31.4		
							9358.3	12.75		
							11370	22.75		
							10364	57.9		
							9970	13.7		
							9492.9	25.8		

Table B-5: DCB test data for Glass-1250, 8×1/8" stitched laminates (Plate #27)

Note: The G_{Ic} could not be computed as the specimens failed in bending during the test.

Specimen Type & #	Width w(mm)	DCB Test #	Starter Crack(a0)	Crack Incre(mm)	WorkDone W(N.mm)	Area A(mm^2)	GIIc J/m^2	Type of Hinges
P27S13 Stitched Glass (1250) 8x1/8"	27.25	P27S13-1	Nominal 2.0"	Invalid	Hinge bond failed			1" Single
P27S14 Stitched Glass (1250) 8x1/8"	27.5	P27S14-1	Nominal 1.0"	Invalid	Hinge bond failed			2" Double
P27S15	specimen failed due to bending				Integral hinge works			

Table B-6: DCB test data for Glass-750, 4×1/4" stitched laminates (Plate #28)

Specimen Type & #	Width w(mm)	DCB Test #	Starter Crack(a0)	Crack Increment(mm)	Work Done W(N.mm)	Area A(mm^2)	GIIc J/m^2		Type of Hinges	
P28S13 Stitched Glass (750) 4x1/4"	25.3	P25S13-1	Nominal 2.0"	Invalid	Hinge bond failed				1" Hinge	
P28S14 Stitched Glass (750) 4x1/4"	27.65	P28S14-1	Nominal	15.25	1348.2	421.6625	3197.36	15.25		
		P28S14-2	1.0"	12.23	Invalid				2"	
		P28S14-3		10.15	2064.29	280.6475	7355.455	37.63	Double	
		P28S14-4		9.75	2116.15	269.5875	7849.585	47.38	-One end	
		P28S14-5		18.825	4102.81	520.5113	7882.27	66.21	trimmed	
P28S15 Stitched Glass (750) 4x1/4"	24.8	P28S15-1	Nominal	10.38	1432.18	257.424	5563.5	10.38	2"	Overall Average Glc= 6379.507
		P28S15-2	1.0"	13.08	2524.72	324.384	7783.12	23.46	Double	
		P28S15-3		11.65	2249.94	288.92	7787.41	35.11	-One end	
		P28S15-4		14.35	1981.18	355.88	5566.99	49.46	trimmed	
		P28S15-5		14.05	2110.09	348.44	6055.83	63.51		
P28S16 Stitched Glass (750) 4x1/4"	24.8	P28S16-1	Nominal	4.2	363.266	104.16	3487.58	4.2	2"	
		P28S16-2	1.0"	14.7	2573.76	364.56	7059.9	18.9	Double	
		P28S16-3		15.8	2729.2	391.84	6965.08	34.7	-One end trimmed	
						For graph of Glc and a	3197.36	15.25		
							7355.454	37.63		
							7849.585	47.38		
							7882.269	66.21		
							5563.5	10.38		
							7783.12	23.46		
							7787.41	35.11		
							5566.99	49.46		
							6055.83	63.51		
							3487.58	4.2		
							7059.9	18.9		
							6965.08	34.7		

Table B-7: DCB test data for Glass-750, 8×1/8" stitched laminates (Plate #29)
Note: The G_{Ic} could not be computed as the specimens failed in bending.

Specimen Type & #	Width w(mm)	DCB Test #	Starter Crack(a0)	Crack Incre(mm)	Work Don W(N.mm)	Area A(mm^2)	GIIc J/m^2	Type of Hinges
P29S13 Stitched Glass (750) 8x1/8"	25.5	P27S13-1 P29S14-2	Nominal 2.0"	10.5 Invalid	287.22 Hinge bond failed	267.75	1072.717	1" Single
P29S14 Stitched Glass (750) 8x1/8"	27.5	P27S14-1	Nominal 1.0"	Invalid	Hinge bond failed			2" Single
P29S15 Stitched Glass 8x1/8"	Specimen failed due to bending							

APPENDIX C
MODE II FRACTURE TOUGHNESS TEST DATA AND SAMPLE CALCULATIONS

The critical mode II strain energy release rate (G_{IIc}) was calculated using Beam theory formula and the two new methods presented in Chapter-4. The ENF test data, measured C-Scan areas, calculated values of the compliance and the a_{eff} along with the G_{IIc} values are shown in Tables C-1, C-2 and C-3 for the Beam Theory formula method, Area method using C-Scan and the Equivalent Area method using compliance of the unloading curve respectively. These tables can be treated as one large table in a spreadsheet for using data from one table to another. Here, these are given in three separate tables for sake of easy presentation. The specimen label numbers are same for all the three tables and are listed in the first column of the Table C-1. The specimen label describes the Plate # and the Specimen # of that plate e.g., P24S4 means specimen #4 of the plate #24.The other nomenclature applicable to these tables is as follows:

a = initial starter crack length

L = half length of the specimen

w = width of the specimen

Pl = linear peak load observed during the ENF loading cycle

GII1 = critical strain energy release rate using Beam theory formula

W = work done calculated from the area under the P- curve

a1 = a+a' where a' is the propagated crack length from C-Scan

A = new crack surface area measured from C-Scan

GII2 = critical strain energy release rate from Area method using C-Scan

C' = compliance of the unloading curve measured at about 500 N load

a2(eff)= effective crack length (a_{eff}) calculated as explained in Chapter-4 for a2<L

a2'(eff)= same as a2(eff) for a2>L

a~ = a1-a2' (to compare the C-Scan crack length with the calculated crack length)

GII3 = critical strain energy release rate from Equivalent Area method using compliance of the unloading curve. Average values of the G_{IIc} for valid specimens are listed in the last column of Table C-3.

Table C-1: Critical strain energy release rate (G_{IIc}) using beam theory formula

Specimen #	a mm	L mm	w mm	PI newton	C mm/N	GII1 J/m^2
P30S4	27.3	50.8	25.71	721.66	0.00303	636.8379
P30S5	27.3	50.8	25.81	729.47	0.00294	628.9227
P30S6	27.3	50.8	25.92	736.06	0.00313	678.8266
P30S7	27.3	50.8	26.54	751.72	0.00313	691.4786
P30S8	27.3	50.8	26.31	749.49	0.00307	680.0993
P30S9	27.3	50.8	25.65	727.25	0.00319	682.4862
P30S10	27.3	50.8	25.91	771.73	0.00292	696.4169
P24S4	27.3	50.8	26.67	910	0.00298	960.0616
P24S5	27.3	50.8	26.52	865	0.003	878.2194
P24S6	27.3	50.8	25.8	850	0.00294	854.257
P24S7	27.3	50.8	25.27	850	0.00288	854.3743
P24S8	27.3	50.8	25.27	880	0.00302	960.2629
P24S9	27.3	50.8	25.78	825	0.00297	813.588
P25S1	27.3	50.8	25.48	1081.5	0.00292	1390.784
P25S2	27.3	50.8	26.67	1114.58	0.00293	1416.088
P25S3	27.3	50.8	26.54	1104.16	0.00256	1220.186
P25S4	27.3	50.8	26.34	1083.3	0.0026	1201.927
P25S5	27.3	50.8	27.25	1145.83	0.00244	1219.795
P25S6	27.3	50.8	27.31	1166.67	0.00231	1194.564
P26S1	27.3	50.8	26.87	681.25	0.00296	530.4692
P26S2	27.3	50.8	26.54	675	0.00297	529.0371
P26S3	27.3	50.8	26.16	631.25	0.00332	524.7183
P26S4	27.3	50.8	26.03	687.5	0.00291	548.261
P26S5	27.3	50.8	25.14	685	0.00303	586.7885
P25S6	27.3	50.8	27.43	675	0.00293	504.978
P27S1	27.3	50.8	26.85	725	0.00254	515.9273
P27S2	27.3	50.8	26.8	718.75	0.00278	556.0179
P27S3	27.3	50.8	26.5	793.75	0.00252	621.649
P27S4	27.3	50.8	25.9	675	0.00233	425.2916
P27S5	27.3	50.8	26.75	775	0.00237	552.1423
P27S6	27.3	50.8	25.5	675	0.0028	519.097
P28S1	27.3	50.8	27.25	800	0.0025	609.2234
P28S2	27.3	50.8	25.85	781.25	0.00286	700.6621
P28S3	27.3	50.8	25.1	768.75	0.00284	693.8059
P28S4	27.3	50.8	26	820	0.00253	678.8877
P28S5	27.3	50.8	26.6	712.5	0.00267	528.716
P28S6	27.3	50.8	25.95	800	0.00267	683.2458
P29S1	27.3	50.8	25.55	775	0.00267	651.2487
P29S2	27.3	50.8	26.25	732.5	0.00306	648.9787
P29S3	27.3	50.8	26.1	800	0.00278	707.306
P29S4	27.3	50.8	26.1	716.25	0.00299	609.7938
P29S5	27.3	50.8	26.3	760	0.00276	628.9319
P29S6	27.3	50.8	26.2	730	0.00276	582.4741

Table C-2: Critical strain energy release rate (G_{IIc}) from area method using C-Scan

Specimen #	W N.mm	a1 mm a+a'	A mm^2 wxa'	GII2 J/m^2 W/A
P30S4	718.07	51.82	630.4092	1139.054
P30S5	379.35	51.81	632.6031	599.6651
P30S6	370.69	52.06	641.7792	577.5974
P30S7	373.92	51.81	650.4954	574.8234
P30S8	410.07	52.06	651.4356	629.4866
P30S9	402.77	53.72	677.673	594.3427
P30S10	391.21	52.7	658.114	594.4411
P24S4	413.4	38.03228	286.23	1444.293
P24S5	1574.71	56.52285	774.99	2031.91
P24S6	4577.19	64.25775	953.51	4800.359
P24S7	388.52	Invalid	Photomicr	Invalid
P24S8	2452.02	Invalid	Photomicr	Invalid
P24S9	4568.37	Invalid	Photomicr	Invalid
P25S1	3494.26	41.87285	371.3162	9410.47
P25S2	3694.41	40.94255	363.8469	10153.75
P25S3	3431.45	39.7285	329.8524	10402.99
P25S4	2927.17	38.34133	290.8286	10064.93
P25S5	2929.7	39.13368	322.4678	9085.249
P25S6	2081.44	Invalid	No C-Scan	Invalid
P26S1	2141.17	45.36906	485.5156	4410.095
P26S2	2956.26	52.5296	669.5937	4415.006
P26S3	2747.89	51.06677	621.7387	4419.686
P26S4	2537.23	51.63181	633.3571	4006.002
P26S5	2809.75	52.19957	625.9751	4488.597
P25S6	2319.25	45.42738	497.234	4664.303
P27S1	3868.2	40.94452	366.3554	10558.6
P27S2	3445.5	40.98932	366.8737	9391.516
P27S3	4115.78	42.20624	395.0152	10419.29
P27S4	3421.39	28.67785	35.68632	95873.99
P27S5	3937.13	31.19649	104.2311	37773.07
P27S6	5171.89	30.90379	91.89656	56279.48
P28S1	5125.4	45.9854	509.1771	10066.05
P28S2	Invalid	Invalid	Invalid	Invalid
P28S3	3476.01	46.20411	474.4932	7325.731
P28S4	3113.31	25.61036	-43.9306	-70868.8
P28S5	Invalid	30.03995	72.88265	Invalid
P28S6	3269.57	31.91459	119.7486	27303.63
P29S1	2574.2	40.65107	341.1198	7546.323
P29S2	2603.07	41.36058	369.0903	7052.664
P29S3	2592.82	46.01955	488.5802	5306.846
P29S4	2538.42	26.51891	-20.3865	-124515
P29S5	3520.68	33.93774	174.5725	20167.44
P29S6	2895.83	25.37669	-50.3906	-57467.6

Table C-3: Critical strain energy release rate (G_{IIc}) from equivalent area method using compliance of unloading curve.

Specimen #	EI mm^2.N	C' mm/N	a2(eff) mm a2<L	a2'(eff) mm a2>L	a~ mm a1-a2'	GII3 W/(w(a2-a	GII3' J/m^2 W/(w(a2'-a))	Av GII1 Av GII2 Av GII3	Stitch Yarn
P30S4	1111221	0.00641	51.78611	33.43629	18.38371	1140.63	4551.546		
P30S5	1145238	0.00492	45.11933	33.01756	18.79244	824.8229	2570.639	670.724	UNSTITCI
P30S6	1075719	0.00488	43.0314	32.91006	19.14994	909.0933	2549.225	672.7729	
P30S7	1075719	0.00508	44.22227	32.97008	18.83992	832.5669	2484.782	884.0744	
P30S8	1096743	0.0051	44.90519	33.00605	19.05395	885.3121	2731.503		
P30S9	1055486	0.00548	45.88001	33.05939	20.66061	845.1304	2726.423		
P30S10	1153082	0.00519	46.86188	33.11555 0	19.58445	771.8482	2596.282		
P24S4	1129866	0.004	38.39516	32.70717	5.325115	1397.057	2866.669		
P24S5	1122333	0.0065	52.45377	33.48508	23.03777	2360.609	9600.234	886.7939	KEVLAR-
P24S6	1145238	0.00692	54.76127	33.66411	30.59365	6460.389	27876.73	3416.134	2790,
P24S7	1169097	0.005	46.18536	33.07659	Invalid	814.1094	2661.562	3297.247	4x1/4"
P24S8	1114901	0.00642	51.92214	33.44612	Invalid	3940.878	15787.65		
P24S9	1133670	0.00767	57.34172	33.88431 0	Invalid	5898.663	26913.39		
P25S1	1153082	0.005	45.78648	33.05417	8.818681	7418.251	23832.7		
P25S2	1149147	0.00518	46.70829	33.1066	7.835953	7137.315	23856.14	1273.891	KEVLAR-
P25S3	1315234	0.00472	47.90985	33.17825	6.550246	6273.384	21995.22	9823.477	2790,
P25S4	1295000	0.00436	45.17943	33.02082	5.320514	6215.536	19425.59	6657.822	8x1/8"
P25S5	1379918	0.004	44.51671	32.98545	6.148229	6244.625	18910.01		
P25S6	1457576	0.00445	49.15429	33.25653 0	Invalid	3487.431	12795.25		
P26S1	1137500	0.0068	54.0857	33.60999	11.75907	2974.955	12628.59		
P26S2	1133670	0.00667	53.45414	33.56068	18.96892	4258.937	17791.8	537.3753	GLASS-
P26S3	1014157	0.00746	53.46899	33.56183	17.50494	4013.975	16774.92	4400.615	1250,
P26S4	1157045	0.0068	54.5599	33.64782	17.98399	3575.703	15355.39	3683.019	4x1/4"
P26S5	1111221	0.0066	52.6022	33.49611	18.70346	4417.171	18037.8		
P25S6	1149147	0.00613	51.47538	33.41403 0	12.01335	3497.425	13829.11		
P27S1	1325591	0.00567	53.28602	33.54777	7.396757	5544.022	23058.97		
P27S2	1211151	0.00547	49.75195	33.29563	7.693685	5726.16	21442.85	531.6875	GLASS-
P27S3	1336111	0.00553	52.8093	33.5116	8.694633	6088.465	25003.61	10123.14	1250
P27S4	1445064	0.00507	52.57332	33.49396	-4.81611	5226.855	21327.24	5600.354	8x1/8"
P27S5	1420675	0.00547	54.2153	33.62026	-2.42377	5468.355	23287.4		
P27S6	1202500	0.00723	57.33796	33.88397 0	-2.98018	6752.097	30805.01		
P28S1	1346800	0.0054	52.36772	33.47872	12.50668	7503.198	30441.28		
P28S2	1177273	Invalid	Invalid	31.47696	Invalid	Invalid	Invalid	649.0901	GLASS-
P28S3	1185563	0.00587	51.13528	33.38999	12.81412	5810.147	22740.01	8695.889	750
P28S4	1330830	0.00587	54.36134	33.6319	-8.02154	4424.861	18911.03	5498.572	4x1/4"
P28S5	1261049	Invalid	Invalid	31.47696	Invalid	Invalid	Invalid		
P28S6	1261049	0.006	53.4715	33.56202 0	-1.64744	4814.205	20120.49		
P29S1	1261049	0.00537	50.369	33.33705	7.314018	4367.396	16688.86		
P29S2	1100327	0.0056	47.69748	33.16531	8.195271	4861.61	16906.95	638.1222	GLASS-
P29S3	1211151	0.0056	50.41303	33.34005	12.6795	4298.086	16447.19	6635.278	750
P29S4	1126087	0.0056	48.35621	33.20585	-6.68694	4618.946	16467.99	4968.818	8x1/8"
P29S5	1219928	0.00553	50.26238	33.32982	0.607921	5829.804	22200.71		
P29S6	1219928	0.0048	46.23551	33.07944	-7.70274	5837.067	19124.33		

Table C-4: A sample calculation for G_{IIc} with variation of crack length.

A	C	D	E	F	G	H	I	J	K
177	752.64	2.979936	753.76	0.01296	1236.873	0.003959	34.3865	7.520579	0.586889
178	754.88	2.992896	756	0.01728	1249.937	0.003965	34.43544	7.086505	0.648917
179	757.12	3.010176	757.12	0.015552	1261.712	0.003976	34.53519	7.135444	0.654544
180	757.12	3.025728	758.24	0.019008	1276.124	0.003996	34.71836	7.235186	0.690563
181	759.36	3.044736	759.36	0.01728	1289.246	0.00401	34.83544	7.418363	0.686476
182	759.36	3.062016	761.6	0.018144	1303.064	0.004032	35.0348	7.535441	0.712627
183	763.84	3.08016	762.72	0.019008	1317.562	0.004032	35.0357	7.734799	0.697765
184	761.6	3.099168	760.48	0.014688	1328.732	0.004069	35.35351	7.7357	0.73416
185	759.36	3.113856	763.84	0.020736	1344.571	0.004101	35.61964	8.053507	0.770374
186	768.32	3.134592	764.96	0.013824	1355.146	0.00408	35.44322	8.319642	0.693621
187	761.6	3.148416	758.24	0.016416	1367.593	0.004134	35.89821	8.143222	0.791808
188	754.88	3.164832	757.12	0.013824	1378.06	0.004192	36.3775	8.598212	0.815925
189	759.36	3.178656	760.48	0.014688	1389.229	0.004186	36.32467	9.0775	0.767926
190	761.6	3.193344	759.36	0.015552	1401.039	0.004193	36.38109	9.024671	0.783673
191	757.12	3.208896	761.6	0.014688	1412.225	0.004238	36.74377	9.081089	0.83122
192	766.08	3.223584	764.96	0.015552	1424.122	0.004208	36.50147	9.443768	0.76649
193	763.84	3.239136	761.6	0.01728	1437.283	0.004241	36.76199	9.201473	0.83167
194	759.36	3.256416	761.6	0.016416	1449.785	0.004288	37.13608	9.46199	0.862088
195	763.84	3.272832	766.08	0.016416	1462.361	0.004285	37.10768	9.83608	0.825461

The table shown above is a part of the spreadsheet used for calculations. The column A is the serial number of data points, C and D are the load (Newton) and Displacement (mm) respectively. These increments can be used to calculate (column E and F) the area under the curve (i.e., work done = W) shown in column G. The column H shows compliance (δ/P). The column I calculates the effective crack length using $c' = (2L^3+3a'^3)/(96EI)$. The column J is crack length ($a'-a_0$), and K is G_{IIc} = (W-$0.5\times P\times\delta$)/(w×crack length) in KJ/m^2.

Table C-5: Details of the effect of contact roller pin friction.

Specimen Label	Drop in peak load at time of unloading (newton)
P24S6	95
P24S9	310
P25S2	40
P26S1	60
P26S2	110
P26S3	70
P26S4	55
P27S1	115
P27S2	105
P27S3	105
P27S4	55
P27S5	45
P27S6	220
P28S1	85
P28S3	55
P29S6	165

Sixteen out of the total 43 stitched specimens that are listed above indicated noticeable drop in peak load at the point of unloading cycle. The loads have been calculated from the respective P-δ curves. The drop for all other specimens is considered less than 30 newtons. An average of about 20% reduction in work done can be attributed to friction in the nonlinear part of the loading regime.

APPENDIX D
TEST DATA OF THIN PLAIN WEAVE LAMINATE SIF AND CAI TESTS

Table D-1: Test data of plain weave laminates

	Specimen	Stitch	density	= 5x1/4"
Specimen	Max.	C-Scan	C-Scan	
Label	Contact	Area	Area	
	Force	(mm2)	(mm2)	
	(N)	Unstitched	Stitched	
10	3000	0	0	
11	3111.3	174.2	114.2	
12	3558.4	163.9	109.6	
13	4003.2	231.6	109	
14	4448	438.1	116.1	
15	4670.4	445.8	403.9	
16	4981.8	629	445.8	
	Specimen	Stitch	density	= 8x1/4"
Unstitched				
2	2800	0		
3	4500	155.9		
4	5500	272.25		
5	4000	19.8		
6	4400	81.67		
7	5100	160.87		
8	5000	No data		
9	3650	4.95		
Stitched				
2	3500		9.9	
3	4800		237.6	
4	6200		334.12	
5	3200		2.47	
6	5100		146.02	
7	5500		188.1	
8	5200		91.57	
9	3650		22.27	

REFERENCES

[1] Tsai, .W. S., Composite Design, (Think Composites: Dayton,Ohio, 1987) pp 1-1, 1-5.

[2] Niu, M.C.Y., Airframe Structural Design: Practical design information and data on aircraft structures, Conmilt Press Ltd., 1990, pp 492-526

[3] Stevens, T., "Commercial composites meet the challenge", Materials Engineering, May 1992, pp 8-10.

[4] Jacobson, K., "ATP Goal: Extend composites' *MAGIC* to *MARKET*", New Technology Week, May 31, 1994, pp 1-3.

[5] Chou, T. W and Ko, F. K., Textile Structural Composites, Composite Material Series Vol.3, Elsevier, 1987, pp 1-24.

[6] Kwon, Y.S. and Sankar, B.V., "Indentation-flexure and low-velocity impact damage in graphite/epoxy laminates", NASA CR 187624, University of Florida, March 1992, pp 1-58 (also published in ASTM Journal of Composites Technology and Research, 1993, Vol 15 (2), pp 101-111.)

[7] Jackson, W.C and Poe, C.C., Jr., "The use of impact force as a scale parameter for the impact response of composite laminates", Journal of Composites Technology and Research, JCTRER, Vol. 15, No. 4, Winter 93, pp 282-289.

[8] Prasad, C.B., Ambur, D.R. and Starnes, J.H., jr., "Response of laminated composite plates to low-speed impact by airgun-propelled and dropped-weight impactors", AIAA paper 93-1402-CP, pp 887-900.

[9] Sankar, B.V., " Low-Velocity Impact response and damage in composite materials", Department of Aerospace Engineering, Mechanics and Engineering Science Report #AeMER-TR-94-1-03, University of Florida, July 1994, pp 1-34 (also being published as a chapter in the book Fracture of Composites by Trans Tech Publications, Ltd., Switzerland).

[10] Teh, K.T. and Morton, J., "Impact damage development and residual compression performance of advanced composite material systems",AIAA paper 93-1401-CP, pp 877-886.

[11] Suemasu, H., "Effects of multiple delaminations on compressive buckling behavior of composite panels", Journal of Composite Materials, Vol. 27, No. 12/1993, pp 1172-1192.

[12] Sierakowski, R.L. and Newaz, G.M., "Key elements in damage tolerance concept for polymeric composites", Proceedings of the 8th annual technical meeting of the American Society of Composites, Cleveland, OH, 1993, pp 640-649.

[13] Lagace, P.A. and Wolf, E., "Impact damage resistance of several laminated material systems", AIAA paper 93-1524-CP, pp 1862-1872.

[14] Mignery, L.A., Tan, T.M. and Sun, C.T., "The use of stitching to suppress delamination in laminated composites", ASTM STP 876, American Society for Testing and Materials, Philadelphia, 1985, pp 371-385.

[15] Dexter, H.B. and Funk, J.G., "Impact resistance and interlaminar fracture toughness of through-the thickness reinforced graphite/epoxy", AIAA paper 86-1020-CP, 1986.

[16] Ogo, Y., "The effect of stitching on in-plane and interlaminar properties of carbon-epoxy fabric laminates", CCM Report Number 87-17, Center for Composite Materials, University of Delaware, Newark, May 1987, pp 1-188.

[17] Pelstring, R. M. and Madan, R.C., "Stitching to improve damage tolerance of composites", 34th International SAMPE Symposium, May 1989, pp 1519-1528.

[18] Byun, J., Gillespie, J.W. and Chow, T., "Mode I delamination of a three-dimensional fabric composite", Journal of Composite Materials, Vol 24, May 1990, pp 497-518.

[19] Chen, V.L., Wu, X.X. and Sun, C.T., "Effective interlaminar fracture toughness in stitched laminates", Proceedings of the 8th annual technical meeting of the American Society of Composites, Cleveland, OH, 1993, pp 453-462.

[20] Jain, L. K. and Mai, Y., "On the effect of stitching on Mode I delamination toughness of laminated composites", Composites Science and Technology, 51 (1994), pp 331-345.

[21] Palmer, R.J., Dow, M.B. and Smith, D.L., "Development of stitching reinforcement for transport wing panels", personal communication.

[22] Reeder, J., "Comparison of the compressive strength for stitched and toughened composite systems", NASA TM 109108, Apr 94, pp 1-44.

[23] Carlsson, L.A. and Pipes, R.B., "Experimental characterization of advanced composite materials", Prentice-Hall. Inc., publication, 1987, pp 157-193.

[24] Hartshron, S., "Three's a charm: Structural adhesives", Materials Engineering, Oct 92, pp 10-11.

[25] Guenon, V.A.E., "Interlaminar fracture toughness of three dimensional composites", M.S. Thesis, University of Delaware, Dec 1987, pp 1-116.

[26] Carlsson, L.A., Gillespie, J.W. and Pipes, R.B., "On the analysis and design of End Notched Flexure (ENF) specimen for Mode II testing", Journal of Composite Materials, Vol.20, Nov 1986, pp 594-605.

[27] Sankar, B., "Scaling of Low-Velocity Impact of Symmetric Laminates", J of Reinforced Plastics and Composites, 1992, Vol 11 (3), pp 296-309.

[28] Poe, C.C. Jr., Jackson, M.A., Portanova, M.A. and Masters, J.E., "Damage tolerance of textile composites", The Proceedings of the fourth NASA/DoD conference, Salt Lake City, June 7-11, 1993.

[29] Portanova, M.A., Poe, C.C. and Whitcomb, J.D., "Open hole and post-impact-compression fatigue of stitched and unstitched carbon/epoxy composites", NASA-TM-102676, Jun 1990, pp 29.

[30] Gong, J.C., and Sankar, B.V.,"Impact properties of three dimensional braided graphite/epoxy composites", Journal of Composite Materials, Vol.25, Jun 91, pp 715-731.

REPORT DOCUMENTATION PAGE

Form Approved
OMB No. 0704-0188

1. AGENCY USE ONLY (Leave blank)	2. REPORT DATE	3. REPORT TYPE AND DATES COVERED
	February 1995	Contractor Report

4. TITLE AND SUBTITLE

Effects of Through-the-Thickness Stitching on Impact and Interlaminar Fracture Properties of Textile Graphite/Epoxy Laminates

5. FUNDING NUMBERS

G NAG1-1226

WU 505-63-50-04

6. AUTHOR(S)

Suresh K. Sharma and Bhavani V. Sankar

7. PERFORMING ORGANIZATION NAME(S) AND ADDRESS(ES)

University of Florida
Center for Studies of Advanced Structural Composites
P.O. Box 116250
Gainesville, FL 32611-6250

8. PERFORMING ORGANIZATION REPORT NUMBER

9. SPONSORING/MONITORING AGENCY NAME(S) AND ADDRESS(ES)

National Aeronautics and Space Administration
Langley Research Center
Hampton, VA 23681-0001

10. SPONSORING/MONITORING AGENCY REPORT NUMBER

NASA CR-195042

11. SUPPLEMENTARY NOTES

Langley Technical Monitor: Wade C. Jackson
Final Report

12a. DISTRIBUTION/AVAILABILITY STATEMENT

Unclassified - Unlimited

Subject Category - 24

12b. DISTRIBUTION CODE

13. ABSTRACT *(Maximum 200 words)*

This study investigated the effects of through-the-thickness stitching on impact damage resistance, impact damage tolerance, Mode I and Mode II fracture toughness of textile graphite/epoxy laminates. Uniweave resin-transfer-molded 48 ply graphite/epoxy (AS4/3501-6) laminates were stitched with Kevlar and glass yarns of different linear densities and stitch spacings. Delaminations were implanted during processing to simulate impact damage. Sublaminate Buckling Tests were performed to determine the effects of stitching on the compressive strength. The results showed outstanding improvements of up to 400% in the compression strength over the unstitched laminates. In impact and static indentation tests the onset of damage occurred at the same level, but the extent of damage was less in stitched laminates. Mode I fracture toughness of 24 ply Uniweave unidirectional (AS4/3501-6) stitched laminates was measured by conducting Double-Cantilever-Beam tests. The critical strain energy release rate (G_{Ic}) was found to be up to 30 times higher than the unstitched laminates. Mode II fracture toughness of the Uniweave laminates was measured by performing End-Notched-Flexure tests. Two new methods to compute the apparent G_{IIc} are presented. The apparent G_{IIc} was found to be at least 5-15 times higher for the stitched laminates.

14. SUBJECT TERMS

Composite laminates; Compression strength; Delamination; Fracture toughness; Graphite/epoxy; Stitching; Textile composites

15. NUMBER OF PAGES

137

16. PRICE CODE

A07

17. SECURITY CLASSIFICATION OF REPORT	18. SECURITY CLASSIFICATION OF THIS PAGE	19. SECURITY CLASSIFICATION OF ABSTRACT	20. LIMITATION OF ABSTRACT
Unclassified	Unclassified		